Electron-vibration interaction in quantum dots and quantum dissipation in Josephson systems

Gianluca Rastelli

Mémoire présenté en vue de l'obtention du
diplôme d'Habilitation à diriger des Recherches

présenté par

Gianluca RASTELLI

à l'Université Grenoble Alpes
Specialité: Physique

Electron-vibration interaction in quantum dots and quantum dissipation in Josephson systems

---

Composition du Jury

Prof. Pascal Simon	(rapporteur/examinateur)
Prof. Alexander Shnirman	(rapporteur/examinateur)
Prof. Christoph Bruder	(rapporteur)
Prof. Elke Scheer	(examinatrice)
Dir. Takis Kontos	(examinateur)
Prof. Wiebke Hasch-Guichard	(examinatrice)
Dir. Denis Basko	(examinateur)

Soutenance prévue le
4 Juillet 2019

dédié à

Frank Hekking

Acknowledgements

This research summary describes a part of my research activities from 2007 until the present in the field of quantum mesoscopic physics.

First of all, I would like to express my gratitude to Dr. Fabio Pistolesi (current director at the laboratory LOMA, Bordeaux) and Dr. Manuel Houzet. They offered me, in 2007, a post-doc position at the LPMMC (Laboratoire de Physique et Modélisation des Milieux Condensés) in Grenoble. During these two years of post-doc experience, I had the possibility to study several topics in mesoscopic physics and quantum transport and to learn new theoretical techniques that are now part of my scientific repertoire. In particular, I am indebted to Dr. Fabio Pistolesi from whom I acquired a successful approach to addressing scientific issues as well as other professional competences.

I also wish to acknowledge Prof. Frank Hekking, who was my academic advisor from 2009 to 2012 at the LPMMC. Prof. Hekking introduced me to the topics of mesoscopic superconductivity and Josephson junction physics. I benefited from his research experience enormously, and it was a great pleasure to interact with him.

In Grenoble, I had also illuminating and interesting discussions with Dr. Thierry Champel, Dr. Markus Holzmann, Dr. Denis Basko and Dr. Robert Whitney. I am also grateful to the experimentalists Dr. Ioan M. Pop and Prof. Wiebke Hasch-Guichard at the Institut Néel. I profited a great deal from my meetings with them; discussing physics from different perspectives enriched my communication and presentation skills.

I also acknowledge the tremendous support and encouragement of Prof. Wolfgang Belzig (Universität Konstanz). Ever since the beginning of our fruitful and robust collaboration at the end of 2012, Prof. Belzig has contributed to a rewarding research experience by giving me intellectual freedom in my work and pushing my research activities towards increasingly wider perspectives.

I must not fail to recognize the various students with whom I have had the chance to work during their PhD studies and who have contributed to the work described in this research summary: Dominik Maile and Dr. Angelo Di Marco. In addition, I had the great pleasure of productive collaboration with Dr. Pascal Stadler, who was a bright and enthusiastic doctoral student. I would also like to thank the graduate students with whom I am currently working at the University of Konstanz: Felicitas Hellbach, Raffael Klees, Mattia Mantovani and Hannes Weisbrich.

I am grateful to the Zukunftskolleg and the collaborative research center SFB 767 in Konstanz for giving me the opportunity to establish important scientific collaborations, especially with Prof. Leonid Glazman (University of Yale), Prof. Carlos Cuevas (Universi-

dad Autónoma de Madrid) and Prof. Michele Governale (Victoria University, Wellington).

I would like to express my special appreciation and thanks to Prof. Andrew Armour (University of Nottingham) and Prof. Mark Dykman (Michigan State University) for their keen scientific insight into the exciting problems on which we are collaborating. I have also benefited from satisfying discussions and collaborations with Prof. Eva Weig and Prof. Elke Scheer at the University of Konstanz. I further convey my deep gratitude to Prof. Sabine Andergassen (Universität Tübingen) as both a colleague and a friend who motivates me to always do my best.

Finally, I thank the three referees, Prof. Pascal Simon (Laboratoire de Physique des Solides, Université Paris Sud), Prof. Alexander Shnirman (KIT, Germany) and Prof. Christoph Bruder (Universität Basel) who warmly accepted the task of reading my habilitation thesis. I am also grateful to the other members of the committee, Dr. Denis Basko (research director at the LPMMC), Prof. Wiebke Hasch-Guichard (Université Grenoble Alpes, Institut Néel), Prof. Elke Scheer (Universität Konstanz, Germany) and Dr. Takis Kontos (research director at Laboratoire Pierre Aigrain, ENS Paris) for their time spent in judging this work and participating in the defence.

Last but not least: I thank my wife Silvia for her endless patience.

Overview

My main contribution to condensed matter physics is at the intersection between nanophysics and quantum many-body problems. During my PhD and my early post-doc period, I worked in the fields of strongly correlated systems (polarons and Wigner crystal) and statistical physics (quantum and classical premelting); since 2007, however, my main research interests have been in the field of mesoscopic quantum physics.

I am currently interested in engineered quantum systems such as quantum electronic devices, superconducting circuits and qubits, and nanomechanical systems. My research objectives are: (i) exploring strategies for creating, detecting and eventually controlling quantum states in these engineered coherent systems; and (ii) understanding the interplay between quantum coherence and interactions. Using a variety of theoretical methods - from path integral and diagrammatic techniques to density matrix equations - I am investigating problems that deal with nonequilibrium quantum states, nonlinear effects, quantum dissipation and decoherence dynamics.

My scientific path is summarized in the table below.

<table>
<tr><th>Period</th><th>2002-2006</th><th>2006-2007</th><th>2007-2009</th><th>2009-2012</th><th>2013-2015</th><th>2015-2020</th></tr>
<tr><th>Type</th><th>PhD</th><th>Post-doc grant (Della Riccia)</th><th>Post-doc (CNRS)</th><th>Post-doc (CNRS)</th><th>Marie-Curie Fellowship</th><th>Zukunftskolleg Research Fellowship</th></tr>
<tr><th>Place</th><th>University of L'Aquila</th><th>Institut Néel Grenoble</th><th colspan="2">LPMMC Grenoble</th><th colspan="2">University of Konstanz</th></tr>
<tr><td></td><td>Method: path integral</td><td></td><td></td><td>Topic: Josephson junctions</td><td colspan="2">→ superconducting circuits / quantum dissipation</td></tr>
<tr><td></td><td colspan="2">Topic: polarons and electron-phonon interaction</td><td>Topic: quantum transport
Method: Keldysh techniques</td><td></td><td colspan="2">→ quantum transport and electron vibration interaction</td></tr>
<tr><td></td><td rowspan="2">Topic: many-body systems (Wigner crystals)</td><td rowspan="2"></td><td rowspan="2"></td><td rowspan="2"></td><td></td><td>→ quantum dissipative phase transitions</td></tr>
<tr><td></td><td>Method: Master equations</td><td>→ decoherence in spin lattices</td></tr>
<tr><td></td><td></td><td>Topic: melting & anharmonic effects</td><td></td><td></td><td></td><td>→ nonlinear and nonequilibrium dynamics in nanoresonators</td></tr>
<tr><td></td><td></td><td></td><td></td><td></td><td></td><td>Topic: Andreev states and topology</td></tr>
</table>

My recent activities can be divided into the following research lines:

(a) quantum transport and electron-vibration interaction;

(b) quantum dynamics in superconducting Josephson systems;

(c) quantum dissipation and decoherence in many-body systems;

(d) Andreev bound states and topological effects;

(e) nonequilibrium dynamics in nonlinear nanoresonators.

In this manuscript I only present an overview of my works on topic (a) in Chapter 1 and on topic (b) in Chapter 2. A publication list of my works on these topics is given on page 7. I briefly outline topic (c) in my last chapter, Chapter 3, which focuses on my future research projects.

Chapter 1 and 2 have a similar introductory structure. The initial sections contain a short overview of the topic - Sections 1.1 and 2.1 - as well as of the state of the art of the experimental nanodevices - Sections 1.2 and 2.2.
I review the theoretical methods employed in the problems addressed by each corresponding chapter: the Keldysh nonequilibrium Green functions in Section 1.3 and the (imaginary) path integral method in Section 2.3. These sections do not seek to be a rigorous and formal introductions to the theoretical techniques; on the contrary, they are intended as a pedagogical overview of the basic concepts.
In Section 1.4, I assess the main results of my publications 2 through 5, whereas Section 1.5 contains the primary findings of my works 6 and 7. In the final section of this chapter (1.6) I outline a recent work, the first on the publication list.
Section 2.4 is a succinct (simple) justification of the standard theoretical modelling of Josephson junction systems. On this topic, for the sake of brevity, I only recapitulate works 13 and 14 in Section 2.5 and 8 and 10 in Section 2.6.

I have learned one good rule from successful theorists, which is to keep things as simple as possible. The idea is not to solve the most complicated problem with the most sophisticated methods. Rather, I always aim to capture the essential features in a simplified model and to work out the crucial aspects in the simplest possible way.

Publications

This research summary is based on the following publications:

Chapter 1

1) P. Stadler, G. Rastelli, W. Belzig,
"Finite frequency current noise in the Holstein model', Physical Review B **97**, 205408 (2018).

2) P. Stadler, W. Belzig, G. Rastelli,
"Charge-vibration interaction effects in normal-superconductor quantum dot", Physical Review B **96**, 045429 (2017).

3) P. Stadler, W. Belzig, G. Rastelli,
"Ground-State Cooling of a Mechanical Oscillator by Interference in Andreev Reflection", Physical Review Letters **117**, 197202 (2016).

4) P. Stadler, W. Belzig, G. Rastelli,
"Control of vibrational states by spin-polarized transport in a carbon nanotube resonator", Physical Review B **91**, 085432 (2015).

5) P. Stadler, W. Belzig, G. Rastelli,
"Ground-state cooling of a carbon nanomechanical resonator by spin-polarized current", Physical Review Letters **113**, 047201 (2014).

6) G. Rastelli, M. Houzet, L. Glazman, F. Pistolesi,
"Interplay of magneto-elastic and polaronic effects in electronic transport through suspended carbon-nanotube quantum dot", *(invited paper) Advances in nano-electromechanical systems*, Comptes Rendus Physique **13**, 410 (2012).

7) G. Rastelli, M. Houzet, F. Pistolesi,
"Resonant magneto-conductance of a suspended carbon nanotube quantum dot", Europhysics Letters **89**, 57003 (2010).

Chapter 2

8) D. Maile, S. Andergassen, W. Belzig, G. Rastelli,
"Quantum phase transition with dissipative frustration", Physical Review B **97**, 155427 (2018).

9) G. Rastelli, I.M. Pop,
"Tunable ohmic environment using Josephson junction chains", Physical Review B **97**, 205429 (2018).

10) G. Rastelli,
"Dissipation-induced enhancement of quantum fluctuations", New Journal of Physics **18**, 053033 (2016).

11) G. Rastelli, M. Vanevic, W. Belzig,
"Coherent dynamics in long fluxonium qubits", New Journal of Physics **17**, 053026 (2015).

12) A. Di Marco, F.W.J. Hekking, G. Rastelli,
"Quantum phase-slip junction under microwave irradiation", Physical Review B **91**, 184512 (2015).

13) G. Rastelli, I. M. Pop, F. W. J. Hekking,
"Quantum phase-slips in Josephson junction ring", Physical Review B **87**, 174513 (2013).

14) G. Rastelli,
"Semi-classical formula for quantum tunneling in asymmetric double-well potentials", Physical Review A **86**, 012106 (2012).

Index

Chapter 1

Electron-vibration interaction in quantum dots

1.1 Context and scientific background

Electronic transport through nanoscale devices is characterized by a variety of interesting phenomena [1, 2]. One of these is the interplay between quantum transport at the level of a single electron and the mechanical motion of localized vibrations in various nanoscale devices.

Nanoelectromechanical systems (acronym NEMS) [3–5] include single-molecule junctions [6–8], suspended carbon nanotube quantum dots (CNT-QDs) [9–14], single-electron transistors [15–19], superconducting single-electron transistors [20–22], single-electron shuttles [23–25] and quantum dots in other suspended nanostructures [26, 27]. In such nanodevices, the motion of the resonator can not only be detected but also manipulated via electron transport. At the same time, the mechanical motion strongly influences the transport itself.

In simple terms, one can describe an electromechanical device as a conductor coupled (capacitively or inductively) to a mechanical resonator. For example, consider a conducting nanowire suspended above a (central) gate electrode to which a gate voltage is applied. The actuation and the detection of the vibrational eigenmodes of the nanowire are implemented via the electrostatic force between the gate and the charge on the nanowire. The flexural displacement of the nanowire thus modulates the gate capacitance. Interestingly, in one class of experiments it is not important to determine the detailed microscopic model; it is sufficient to assume that the conductor is a black box characterized by a transconductance, viz. the conductance depends on the gate capacitance. Even within this framework, NEMS have important applications as ultrasensitive detectors at the nanoscale [28] and constitute a platform for the investigation of fundamental questions about classical nonlinear dynamics and nonequilibrium fluctuations [29].

In another class of experiments, the quantum nature of the conductor is important.

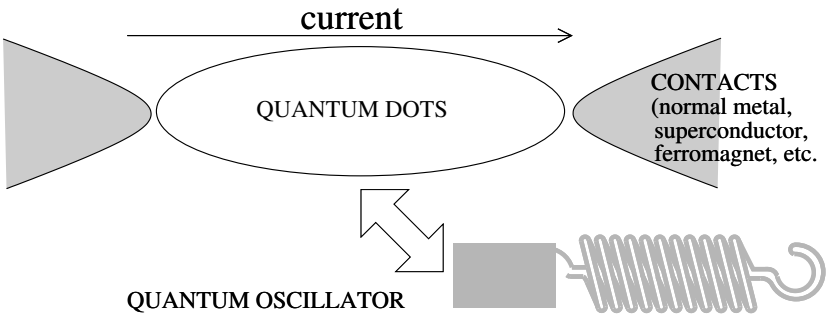

Figure 1.1: General theoretical model discussed in the text. A central quantum dot is in contact with two lateral leads of various type (normal metal, superconductor, ferromagnet) and interacts with a quantum harmonic oscillator. The latter object can represent either a vibrational mode of a molecule or of a nanomechanical resonator or an electromagnetic mode of a photon cavity.

Here, the current is due to a temporally discrete set of events whereby electrons can tunnel quantum-mechanically, one-by-one, from the source to the drain electrode through, for instance, a central island. Moreover, the action of the quantum conductor alters the vibrational motion in a fundamental way, such that the transport itself is correlated to the vibrational states. For example, because the probability for quantum mechanical tunnelling is exponentially sensitive to the tunnelling distance, it follows that the position of a metallic island oscillating between two electrodes is crucial: even small oscillations can significantly amplify the probability of transmission and, in the meantime, excitations of the vibration can be generated by the tunnelling of electrons from the leads, e.g. the so-called shuttle mechanism [24, 25].

More generally, charge-vibration interaction leads to a plethora of novel and unexpected behaviors of the nanoresonators. Electromechanical backaction effects - such as oscillator frequency shift and electromechanical damping - have been reported in experiments for the flexural modes in suspended carbon nanotube quantum dots [11, 12, 14] and in quantum dots coupled to a piezoelectric nanoresonator [27]. Further increasing the coupling strength, current suppression is expected due to the Franck-Condon blockade mechanism, which has been experimentally observed [9]. Mechanical bistabilities and blocked-current states are also theoretically predicted beyond a critical threshold of the charge-vibration coupling strength for low-frequency classical nanoresonators [30–32]. Other theoretical studies have reported self-sustained mechanical oscillations [33].

In many of the experiments and theoretical studies mentioned above, the oscillator acts as a *classical* moving object interfaced with a quantum conductor. However, this does not necessarily have to be the case. In *quantum* nanomechanical systems, one has the possibility of studying the quantum mechanical behavior of macroscopic moving objects, using nanoscaled resonators near the ground state of motion. Simply put, this regime can occur when the temperature T is much smaller the vibrational quantum energy associated

with a single vibrational mode of frequency ω, namely $k_BT \ll \hbar\omega$ with k_B denoting the Boltzmann constant and $\hbar$ the Planck constant. In this case, a full quantum theoretical approach is required [5]. This is also the domain of the single molecule devices. Here, the quantum tunnelling of electrons from the lateral electrodes (source and drain) through the central quantum dot can excite localized vibrational modes, such as the longitudinal or radial (breathing) modes in suspended carbon quantum dots [9, 10].

Before concluding this introduction, it is worthy mentioning that single-electron quantum conductors coupled to other types of localized resonators, such as microwave photon cavities, have now become a commonly studied system [34–37]. These hybrid structures, which combine electronic and photonic degrees of freedom in on-chip circuit-QED architectures, are currently undergoing rapid development. This opens the path to exploration of the correlations between the charge transport and the nonequilibrium regime of the photon cavity [38–40].

1.2 Electromechanical systems with quantum dots: experimental overview

Suspended carbon nanotube quantum dots (CNT-QDs) are particularly interesting electromechanical systems. These suspended nanostructures have outstanding mechanical properties as carbon nanoresonators can have frequencies in the range $f \sim$ MHz-GHz and yet large quantum zero-point fluctuations $u_0 \sim 10\,\mathrm{pm}$, making them ideal candidates for observing quantum mechanical effects. With regard to their transport properties, the state of the art in suspended CNT-QD has achieved accurate control of the number of the electrons in the quantum dot, of the tunnelling barriers as well as of the position of the dot in the nanotube, see Fig. 1.2. Quantized vibrational modes appear in low temperature transport spectroscopy (longitudinal and breathing modes) [9, 10, 41, 42]. In contrast, flexural modes have been mainly investigated experimentally and theoretically in the context of *classical* resonators coupled to quantum dots [43].

To achieve the quantum regime of the mechanical motion, a crucial requirement is cooling the system to a temperature much lower than the characteristic frequency, viz. $k_BT \ll \hbar\omega$. In this way, starting from the ground state, one aims to have access to and control of only a few low-energy excitations of the quantum oscillator. Ground-state cooling, i.e. the average vibrational quanta $n \ll 1$, has been achieved in certain nanomechanical devices, for instance, in oscillators of GHz frequency using standard dilution refrigeration techniques [44].

This goal still remains to be achieved in the flexural mechanical modes of suspended CNTs, which are related to the oscillations of the center of mass of the entire mechanical object. This accomplishment is hindered by the difficulty of cooling such low-frequency modes to temperatures of quantum regime. The flexural modes have typical values around hundreds of MHz or below. This implies that the electromechanical devices would have to be cooled to extremely cryogenic temperature below a few millikelvin which is a demanding

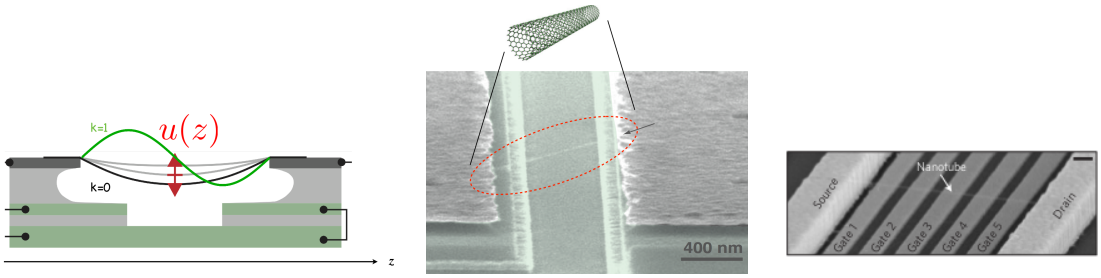

Figure 1.2: **Left:** Schematic picture of a suspended carbon nanotube quantum dot between two conducting contacts, with the flexural modes labelled by the index k and with $u(z)$ as the local displacement (from [11]). **Center**: Scanning electron microscopy image of a typical device, with the arrow showing the position of a nanotube (from [11]). **Right:** Scanning electron microscopy of a carbon nanotube (length $\sim 0.9\mu$m) suspended above five gate electrodes (from [14]). A quantum dot is formed when a few electrons are confined in a small region of the suspended carbon nanotube using the underlying gate electrodes.

task in the field of low-temperature electronic circuitry.

In the next sections, I discuss two proposals for controlling the vibrational states of a suspended carbon nanotube using either spin-vibration interaction with spin-polarized current or charge-vibration interaction in a normal-superconductor quantum dot.

Experiments in recent years have achieved a relevant coupling regime for flexural modes, such that the intrinsic mechanical damping can be much smaller than the induced electromechanical damping [14, 45]. The latter condition is important to attain quantum ground state cooling of the mechanical motion, as I explain in the following section.

Furthermore, suspended CNT-QDs are versatile systems, and they can be in contact with electrodes of different types. For instance, spin-current injection has been experimentally reported in CNT-QDs in a spin-valve geometry with gate field control and with ferromagnetic nanocontacts [46]. Moreover, the coherent coupling between the electron spin and its orbital magnetic moment has been studied theoretically and proved experimentally [47]. Although a priori, for vanishing magnetic field and spin-orbit interaction, the localized electronic levels of a CNT-QD shell are at least fourfold degenerate owing to the spin and circumferential orbital degree of freedom, the magnetic field and the spin-orbit interaction remove this degeneracy. This feature opens up the possibility of tuning individual spin levels in suspended CNT-QD and of coupling the spin with the mechanical flexural modes [48, 49].

In addition, a set-up involving CNT-QDs with the nanotube embedded between a normal metal and a superconductor has also been experimentally implemented [50, 51].

In normal-superconductor quantum dots, one would expect the role of the superconducting contact to be unessential when the superconducting gap is much smaller than the typical vibrational frequency $\Delta \ll \hbar\omega$ as the vibrational frequency sets the energy scale of the inelastic tunneling of electrons. The interesting and relevant regime is thus expected

for $\Delta \sim \hbar\omega$ or $\Delta \geq \hbar\omega$, which corresponds to a demanding condition in single-molecule junctions characterized by typical high-frequency vibrations due to the low mass of the molecules. This regime can occur naturally in CNT-QDs for a quantum dot coupled to the flexural modes with a lower frequency range.

1.3 Overview of the theoretical technique

The technique of the Keldysh Green's functions is a useful theoretical method for analyzing problems of quantum transport in the presence of interaction and in nonequilibrium regime. Many books present a complete introduction to this method, including that of Rammer [52]. In this section, I present a short overview. For the notations, I refer to the book of Rammer [52] (and set $\hbar = 1$, except for the conductance quantum).

1.3.1 The Keldysh nonequilibrium Green's functions

Let us assume that in the distant past t_0, the system was in a state specified by a (many-body) density matrix $\hat{\rho}(t_0) = \hat{\rho}_0$. Setting the Hamiltonian as $\hat{H} = \hat{H}_0 + \hat{H}_I$ with $\hat{H}_I$ assumed to be the perturbation, we set $\hat{H}_I = 0$ before the time t_0. At time t_0 the perturbation $\hat{H}_I$ is switched on. Then, the precise form of $\hat{\rho}_0$ is of no importance as long as we consider the steady regime of the system at a time t sufficiently far away from t_0 (eventually $t_0 \to -\infty$). The physical explanation is that over this large time elapse dissipative irreversible processes occur such that the system losses memory of the initial state. For instance, this is the case for a central dot coupled to two lateral leads. Here the dot represents an open quantum system coupled to the two fermionic reservoirs at temperature T such that, even if the interactions are not present in the leads (which form a continuum anyways), the state of the dot becomes uncorrelated to its initial state after some time.

The unitary time evolution operator in the interaction picture is $\hat{U}_I(t, t_0) = \hat{T} e^{-i \int_{t_0}^{t} dt' \hat{H}_I(t')}$, whereas the operators are characterized by the Heisenberg evolution according to an unperturbed Hamiltonian $\hat{H}_0$, for instance, $\hat{H}_I(t') = e^{i\hat{H}_0 t'} \hat{H}_I e^{-i\hat{H}_0 t'}$. $\hat{T}$ is the time ordering on the time axis, namely $\hat{T}\hat{A}(t_1)\hat{A}(t_2) = \theta(t_1 - t_2)\hat{A}(t_1)\hat{A}(t_2) + \theta(t_2 - t_1)\hat{A}(t_2)\hat{A}(t_1)$ ($\hat{T}'$ is the time anti-ordering). The density matrix evolves as $\hat{\rho}(t) = \hat{U}_I(t, -\infty)\hat{\rho}_0\hat{U}_I^\dagger(t, -\infty)$. Then, the expectation value of an observable is calculated at a time t $\langle \hat{O} \rangle = \mathrm{Tr}\left[\hat{O}_I(t)\hat{\rho}_I(t)\right]$, or more explicitly

$$\langle \hat{O} \rangle \;=\; \mathrm{Tr}\left[\hat{U}_I^\dagger(t, -\infty)\hat{O}_I(t)\hat{U}_I(t, -\infty)\hat{\rho}_0\right] = \langle \hat{T}_c\, e^{-i \oint_c dt' \hat{H}_I(t')}\, \hat{O}_I(t) \rangle \,. \tag{1.1}$$

In the equation above, I have introduced the close time path which starts at t_0 and proceeds along the real time axis to time t (upper branch) and then goes back to t_0 (lower branch). This path is the so-called Keldysh close time contour c depicted in Fig. 1.3(a) upon which one can define a time ordering operator $\hat{T}_c$ acting on it. One can generalize

the previous expression to the two operators (correlators) function, for instance, for the Green's functions defined as

$$\hat{\mathcal{G}}_{\lambda,\mu}(t,t') = -i\langle \hat{T}_c\, e^{-i\oint_c dt'' \hat{H}_I(t'')}\, \hat{c}_\lambda(t)\hat{c}^\dagger_\mu(t')\rangle \equiv -i\langle \hat{T}_c\, \hat{S}_c\, \hat{c}_\lambda(t)\hat{c}^\dagger_\mu(t')\rangle \tag{1.2}$$

where $\hat{c}_\lambda$ and $\hat{c}^\dagger_\lambda$ are the annihilation and creation fermionic operator with respect to a single particle set basis λ, μ in the interaction picture. I have also introduced the notation $\hat{S}_c$ for the exponential operator appearing in Eq. (1.2). A similar definition holds for the phonon propagator with the operator $\hat{u} = \hat{b} + \hat{b}^\dagger$, where $\hat{b}$ and $\hat{b}^\dagger$ are the annihilation and creation bosonic operators

$$\hat{D}(t,t') = -i\langle \hat{T}_c\, \hat{S}_c\, \hat{u}(t)\hat{u}^\dagger(t')\rangle\,. \tag{1.3}$$

By introducing the Keldysh close time contour and the time ordering on it, the Keldysh Green functions method appears formally equivalent to the zero-temperature diagrammatic method for calculating the ground state of many-body systems or the Matsubara method for evaluating the response functions of many-body systems at thermal equilibrium [52]. However, such formalism enables us to describe nonequilbrium states and even at finite temperature. The price we must pay is that the Green's functions are matrices since the time t and t' in the Eq. (1.2) and Eq. (1.3) can belong to the upper or lower branch of the Keldysh close time contour. As a simple example, I consider the case of a single electron level of an isolated quantum dot without any interaction, with $\hat{d}$ the annihilation fermionic operator for the dot's level. Then the Keldysh Green's function matrix reads as

$$\hat{g}_d(t,t') = \begin{pmatrix} g_d^{++}(t,t') & g_d^{+-}(t,t') \\ g_d^{-+}(t,t') & g_d^{--}(t,t') \end{pmatrix} = -i \begin{pmatrix} \langle \hat{T}\hat{d}(t)\hat{d}^\dagger(t')\rangle & -\langle \hat{d}^\dagger(t')\hat{d}(t)\rangle \\ \langle \hat{d}(t)\hat{d}^\dagger(t')\rangle & \langle \hat{T}'\,\hat{d}(t)\hat{d}^\dagger(t')\rangle \end{pmatrix}, \tag{1.4}$$

where the signs + and − refers to the fact that the times t, t' can belong to the upper (+) or lower (−) branch.

Both the Wick theorem and the Dyson equation can be reformulated on the Keldysh close time contour, provided that one defines the Green's functions as matrices with respect to the position of the two times t and t' in the lower or upper branch.

1.3.2 Exactly solvable model of a quantum dot

In this section, I describe the method of Keldysh nonequilibrium Green's functions in more detail for the specific case of the impurity model, namely a quantum dot between two fermionic reservoirs, Fig. 1.3(b). The latter systems are bulk leads, described as two Fermi gases at thermal equilibrium and characterized by a temperature T. To simplify the notation, I discuss spinless fermions. The Hamiltonian of the entire system is given by s

$$\hat{H}_0 = \sum_{\nu=l,r}\sum_k (\varepsilon_{\nu k} - \mu_\nu)\,\hat{c}^\dagger_{\nu k}\hat{c}_{\nu k} + \underbrace{\sum_{\nu=l,r}\sum_k \left(t_\nu\ \hat{d}\ \hat{c}^\dagger_{\nu k} + \text{h.c.}\right)}_{\hat{H}_{tun}} + \varepsilon_0 \hat{d}^\dagger\hat{d}\,, \tag{1.5}$$

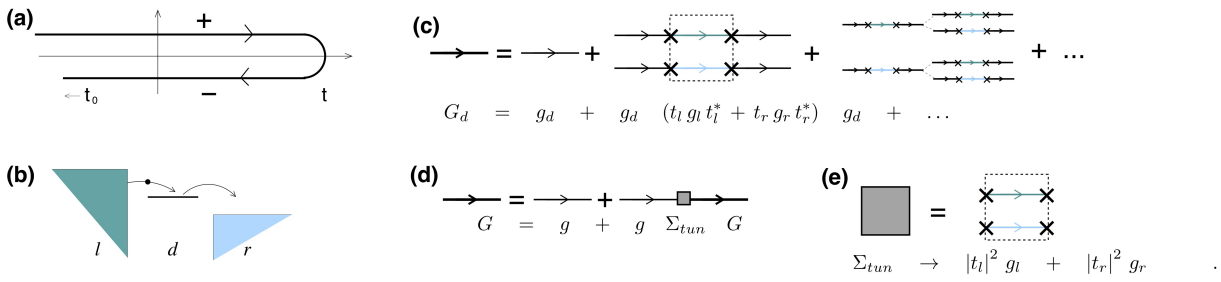

Figure 1.3: **(a)** The Keldysh closed time contour with the positive branch and negative branch for the initial time $t_0 \to -\infty$. **(b)** Sketch of the exactly solvable impurity model in the simplest case: a quantum dot d coupled to the two lateral norma leads (l left and r right). **(c)** Schematic diagrammatic of the perturbation theory for the model in (b). The tunneling is treated as the perturbation (cross). The exact electron Green's function G_d is the solid (thick) line whereas the thin lines are the bare Green's functions g_d, g_l, g_r for vanishing tunneling (see text). The tunneling amplitudes are t_l and t_r. **(d)** The Dyson equation for the dot Green function $G \equiv G_d$ (solid line) of the quantum dot coupled to the lateral leads. **(e)** The self energy Σ_{tun} is given simply by the sum of two terms related to the bare Green's functions of the leads (see text).

where the first term is the Hamiltonian for the left and right leads the second term is the tunnelling Hamiltonian and the third term is the dot's level. The operators $\hat{c}^\dagger_{\nu k}$ ($\hat{c}_{\nu k}$) and $\hat{d}^\dagger$ ($\hat{d}$) are creation (annihilation) operators for the corresponding electronic states in the leads and the dot.

Let us assume that in the distant past t_0, the whole system formed by the dot and the leads is described by the density matrix $\hat{\rho}_0 = \rho_l\,\rho_r\,\rho_d$ with ρ_l and ρ_r as the density matrices of a Fermi gas at temperature T and chemical potential μ_ν. Before time t_0, a bias-voltage is applied across the two leads, with no tunnelling between the dot and the leads. At time t_0, the tunnelling with the quantum dot is switched on. Considering the tunnelling term as the perturbation (interaction) on the dot in contact with two lateral leads, we write the Green's function of the dot as

$$\hat{G}_d(t,t') = -i\langle \hat{T}_c\, e^{-i\oint_c dt'' \hat{H}_{tun}(t'')}\, \hat{d}\ (t)\hat{d}^\dagger(t')\rangle\,. \tag{1.6}$$

By expanding the exponential, one generates a series of different terms of increasing order in the tunnelling amplitudes t_ν. Since we average on the thermal fermionic distribution of the leads, the first non-vanishing term is second order in the tunnelling. By applying Wick's theorem we obtain, for example, the following pairing

$$\langle \hat{T}_c\ \overbrace{\hat{d}\ (t)\,\big[\hat{d}(t_1)\,\hat{c}^\dagger_{lk}(t_1)\hat{c}_{lk}(t_2)\,\hat{d}^\dagger(t_2)\big]}\ \overbrace{\hat{d}\ (t')}\rangle \ \propto\ \hat{g}_d(t,t_1)\,\hat{g}_{lk}(t_1,t_2)\,\hat{g}_d(t_2,t')\,, \tag{1.7}$$

where the times t_1 and t_2 vary on the close path and $\hat{g}_{lk}(t_1,t_2)$ is the Keldysh Green's

function of the fermionic state k on the left lead l. Proceeding in this way, one obtains

$$\hat{G}_d(t,t') = \hat{g}_d(t,t') + \oint\!\!\oint dt_1 dt_2\, \hat{g}_d(t,t_1) \left(\sum_{\nu,k} |t_\nu|^2 \hat{g}_{\nu k}(t_1,t_2) \right) \hat{g}_d(t_2,t') + \dots . \tag{1.8}$$

The factor two coming from the exponential is compensated by the number of permutations of the indices of the internal time t_1, t_2. This is also true at any order: the factorial term $(n!)$ at the denominator is compensated by the number of possible terms that can be obtained by permuting the internal time $t_1, \dots, t_n$. This second order result illustrates very well the simple rules for constructing the diagrams at any order, as depicted graphically in Fig. 1.3(c). The graphic rules are: (i) consider only an even number of combinations of the tunnelling Hamiltonian for the left and right leads, (ii) after the bare dot Green's function g_d (without tunnelling,) one must insert a bare Green's function $\hat{g}_{\nu k}$ of the left or right lead and sum over k, and (iii) each tunnelling event is represented by a cross corresponding to a factor $|t_\nu|^2$. Then, one can graphically realize the validity of the Dyson equation - Fig. 1.3(c) - which reads explicitly as

$$\hat{G}_d(t,t') = \hat{g}_d(t,t') + \oint\!\!\oint dt_1 dt_2\, \hat{g}_d(t,t_1) \left(\hat{\Sigma}_t(t_1,t_2) \right) \hat{G}_d(t_2,t')\,, \tag{1.9}$$

and the self energy defined with respect to the tunnelling Hamiltonian $\hat{H}_{tun}$ is simply $\hat{\Sigma}_t(t_1,t_2) = \sum_{\nu,k} |t_\nu|^2 \hat{g}_{\nu k}(t_1,t_2)$. In summary, using the perturbative expansion and drawing the diagrams as in Fig.1.3(c), we have shown that the self energy is formed simply by the sums of two terms as a consequence of the fact that the electron can tunnel only to one lead per time before returning to the dot.

Using the matrix formalism, one reduces the integration on the complex contour to the integration on the real axis

$$\hat{G}_d(t,t') = \hat{g}_d(t,t') + \iint_{-\infty}^{+\infty} dt_1 dt_2\ \hat{g}_d(t,t_1)\, \hat{\sigma}_z\, \hat{\Sigma}_t(t_1,t_2)\, \hat{\sigma}_z\, \hat{G}_d(t_2,t')\,, \tag{1.10}$$

where $\hat{\sigma}_z$ is the diagonal Pauli matrix. The latter equation suggests the use of a rotation known as the Larkin-Ovchinnikov rotation defined by the matrix $\hat{L}$ that removes the Pauli matrix in the Dyson equation such that one must simply carry out a matrix product operation:

$$\check{G}_d(t,t') = \hat{L}\hat{G}_d(t,t')\hat{L}^\dagger = \check{g}_d(t,t_1) + \iint_{-\infty}^{+\infty} dt_1 dt_2\ \check{g}_d(t,t_1)\, \check{\Sigma}_t(t_1,t_2)\, \check{G}_d(t_2,t') \tag{1.11}$$

with $\hat{L} = \begin{pmatrix} 1 & -1 \\ 1 & 1 \end{pmatrix} / \sqrt{2}$ and $\hat{L}\hat{L}^\dagger = 1$. The new matrices are triangular with three components: the retarded, the advanced and the Keldysh components.

$$\check{g}_d = \begin{pmatrix} g_d^R(t,t') & g_d^K(t,t') \\ 0 & g_d^A(t,t') \end{pmatrix},\ \check{G}_d = \begin{pmatrix} G_d^R(t,t') & G_d^K(t,t') \\ 0 & G_d^A(t,t') \end{pmatrix},\ \check{\Sigma}_t = \begin{pmatrix} \Sigma_t^R(t,t') & \Sigma_t^K(t,t') \\ 0 & \Sigma_t^A(t,t') \end{pmatrix}. \tag{1.12}$$

The Dyson equation 1.11 now reads as a time convolution product, and in the frequency space, it corresponds to

$$\check{G}_d(\omega) = \check{g}_d(\omega) \, + \, \check{g}_d(\omega)\, \check{\Sigma}_t(\omega)\, \check{G}_d(\omega)\,. \tag{1.13}$$

To obtain the self energy we must sum over the k vector of the Green's functions for the leads $\nu = l, r$ which are given by

$$g^{R,A}_{\nu k}(\omega) = \frac{1}{\omega - \varepsilon_{\nu k} \pm i\eta} \quad , \quad g^{K}_{\nu k}(\omega) = -2\pi i \delta(\omega - \varepsilon_{\nu k})\,[1 - 2f_\nu(\omega)] \tag{1.14}$$

and the fermi function of the leads $f_\nu(\omega) = 1/(1 + e^{\beta(\omega - \mu_\nu)})$. In this exactly solvable problem, the self energy has only a single diagram:

$$\check{\Sigma}(\omega) = \sum_k \left(|t_l|^2 \check{g}_{lk}(\omega) + |t_r|^2 \check{g}_{rk}(\omega) \right) = -i\Gamma \begin{pmatrix} 1 & 2\left[1 - 2\frac{\Gamma_l f_l(\omega) + \Gamma_r f_r(\omega)}{\Gamma}\right] \\ 0 & -1 \end{pmatrix} \tag{1.15}$$

where I set $\Gamma = \Gamma_l + \Gamma_r$, $\Gamma_\nu = \pi \rho_\nu |t_\nu|^2$ and I have utilized the wide-band approximation in which one neglects the energy dependence in the density of the states of the normal metal, assuming that its characteristic energy variation is larger than the energy scales involved in the problem (temperature, bias voltages, tunnelling rates).

Incorporating Eq. (1.15) into Eq. (1.13), one obtains the exact electron Green's function of the quantum dot coupled to the two leads. This quantity plays a crucial role in the transport. For instance, one can show that the current is given by

$$I = \frac{e\Gamma}{\pi} \int d\omega \; \mathrm{Im}\left[G^R_d(\omega)\right] \;\; (f_l(\omega) - f_r(\omega)) \;, \tag{1.16}$$

with e denoting the electron charge. The equation 1.16 is known as the Meir-Wingreen formula, and it is valid if the interactions are confined in the central part of the system (the dot) with proportional coupling for the tunnelling amplitudes between the dot and the leads [53]. The effective energy-dependent transmission function appearing in Eq. (1.16) reads as

$$\mathrm{Im}\left[G^R_d(\omega)\right] = \frac{\Gamma_l \Gamma_r}{\Gamma} \frac{1}{(\omega - \varepsilon_0)^2 + \Gamma^2}\,. \tag{1.17}$$

Applying a large bias voltage $\mu_l - \mu_r = eV \gg (k_B T, \Gamma)$ and $|\mu_\nu - \varepsilon_0| \gg (k_B T, \Gamma)$, the current saturates to

$$I_{max} = e\, \frac{\Gamma_l \Gamma_r}{\Gamma_l + \Gamma_r}\,. \tag{1.18}$$

The latter result can be obtained by a simple rate equation in which one electron can tunnel into the dot from the left lead with rate Γ_l and can exit the dot to the right lead with rate Γ_r.

1.3.3 Extended Green's functions: spin degree and superconductivity

The previous example can be generalized to treat other systems with an arbitrary number of tunnelling junctions and with contacts of different types. In the general case, it is important to consider the spin degree of freedom (for example, with ferromagnetic leads) and the particle/hole nature of excitations in the leads (for example, for dots with superconducting contacts). As long as the full Hamiltonian is quadratic in the fermionic operators (in the case of the superconductor with the mean-field BCS Hamiltonian), the problem of the transport (current, noise, charge occupation, etc.) can be solved exactly: the self energies are formed by a single term, and the Dyson equations can be solved exactly.

For instance, in the case of spin-dependent transport, we must increase the dimension of the Keldysh Green's functions and consider the spin index as follows:

$$\check{g}_d^{\sigma\sigma'} = \begin{pmatrix} \check{g}_d^{\uparrow\uparrow} & \check{g}_d^{\uparrow\downarrow} \\ \check{g}_d^{\downarrow\uparrow} & \check{g}_d^{\downarrow\downarrow} \end{pmatrix} = -i \begin{pmatrix} \langle \hat{T}_c \hat{d}_\uparrow(t) \hat{d}_\uparrow^\dagger(t') \rangle & \langle \hat{T}_c \hat{d}_\uparrow(t) \hat{d}_\downarrow^\dagger(t') \rangle \\ \langle \hat{T}_c \hat{d}_\downarrow(t) \hat{d}_\uparrow^\dagger(t') \rangle & \langle \hat{T}_c \hat{d}_\downarrow(t) \hat{d}_\downarrow^\dagger(t') \rangle \end{pmatrix} \tag{1.19}$$

or simply

$$\check{g}_d^{\sigma\sigma'} = -i \left\langle \hat{T}_c \left[\begin{pmatrix} \hat{d}_\uparrow(t) \\ \hat{d}_\downarrow(t) \end{pmatrix} \left(\hat{d}_\uparrow^\dagger(t'), \hat{d}_\downarrow^\dagger(t') \right) \right] \right\rangle = -i \left\langle \hat{T}_c \, \hat{\psi}_d(t) \hat{\psi}_d^\dagger(t') \right\rangle \tag{1.20}$$

where we have introduced the spin dependent spinor $\hat{\psi}_d^\dagger = \left(\hat{d}_\uparrow^\dagger, \hat{d}_\downarrow^\dagger \right)$. Here each of the functions such as $\langle \hat{T}_c \hat{d}_\uparrow(t) \hat{d}_\uparrow^\dagger(t')$ is a matrix (the time on the upper or lower branch of the Keldysh close time contour).

In a similar way, one introduces a spinor notation to address the problem with superconducting contacts where the quasi-particle excitations are (coherent) linear combinations of the electron and hole states of the normal phase. As shown in the following sections, one of the leads can be described by the BCS Hamiltonian with the pairing potential Δ. A superconductor is characterized by the so-called anomalous averages, for instance, the Green's function $\left\langle T_c \hat{d}_\uparrow(t) \hat{d}_\downarrow(t') \right\rangle \neq 0$ does not vanish. In this case, it is useful to introduce the spinor for each individual spin channel

$$\check{G}_d^{\nu\mu} = -i \left\langle \hat{T}_c \left[\begin{pmatrix} \hat{d}_\uparrow(t) \\ \hat{d}_\downarrow^\dagger(t) \end{pmatrix} \left(\hat{d}_\uparrow^\dagger(t'), \hat{d}_\downarrow(t') \right) \right] \right\rangle = -i \left\langle \hat{T}_c \, \hat{\Psi}_d(t) \hat{\Psi}_d^\dagger(t') \right\rangle \tag{1.21}$$

where the index $\nu, \mu = e, h$ (electron-hole) and the spinor $\hat{\Psi}_d^\dagger = \left(\hat{d}_\uparrow^\dagger, \hat{d}_\downarrow \right)$.

1.3.4 Diagrams with electron-vibration interaction

Finally, in this section, we analyze the case of the quantum dot with the charge-vibration interaction. Again, I illustrate the general approach for the simplest case of a single level

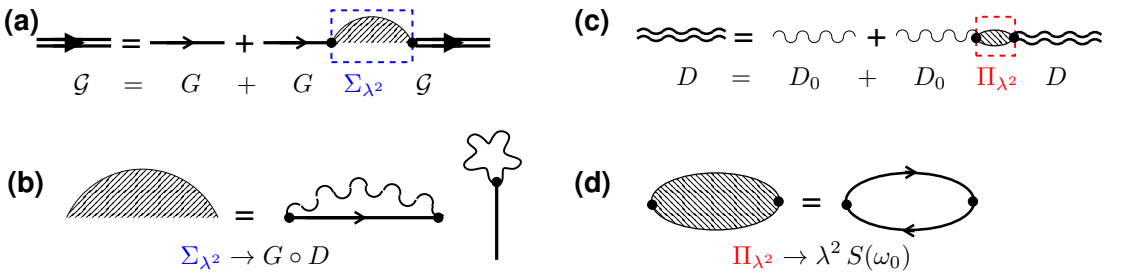

Figure 1.4: **(a)** Diagram of the Dyson equation for the renormalized electron Green's function $\mathcal{G}$ (double solid lines) in the spresence of electron-vibration interaction. **(b)** The self energy Σ is calculated to the lowest order in the coupling $\sim \lambda^2$ corresponding to the rainbow diagram and the tadpole diagram, related to the bare dot Green's function G and the bare phonon Green's function D_0 (wavy line). **(c)** Diagram of the Dyson equation for the renormalized phonon Green's function D (double wavy line). **(d)** The phonon self energy Π is calculated to the lowest order in the coupling $\sim \lambda^2$ corresponding to the bubble diagram related to the correlator of the dot's operator coupled to the resonator, see Eq. (1.36), e.g. the non-symmetrized noise.

of a dot linearly coupled to a harmonic oscillator,

$$\hat{H}_{\text{e-ph}} = \hat{H}_0 + \omega_0 \hat{b}^\dagger \hat{b} + \underbrace{\lambda\, \hat{d}^\dagger \hat{d} \quad \left(\hat{b} \;\; + \hat{b}^\dagger\right)}_{\hat{H}_{int}}, \tag{1.22}$$

with $\hat{H}_0$ given by Eq. (1.5). We now consider the Green's functions obtained for the full tunnelling problem (for instance, for the dot G_d) as the unperturbed functions. The perturbative term is $\hat{H}_{int}$. Using the perturbation expansion to the time evolution operator and applying Wick's theorem, one can write the perturbative series as a function of the coupling constant λ. Due to the pairing rule for the bosonic propagator, the non-vanishing terms are only the terms even in λ. Thus, the first leading term is of order λ^2. For example, the electron Green's function in the dot has the following form in the real time representation:

$$\begin{aligned}
\hat{\mathcal{G}}_d(t,t') &= \hat{G}_d(t,t') + \iint_{-\infty}^{+\infty} dt_1 dt_2 \;\; \hat{G}_d(t,t_1)\,\hat{\sigma}_z \;\left[\lambda^2 \hat{G}_d(t_1,t_2)\hat{D}_0(t_1,t_2)\right]\; \hat{\sigma}_z\, \hat{G}_d(t_2,t') \;\; + \ldots \\
&= \hat{G}_d(t,t') + \iint_{-\infty}^{+\infty} dt_1 dt_2 \;\; \hat{G}_d(t,t_1)\,\hat{\sigma}_z \;\left[\hat{\Sigma}^{rbw}_{\lambda^2}(t,t')\right]\; \hat{\sigma}_z\, \hat{G}_d(t_2,t') + \ldots .
\end{aligned} \tag{1.23}$$

Here, $\hat{G}_d$ still denotes the exact Green's function of the dot coupled via tunneling to the leads, whereas $\hat{D}_0$ is the bare phonon propagator. In Eq. (1.23), we write a first term that represents the electron self energy - the irreducible representation of the interacting diagram at the order λ^2. The latter quantity is given by the product of $\hat{G}_d$ with $\hat{D}_0$ and is known as the rainbow diagram. A second possible kind of diagram is the tadpole

diagram, see Fig. 1.4(b). The latter diagram corresponds physically to the average force that induces a displacement on the position of the oscillator from zero $\langle \hat{u} \rangle = 0$ to a finite value $\langle \hat{u} \rangle = \lambda^2 \langle \hat{d}^\dagger \hat{d} \, \rangle_{\lambda=0} \neq 0$. Using the perturbative expansion in the electron-vibration interaction, it is possible to show that the current can be decomposed as follows:

$$I = I^{(0)} + I^{(\lambda^2)} + \dots \,, \tag{1.24}$$

and the condition $I^{(\lambda^2)} \gg I^{(\lambda^4)}$ justifies the perturbation theory a priori.

For the phonon Green's function, the perturbation expansion leads to the following result:

$$\begin{aligned} \hat{D}(t,t') &= \hat{D}_0(t,t') + \iint_{-\infty}^{+\infty} dt_1 dt_2 \;\; \hat{D}_0(t,t_1)\, \hat{\sigma}_z \;\; \Big[\lambda^2 \hat{G}_d(t_1,t_2) \hat{G}_d(t_2,t_1)\Big] \;\; \hat{\sigma}_z \, \hat{D}_0(t_2,t') \;\; + \dots \\ &= \hat{D}_0(t,t') + \iint_{-\infty}^{+\infty} dt_1 dt_2 \;\; \hat{D}_0(t,t_1)\, \hat{\sigma}_z \;\; \Big[\hat{\Pi}_{\lambda^2}(t,t')\Big] \;\; \hat{\sigma}_z \, \hat{D}_0(t_2,t') + \dots \,. \end{aligned} \tag{1.25}$$

In this case, the leading order of the phonon self energy $\hat{\Pi}$ is given by a bubble diagram formed of two fermionic propagators forming a loop, see Fig. 1.4(c,d). This corresponds to the calculation of a Green's function with four fermionic operators, and it is indeed related to the correlator of the dot's operator coupled to the vibration, in this case the charge occupation of the single level $\langle \hat{d}^\dagger(t) \hat{d}(t) \, \hat{d}^\dagger \hat{d} \, \rangle$. Thus, the associated Dyson equation of the phonon propagator in the lowest order in λ reads as

$$\hat{D}(t,t') = \hat{D}_0(t,t') + \iint_{-\infty}^{+\infty} dt_1 dt_2 \;\; \hat{D}_0(t,t_1)\, \hat{\sigma}_z \;\; \Big[\hat{\Pi}_{\lambda^2}(t,t')\Big] \;\; \hat{\sigma}_z \, \hat{D}(t,t') \,. \tag{1.26}$$

Using the Larkin-Ovchinnikov rotation, in the frequency space, we have

$$\check{D}(\omega) = \check{D}_0(\omega) + \;\; \check{D}_0(\omega)\, \check{\Pi}_{\lambda^2}(\omega)\, \check{D}(\omega) \,. \tag{1.27}$$

We note that the phonon self energy $\check{\Pi}_{\lambda^2}$ in the triangular form, after the Larkin-Ovchinnikov rotation, is related to special combinations of the convolution products (in the frequency space) of the two electron Green's functions forming the bubble diagram.

By utilizing the electron Green's function G_d, one can obtain the phonon self energy. In this way the renormalized phonon propagator $\hat{D}$ is the solution of the Dyson equation Eq. (1.27). For example, the retarded component reads as

$$D^R(\omega) = \frac{2\omega}{\omega^2 - \omega_0^2 - 2\omega \Pi^R(\omega)} \simeq \sum_{s=\pm} \frac{1}{\omega - s\,[\omega_0 + \operatorname{Re} \Pi^R(\omega_0)] - i \operatorname{Im} \Pi^R(\omega_0)} \,, \tag{1.28}$$

where we used the symmetry of the self energy $\operatorname{Re} \Pi^R(\omega_0) = \operatorname{Re} \Pi^R(-\omega_0)$ and $\operatorname{Im} \Pi^R(\omega_0) = -\operatorname{Im} \Pi^R(-\omega_0)$. By comparison with the bare phonon propagator

$$D_0^R(\omega) = \lim_{\eta \to 0} \sum_{s=\pm} \frac{1}{\omega - s\omega_0 + i\eta} \,, \tag{1.29}$$

with η denoting an infinitesimally small (damping) constant, one can conclude that the interaction with the dot's charge results in two effects. The first one is a renormalization of the oscillator's frequency. As seen in Eq. (1.28), the real part of the retarded component of the phonon self energy renormalizes the oscillator's frequency, namely $\omega_0 \to \omega_0 + \mathrm{Re}\,\Pi^R(\omega_0)$. Hereafter, we will implicitly assume such a renormalization. The second effect is that the renormalized phonon Green's function acquires a finite imaginary part in the denominator, which corresponds to a damping of the mechanical oscillator. Hence, one defines the electro-phonon damping of the oscillator as

$$\gamma = -\mathrm{Im}\,\Pi^R(\omega_0)\,. \tag{1.30}$$

The approximated expression appearing in Eq. (1.28) that allowed us to introduce the damping γ is valid in the underdamped regime when the friction is weak enough $\gamma \ll \omega_0$, such that one approximates the phonon propagator as the sum of two Lorentzians centered at $\pm\omega_0$.

We conclude this section by reporting the result for the Keldysh component of the phonon propagator in the underdamping (Markovian) regime. One can show that

$$D^K(\omega) \simeq \sum_{s=\pm} \frac{\Pi^K(\omega_0)}{\omega - s\omega_0 + i\gamma}\,. \tag{1.31}$$

This quantity plays a special role. From it, one can obtain the nonequilibrium average phonon occupation of the quantum oscillator, namely

$$\langle \hat{b}^\dagger \hat{b} \,\rangle = \frac{i}{8\pi}\mathrm{Im}\int d\omega D^K(\omega) - \frac{1}{2} \simeq \frac{i}{4}\mathrm{Im}\left(\frac{\Pi^K(\omega_0)}{\gamma}\right) - \frac{1}{2}\,. \tag{1.32}$$

1.4 Ground state cooling by electron transport

1.4.1 Active cooling: state of the art

Active ground-state cooling was obtained in an opto-mechanical setup in which one mechanical mode of the resonator was coupled to a microwave electromagnetic cavity, using the so-called side-band method [54, 55]. The mechanism of side-band cooling is based, in a scattering picture, on the enhancement of phonon absorption due to the matching of the mechanical resonator's frequency ω_0 with the detuning between the cavity frequency and the frequency of laser pumping the cavity. Alternatively, several interesting theoretical proposals for the attainment of active cooling through electron transport have been analyzed [56–61]. I I emphasize that active cooling by pure electron transport has been experimentally achieved thus far using a superconducting single electron transistor [20]. In this section, I discuss two proposals for cooling a resonator using electron transport.

The first system is a spin-valve quantum dot with ferromagnetic nanocontacts [46]. The spin of discrete electron levels in the dot is theoretically predicted to couple to the

flexural vibrations due to the presence of an external magnetic gradient [48] or due to the mediation of the intrinsic spin-orbit interaction [49]. I combined these two ingredients and proposed the system outlined in Fig. 1.5(a,b) (articles 4 and 5 on the publications list).

The second system is a quantum dot connected to one superconducting contact and a normal metal, as shown in Fig. 1.5(c,d). In this system, for energy scales involved in the transport and smaller than the superconducting gap Δ, finite current flows via Andreev reflection (AR) in which, for instance, an incoming electron from the normal lead is reflected as a hole with the concurrent formation of a Cooper pair in the superconductor. In the presence of an interaction of the quantum dot with bosonic modes of the environment, AR can be inelastic, and experimental observations of such inelastic reflections in CNT-QD have been reported [51]. I analyzed a microscopic model of charge-vibration interaction in the QD with phonon emission or absorption in the vibration-assisted Andreev reflection (articles 2 and 3 on the publications list).

1.4.2 Electromechanical model

Quantum dots in real devices can be modeled as a single-impurity Holstein model in which one assumes a linear coupling between the electron occupation on the quantum dot and the oscillation amplitude of one or more oscillators representing the local vibrations [62–66]. Here I generalize this model and consider the following Hamiltonian:

$$\hat{H} = \sum_{\nu=l,r} \left(\hat{H}_\nu + \hat{H}_{\nu,tun} \right) + \sum_{\sigma=\uparrow,\downarrow} \varepsilon_\sigma \hat{n}_\sigma + \lambda \, \hat{F}_d \, (\hat{b} \ + \hat{b}^\dagger) + \omega_0 \, \hat{b}^\dagger \hat{b} \ , \tag{1.33}$$

where $\hat{H}_\nu$ is the Hamiltonian for the left and right lead ($\nu = l, r$) and $\hat{H}_{\nu,tun}$ is the tunnelling Hamiltonian between the dot and the lead ν. The nature of these contacts will be specified in the next two sections for two different cases. The operators $\hat{b}$ and $\hat{b}^\dagger$ are the (bosonic) creation and annihilation operators of the harmonic oscillator of frequency ω_0, and $\hat{d}_\sigma$ and $\hat{d}_\sigma^\dagger$ are the corresponding fermionic operators for the dot's levels. The coupling strength of the interaction is λ. The operator $\hat{F}_d$ is the force acting on the oscillator. We will study the case in which $\hat{F}_d$ corresponds to the x component of the local spin operator $\hat{F}_d = \hat{s}_x = \hat{d}_\uparrow^\dagger \hat{d}_\downarrow + \hat{d}_\downarrow^\dagger \hat{d}_\uparrow$ in Section 1.4.3, whereas in Section 1.4.5 we analyze the case in which $\hat{F}_d$ corresponds to the dot charge $\hat{F}_d = \hat{n}_d = \hat{d}_\uparrow^\dagger \hat{d}_\uparrow + \hat{d}_\downarrow^\dagger \hat{d}_\downarrow$.

Furthermore, we assume the weak coupling limit regime given by

$$\lambda \ll \omega_0 \, . \tag{1.34}$$

This means that the variation of the charge or the spin in the dot induces a displacement of the energy of the order of λ, which is small compared to the level separation of the harmonic oscillator. In this case, the bare levels and states of the harmonic oscillator are meaningful starting points in the presence of the electron-vibration interaction and current flowing through the dot. We focus on the sharp resonance transport regime, such that we

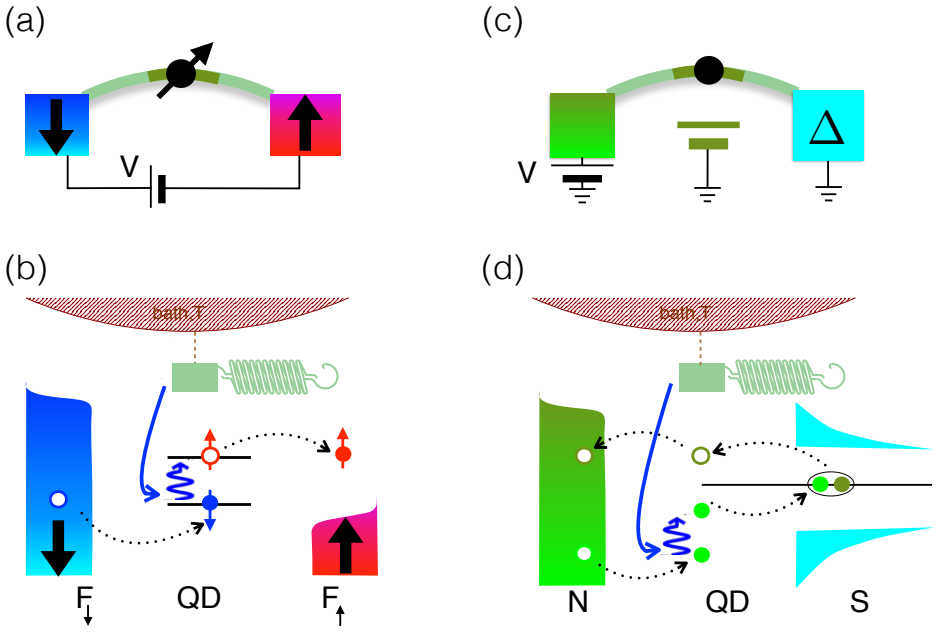

Figure 1.5: **(a)** The spin of the quantum dot states is coupled to the flexural modes of the nanotube suspended between two ferromagnetic contacts of opposite polarization. **(b)** Microscopic model of (a). The dot corresponds to two spin levels with a Zeeman splitting and a single flexural mode to an oscillator. The spin-vibration interaction leads to vibration-assisted inelastic spin-flip processes accompanied by the exchange (e.g. absorption) of energy with the oscillator. **(c)** The charge of the quantum dot states is coupled to the flexural modes of the suspended nanotube between a normal metal N and a superconductor S with gap Δ. **(d)** Microscopic model of (c). The dot corresponds to two spin-degenerate levels and a single flexural mode to an oscillator. At bias voltage V smaller than the superconducting gap, the charge-vibration interaction leads to vibration-assisted inelastic Andreev reflections accompanied by the exchange (e.g. absorption) of energy with the oscillator.

also require another condition for the typical tunneling rate Γ controlling the hopping of the electrons from the leads to the dot:

$$\Gamma \ll \omega_0 \,. \tag{1.35}$$

Because the inverse of the tunneling rate $\hbar/\Gamma$ is related to the dwell time of the electron in the dot, the latter condition is known as the anti-adiabatic limit.

Assuming weak coupling and the anti-adiabatic limit, we calculate two important quantities: the nonequilibrium occupancy of the harmonic oscillator $\bar{n}_c$ and the inelastic current through to the dot I_{in} due to the electron- vibration interaction in the leading order of λ^2. These quantities have been computed in articles 2-5 on the publications list using the Keldysh Green's function technique and for arbitrary ranges of other transport parameters. Here, I introduce a simple heuristic approach to derive these quantities, focusing on

specific transport regimes to emphasize the underlying mechanism of cooling via electron transport.

When a voltage bias is applied, the electrons tunneling through quantum dot behave as an effective environment characterized by an electromechanical damping γ and a force noise acting on the oscillator. Then the crucial quantity is the unperturbed, non-symmetrized noise of the electron force operator (charge or spin) of the dot

$$S(\omega) = \int_{-\infty}^{+\infty} dt\, e^{i\omega t} \langle \hat{F}_d(t)\hat{F}_d(0)\rangle_{\lambda=0}\,, \tag{1.36}$$

with $\langle \dots \rangle_{\lambda=0}$ denoting the quantum statistical average taken over the electron system for $\lambda = 0$. Using $S(\omega)$, it is possible to show that the electromechanical damping reads as

$$\gamma = \lambda^2 \left[S(\omega_0) - S(-\omega_0)\right] \equiv \gamma_+ - \gamma_-\,. \tag{1.37}$$

Indeed, the absorption of an energy quantum ω_0 is connected to the intrinsic non-symmetrized noise at the positive frequency of the open dot (non-interacting with the vibration), whereas the emission of an energy quantum ω_0 is connected to the non-symmetrized noise at the negative frequency. A simple way to understand the relationship between the non-symmetrized noise and the probability of absorption or emission of a phonon of energy ω_0 is based on Fermi's Golden rule. For the probability per unit time of one phonon absorption (+) or emission (−), the Golden rule gives us

$$p_\pm = 2\pi \sum_n \sum_{i,f} P_n\, P_i \left|\langle n \mp 1, \psi_f|\, \hat{H}_{int}\, |n, \psi_i\rangle\right|^2 \delta\left[\omega_0 \pm (E_i - E_f)\right]\,, \tag{1.38}$$

where ψ_i and ψ_f are the initial and final states of the open dot, with energies E_i and E_f, and P_i is the probability of occupation of the initial state, whereas P_n is the probability of occupation of the Fock state $|n\rangle$. Using the integral representation for the δ-function and the interaction $\hat{H}_{int} = \lambda \hat{F}_d(\hat{b} + \hat{b}^\dagger)$, one obtains for the case of absorption

$$p_+ = \lambda^2 \sum_n nP_n \sum_{i,f} P_i\, \langle\psi_i|\, \hat{F}_d\, |\psi_f\rangle \langle\psi_f|\, \hat{F}_d\, |\psi_i\rangle \int_{-\infty}^{+\infty} dt\, e^{i\left[\omega_0 + E_i - E_f\right]t} \tag{1.39}$$

$$= \lambda^2 \bar{n} \int_{-\infty}^{+\infty} dt\, e^{i\omega_0 t} \Big\langle \hat{F}_d(t)\hat{F}_d(0)\Big\rangle_{\lambda=0} = \bar{n}\ \gamma_+\,, \tag{1.40}$$

in which I have used the completeness of the dot's states and $\bar{n} = \sum_n nP_n$. A similar calculation for the emission of one phonon leads to

$$p_- = (\bar{n} + 1)\ \gamma_-\,. \tag{1.41}$$

In order to calculate the steady-state nonequilibrium occupation n due to the charge-vibration interaction, we neglect in a first approximation the thermal bath and use a phenomenological equation rate

$$0 = \frac{d\bar{n}}{dt} = \bar{n}\gamma_+ - (\bar{n} + 1)\,\gamma_- \longrightarrow \bar{n} = \frac{\gamma_-}{\gamma_+ - \gamma_-} \equiv \bar{n}_c\,. \tag{1.42}$$

The result for n in Eq. (1.42) clearly indicates that ground state cooling with $\bar{n}_c \ll 1$ can be achieved for $\gamma_+ \gg \gamma_-$. In other words, one must create a strong asymmetry between the two processes in order to cool the oscillator. Hereafter, we call the coefficients $\gamma_\pm$ the *intrinsic* rates or simply *rates for the phonon emission and absorption*, since they are a property of the intrinsic system without the interaction with the resonator.

One can generalize Eq. (1.42) by taking into account the (unavoidable) interaction of the oscillator with a thermal bath with an intrinsic damping rate γ_0. Then, the general steady occupation of the oscillator is given by the competition between the interaction of the oscillator with the effective environment - the quantum dot - and the thermal bath

$$\bar{n} = \frac{\gamma\,\bar{n}_c\, + \gamma_0\, n_B}{\gamma + \gamma_0}\,, \tag{1.43}$$

with n_B denoting the Bose distribution at frequency ω_0 and temperature T. Thus, ground state cooling $\bar{n} \ll 1$ also requires that the electromechanical damping dominates over the intrinsic damping $\gamma_0\, n_B \ll \gamma\, \bar{n}_c$. The latter inequality means that $\gamma_0/\gamma \ll \bar{n}_c/n_B \ll 1$ which is a realistic condition for suspended CNT-QD characterized by huge quality factors $Q_0 = \omega_0/\gamma_0 \sim 10^6$.

Finally, I conclude this section by summarizing the result for the inelastic current associated with the electron-vibration interaction. This current results from vibration-assisted tunnelilng processes in which an electron hops from a lead to the dot, s exchanging energy with the oscillator. Both phonon emission and phonon absorption make a contribution to the inelastic current. Hence, based on the discussion in the previous section, one would intuitively expect the following expression for the inelastic current:

$$I_{in} = \, q^* \, [\, \gamma_- \, (\bar{n} + 1) \, + \, \gamma_+ \bar{n} \,] \, . \tag{1.44}$$

In Section 1.4.3, I discuss the result for the case of a quantum dot coupled to the vibration via the dot's spin, $\hat{F}_d = \hat{s}_x$. In this case, for the fully spin-polarized electrons in the ferromagnetic leads and in the limit of large applied voltage V, the inelastic current indeed takes the form given by Eq. (1.44) with $q^* = e$. Similarly, in Section 1.4.5, I discuss the case of a quantum dot coupled to the vibration via the dot's charge, $\hat{F}_d = \hat{n}_d$. Again, in the regime of subgap transport in which the current is mainly determined by Andreev reflections and in the limit of large applied voltage V (but still $eV \ll \Delta$ with Δ denoting the superconducting gap), the inelastic current reduces to Eq. (1.44) with $q^* = 2e$ since two electrons are involved in the current in order to form a Cooper pair in the superconductor.

1.4.3 Spin-vibration interaction and inelastic spin-flip tunneling

Hereafter, we focus on the range of parameters around the cross point of the two spin levels (see articles 4 and 5). In this case, the quantum dot is described by two spin levels with an effective Zeeman splitting $\Delta\varepsilon_z = \varepsilon_\uparrow - \varepsilon_\downarrow$ which is tunable by a uniform field B_z,

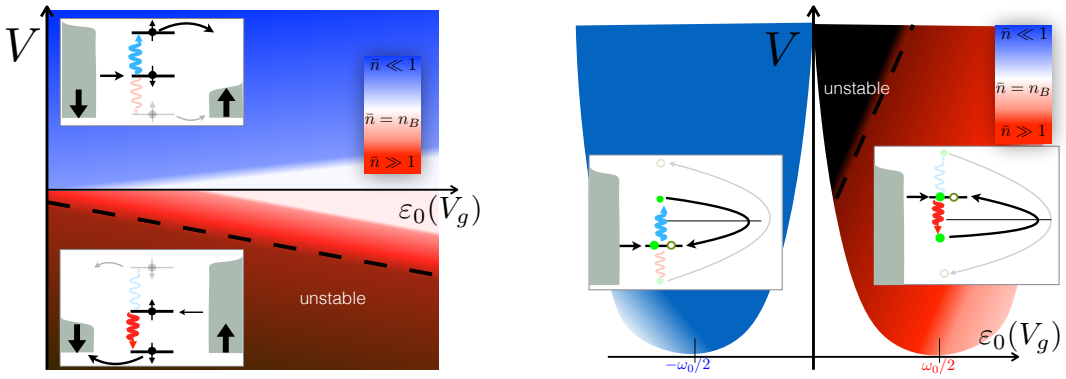

Figure 1.6: Schematic picture of the average phonon occupancy as a function of the bias voltage V and the average dot's energy ε_0 (controlled by a gate voltage V_g). **Left:** In the nanomechanical spin-valve, the figure represents the case of fully polarized leads at the resonance $\omega_0 = \Delta\varepsilon_z$. At fixed configuration of the Zeeman splitting in the dot and polarization of the leads, the phonon absorption is enhanced at positive voltage (see text). At the negative voltage, the opposite regime occurs. **Right:** In the system with a superconducting lead, at positive high voltage (see text), the Andreev reflections are essentially given by incoming electrons from the normal lead to the dot. The phonon absorption is enhanced when the reflected hole appears at the same energy of the incoming electron (see text). This is possible if, for example, the electron enters the dot at energy $\varepsilon_0 = -\omega_0/2$, such that it enters the superconductor at energy $\varepsilon_e = \omega_0/2$ after the absorption of a phonon. Then, the hole is reflected at energy $\varepsilon_h = -\omega_0/2$. The opposite regime occurs when the electron enters the dot at energy $\varepsilon_0 = \omega_0/2$.

namely

$$\sum_{\sigma=\uparrow,\downarrow} \varepsilon_\sigma \hat{n}_\sigma = \sum_{\sigma=\uparrow,\downarrow} \left(\varepsilon_0 + \sigma \frac{\Delta\varepsilon_z}{2}\right) \hat{d}^\dagger_\sigma \hat{d}_\sigma \,, \tag{1.45}$$

and the average energy $\varepsilon_0 = (\varepsilon_\uparrow + \varepsilon_\downarrow)/2$. To model the spin-valve CNT-QD embedded between ferromagnetic leads and to simplify the discussion, I restrict the analysis to the case of fully polarized leads such that we can identify $\alpha = l \leftrightarrow \sigma = \downarrow$ and $\beta = r \leftrightarrow \sigma = \uparrow$ in the Hamiltonian

$$\sum_{\nu=l,r} \left(\hat{H}_\nu + \hat{H}_{\nu,tun}\right) = \sum_{\sigma=\uparrow,\downarrow} \sum_k \left[\varepsilon_{k\sigma} \hat{c}^\dagger_{k\sigma} \hat{c}_{k\sigma} + t_\sigma \hat{c}^\dagger_{k\sigma} \hat{d}_\sigma + t^*_\sigma \, \hat{d}^\dagger_\sigma \hat{c}_{k\sigma}\right] . \tag{1.46}$$

I also assume symmetric contacts such that the tunneling rates $\Gamma^\uparrow_l = \Gamma^\downarrow_r = \Gamma$. In simple terms, for fully polarized leads, the current can flow through the system only if the spin is flipped when the electrons pass through the dot. This process occurs inelastically with the absorption or the emission of one single phonon (weak coupling regime). Basically, the system acts as a nanomechanical spin-valve in which spin-polarized electrons tunnelling through the dot's levels can exchange energy with the oscillator by flipping their spins.

At large bias voltage V compared to the other energies (temperature T, the tunnelling rate Γ and the separation of the energy spin level ε_σ from the chemical potentials) the electrons practically flow from the left to the right, as shown in the upper inset of Fig. 1.6(a). In the electromechanical damping $\gamma = \gamma_+ - \gamma_-$, the coefficients $\gamma_\pm$ correspond to the rates for vibration-assisted inelastic processes in which a spin flip occurs for one electron tunneling from the left lead to the right accompanied by the absorption ($s = +$) or emission ($s = -$) of a vibrational energy quantum ω_0

$$\gamma_\pm = \lambda^2\Gamma^2 \int d\omega \; T_\pm(\omega) \; f_l(\omega)\,[1-f_r(\omega \pm \omega_0)] \simeq \lambda^2\Gamma^2 \int d\omega \; T_\pm(\omega) \;\; , \tag{1.47}$$

where $f_{l,r}(\omega) = 1/\{1 + \exp[(\omega - \mu_{l,r})/T]\}$ the Fermi functions of the lead, $\mu_l - \mu_r = eV$ (approximately $f_l(\omega) \simeq 1$ and $f_r(\omega) \simeq 0$ for high voltage), whereas the transmission functions are given by

$$T_\pm(\omega) = \frac{1}{\pi} \frac{\Gamma^2}{[\Gamma^2 + (\omega - \varepsilon_\downarrow)^2]} \frac{\Gamma^2}{[\Gamma^2 + (\omega + s\omega_0 - \varepsilon_\uparrow)^2]} \, . \tag{1.48}$$

The equation 1.47 can be evaluated analytically. We report the result for the resonance case $\varepsilon_\uparrow - \varepsilon_\downarrow = \omega_0$, which reads as

$$\gamma_+ = \frac{\lambda^2}{2\Gamma} \, , \qquad \gamma_- = \gamma_+ \frac{\Gamma^2}{\Gamma^2 + \omega_0^2} \simeq \gamma_+ \left(\frac{\Gamma}{\omega_0}\right)^2 , \tag{1.49}$$

from which we extract the minimum values of the phonon occupations that can be achieved, namely $n_{min} \simeq \gamma_-/\gamma_+ = (\Gamma/\omega_0)^2$. The situation changes at negative voltage, where we find a region of increase for the phonon occupation $n \gg 1$ for $\gamma_+ \gtrsim \gamma_-$ and an instability region when $\gamma_+ < \gamma_-$. These two regions are beyond the validity of the perturbative approach, and the phase diagram represents only a qualitative description.

The results of Eqs. (1.47,1.48,1.49) enlighten the ultimate mechanism for the cooling. The two Lorentzian functions in the integral of Eq. (1.47) completely overlap for the case of the absorption rate $s = +$ in the cooling region. In other words, the inelastic spin-flip occurs through the two peaked spin levels of the dot's density of states. Conversely, in the case of emission $s = -$, the two Lorentzian functions in the integral of Eq. (1.47) are well separated: phonon emission is still possible but arises through only one peak associated with the spin down, whereas the passage through the spin up can be seen as a cotunnelling process (a virtual occupation of the level) whose amplitude scales as $\sim (\Gamma/\omega_0)^2 \ll 1$.

The behavior of the inelastic current is intuitively understandable in the limit case in which the oscillator is strongly affected by the quantum dots and the steady-state phonon occupation saturates to $\bar{n} \simeq \bar{n}_c$. In this regime, the current clearly reflects the behavior of the phonon occupancy. At large positive voltage, in the cooling regime, we have $\bar{n}_c \ll 1$ and $\gamma_- \ll \gamma_+$

$$I_{in}^{eV>0} \simeq e\gamma_- = I_0 \left(\frac{\lambda^2}{2\omega_0^2}\right) \tag{1.50}$$

with $I_0 = e\Gamma$. In the cooling regime, the inelastic current is strongly suppressed with respect to the elastic current. At negative voltage with $\gamma_+ \gtrsim \gamma_-$ we have $\bar{n}_c > 1$ such that we can approximate

$$I_{in}^{eV<0} \simeq e\,\gamma\,\bar{n}_c\,. \tag{1.51}$$

Because the phonon occupation scales as $\bar{n}_c \sim \gamma_-/(\gamma_+ - \gamma_-)$, it increases indefinitely as long as $\gamma_+ \to \gamma_-$ until the instability line $\gamma_+ - \gamma_- = 0$. In summary, a strong asymmetry emerges in the inelastic current that reflects the behavior of the nonequilibrium average phonon occupation $\bar{n}_c$.

1.4.4 Andreev reflection: qualitative picture

Before discussing the quantum dot with charge vibration, I review the quantum transport occurring at the interface between a normal metal and a superconductor and, in particular, when a quantum dot is embedded between these two different contacts.

In discussing the current through the system, one must start by considering the probability of tunneling of electrons and holes from the normal metal to the superconductor. In the system with normal-superconductor interfaces, one distinguishes between two different mechanisms of transport.

The first mechanism is based on the semiconducting model, and it is associated with the quasi-particle excitations. A single electron excitation of energy higher than the gap $\varepsilon - \mu_S > \Delta$, with Δ denoting the superconducting gap and μ_S the chemical potential of the superconductor, can in principle tunnel into the superconductor, with some transmission probability related to the details of the barrier at the interface. At the same level, a hole excitation of energy $\mu_S - \varepsilon > \Delta$ in the normal metal can tunnel into the superconductor. At small but finite temperature $k_BT \ll \Delta$, viz. electrons and holes are present in the normal metal above and below the chemical potential, the net charge current is zero when the chemical of the normal metal equals that of the superconductor $\mu_N = \mu_S$. By applying a finite voltage, for instance $\mu_N = eV + \mu_S$, one creates an asymmetry in the flux and a net charge current flows through the interface. This description is similar to the tunneling of one electron from a metal to a (gapped) semiconductor. As a consequence, in the limit of $k_BT \to 0$, the current can flow only if the particle excitations have enough energy, namely for applied voltage $|eV| > \Delta$. This leads to a sharp feature in the I vs V characteristic. In the limit $T \to 0$ and $|eV| < \Delta$, no current is expected according to this scenario.

In the latter regime, known as sub-gap regime $eV \ll \Delta$, the second mechanism of transport occurs: the Andreev reflection (AR). This leads to a substantial current at the interface between a superconductor and a normal conductor.

The basis of such processes lies in the impossibility of electrons from the normal region of penetrating into the superconductor due to the energy gap formed in the latter: in order to enter into the superconducting condensate (formed by Cooper pairs), another electron must be picked up from the normal metal, leaving a (reflected) hole in it. Simply put, the AR corresponds to an effective injection of two electrons of opposite spin into the superconductor at the chemical potential μ_S. When we consider a quantum dot with two

spin-degenerate levels, the net effect is that this process is characterized by an effective energy-dependent transmission function for the two electrons entering the superconductor.

The model Hamiltonian for the normal lead and the superconductor with the tunnelling to the quantum dot reads as

$$\sum_{\nu=N,S}\left[\hat{H}_\nu+\hat{H}_{\nu,tun}\right]=\sum_{\nu=N,S}\sum_{\sigma,k}\left[\frac{1}{2}\left(\varepsilon_{k\sigma}-\mu_\nu\right)\hat{c}^\dagger_{k\sigma\nu}\hat{c}_{k\sigma\nu}+t_\nu\hat{c}^\dagger_{k\sigma\nu}\hat{d}_\sigma+\delta_{\nu S}\Delta\hat{c}^\dagger_{-k\downarrow}\hat{c}^\dagger_{k\uparrow}+\text{h.c.}\right]. \tag{1.52}$$

The superconducting lead $\nu = S$ is described by the mean-field BCS Hamiltonian with the superconducting pairing Δ. The dot is formed by a spin degenerate level

$$\sum_{\sigma=\uparrow,\downarrow}\varepsilon_\sigma\hat{n}_\sigma=\varepsilon_0\sum_{\sigma=\uparrow,\downarrow}\hat{d}^\dagger_\sigma\hat{d}_\sigma\,. \tag{1.53}$$

The Hamiltonian is quadratic in the fermionic field and the Green's functions can be solved exactly by generalizing the formalism of the Keldysh Green's functions with the use of the spinor for the electron and hole excitations, as explained in the previous section. Hereafter, we primarily focus on the strong subgap regime defined by the condition that the gap is the largest energy scale in the problem. In this case, the transport through the system is captured by the effective low energy Hamiltonian,

$$\hat{H}_S+\hat{H}_{S,tun}+\varepsilon_0\sum_{\sigma=\uparrow,\downarrow}\hat{d}^\dagger_\sigma\hat{d}_\sigma\;\longrightarrow\;\hat{H}_{dS}=\varepsilon_0\sum_{\sigma=\uparrow,\downarrow}\hat{d}^\dagger_\sigma\hat{d}_\sigma-\Gamma_S\left(\hat{d}^\dagger_\uparrow\hat{d}^\dagger_\downarrow+\hat{d}_\downarrow\hat{d}_\uparrow.\right) \tag{1.54}$$

Here, the parameter Γ_S is given by $\Gamma_S=\pi\rho|t_S|^2$ - with ρ the density of state of the superconducting lead in the normal phase. Above the critical temperature, the superconductor behaves as a normal metal and the parameter Γ_S corresponds to the tunnelling rate between the lead and the dot. However, in the superconducting phase and in the large superconducting gap limit defined by Eq. (1.54), the parameter Γ_S plays the role of coupling strength for the intradot pairing due to the proximity to the superconductor.
One can compute the Green's functions and calculate the current through the system (at the normal lead). The result for this subgap current is given by

$$I_{AR}=e\int\frac{d\omega}{2\pi}\;\mathrm{T}_{AR}(\omega)\;\Big[f_e(\omega)\left(1-f_h(\omega)\right)-f_h(\omega)\left(1-f_e(\omega)\right)\Big], \tag{1.55}$$

with $f_e(\omega)=\left(1+\exp[\frac{\omega-\mu_S-eV}{k_BT}]\right)^{-1}$ as the conventional Fermi function and $f_h(\omega)=1-f_e(-\omega)$ as the *hole* distribution. Hereafter, I set the chemical potential of the superconductor $\mu_S=0$. The transmission function for the AR is

$$\mathrm{T}_{AR}(\omega)=\frac{8\Gamma_N^2\Gamma_S^2}{\left|\left(\omega-\varepsilon_0+i\Gamma_N\right)\left(\omega+\varepsilon_0+i\Gamma_N\right)-\Gamma_S^2\right|^2}=\frac{8\Gamma_N^2\Gamma_S^2}{\left|\omega^2-E_A^2-\Gamma_N^2+2i\omega\Gamma_N\right|^2}, \tag{1.56}$$

with the Andreev energy defined as $E_A^2=\varepsilon_0^2+\Gamma_S^2$. In the large gap limit (neglecting the tunnelling with the normal lead), the eigenstates of the Hamiltonian $\hat{H}_{dS}$ are given by the

singly occupied states of the dot (spin up and down) and the coherent superposition of the double occupied state (singlet) and the vacuum with energy $\pm E_A$.

In the limit of high voltage $eV \gg \Gamma_S, \Gamma_N, |\varepsilon_0|, k_B T$ (but still $eV \ll \Delta$), we find that the electronic states are all occupied in the normal lead $f_e(\omega) \simeq 1$, which means that the hole state are all empty $f_h(\omega) \simeq 0$. By integrating Eq. (1.57) within this approximation, one obtains

$$I_{AR} = \frac{e\Gamma_N \Gamma_S^2}{E_A^2 + \Gamma_N^2} \simeq \frac{e\Gamma_N \Gamma_S^2}{\varepsilon_0^2 + \Gamma_S^2}\,, \tag{1.57}$$

where the approximated expression is valid for $\Gamma_N \ll \Gamma_S$. The result Eq. (1.57) can be again obtained via a rate equation in which one assumes the dot is coherently pumped in the singlet state (doubly occupied) - coupled to the vacuum - that eventually decays into a single occupied state [67].

1.4.5 Charge-vibration interaction and inelastic Andreev reflection

The model Hamiltonian for a superconductor/normal metal quantum dot was introduced in the previous section. In the strong subgap regime, defined by the condition that the gap Δ is the largest energy scale in the problem, the charge transport through the quantum dot occurs via AR, whose transmission amplitude is independent of Δ. In this case, the relevant quantities are the tunnelling rates from the normal lead to the dot Γ_N and the parameter Γ_S.

An electron at energy much lower than the energy gap and tunnelling on the quantum dot from the normal metal can be either inelastically reflected as electron (normal reflection, NR) or inelastically reflected as hole (Andreev reflection, AR). Thus the electromechanical damping is associated with these two inelastic processes $\gamma = \gamma_{NR} + \gamma_{AR}$. However, the normal reflection can drive the oscillator only to the thermal equilibrium: in these processes, the oscillator sees only one fermionic reservoir at a unique temperature T. Hence, inelastic normal reflection forms an additional mechanism of normal damping, and γ_{NR} sums up to the intrinsic damping γ_0. By contrast, the inelastic ARs can drive the resonator towards a nonequilibrium steady state. From now on, we focus on the inelastic Andreev reflection processes. sConsidering the high voltage limit (but still $eV \ll \Delta$), the current is given by the impinging electrons that are reflected as holes. Then, the emission/absorption rates read as

$$\gamma_\pm = s\lambda^2 \int d\omega\; T_\pm(\omega)\; f_e(\omega)\,[1 - f_h(\omega \pm \omega_0)] \simeq \lambda^2\,\Gamma_N^2 \int d\omega\; T_\pm(\omega)\;, \tag{1.58}$$

where the transmission function for the inelastic Andreev reflection is

$$T_\pm(\omega) = \frac{\Gamma_N^2}{4\pi} |G_e(\omega)\, F^*(\omega + s\omega_0) - F(\omega)\, G_h^*(\omega + s\omega_0)|^2\,, \tag{1.59}$$

and the Green's functions are defined as

$$G_{e/h}(\omega) = G_{+/-} = \frac{\omega \pm \varepsilon_0 + i\Gamma_N}{(\omega + \varepsilon_0 + i\Gamma_N)(\omega - \varepsilon_0 + i\Gamma_N) - \Gamma_S^2}, \tag{1.60}$$

$$F(\omega) = \frac{\Gamma_S}{(\omega + \varepsilon_0 + i\Gamma_N)(\omega - \varepsilon_0 + i\Gamma_N) - \Gamma_S^2}. \tag{1.61}$$

As shown in the previous section, the quantity $\sim \Gamma_N^2 |F(\omega)|^2$ plays the role of transmission function in the formula for the elastic current associated with ARs through the dot (for instance, an incoming electron at energy ω). Thus one can regard it as the effective amplitude for the AR. The other two functions $G_{e/h}(\omega)$ are the electron and hole Green's functions of the dot in tunneling contact with the superconductor, and they play the role of transmission functions of the tunnelling electron (for instance, an incoming electron at energy ω), in the limit case $\Gamma_S \ll \Gamma_N$. In other words, the transmission function Eq. (1.59) consists of a coherent sum of two amplitudes that are associated with the two possible paths in which the phonon is emitted or absorbed before or after an AR. The integral of the transmission function in the last term of Eq. (1.58) can be computed analytically and, at $\varepsilon_0 = -\omega_0/2$, it reads as

$$\gamma_+ = \Lambda \Gamma_N^2, \tag{1.62}$$

$$\gamma_- = \Lambda \left[\frac{\omega_0^2}{4} + \Gamma_N^2 \right], \tag{1.63}$$

with

$$\Lambda = \frac{\lambda^2 \Gamma_S^2 \Gamma_N \left(E_A^2 + \frac{\omega_0^2}{4} + 5\Gamma_N^2 \right)}{\left(E_A^2 + \Gamma_N^2 \right) \left(\frac{\omega_0^2}{4} + \Gamma_N^2 \right) \left[(\omega_0/2 - E_A)^2 + \Gamma_N^2 \right] \left[(\omega_0/2 + E_A)^2 + \Gamma_N^2 \right]}. \tag{1.64}$$

Remarkably, the rate for phonon emission is strongly suppressed such that the resonator approaches the ground state with minimum phonon occupation $n_{min} = \gamma_-/\gamma_+ \propto (\Gamma_N/\omega_0)^2$, see Fig. 1.6(b). At the symmetric point $\varepsilon_0 = \omega_0/2$, the rate for phonon absorption is strongly reduced, and we are in the full region of instability $\gamma_+ \ll \gamma_-$, see Fig. 1.6(b). The final result found in Eqs. (1.62, 1.63) is a consequence of the form of the transmission function Eq. (1.59). In other words, ground state cooling is achieved due to the destructive interference of the two amplitudes associated with the charge transmission with phonon emission.

With regards to the system discussed above, I show the behavior of the inelastic current in the limit case in which the oscillator is strongly affected by the quantum dots and the steady-state phonon occupation saturates to $\bar{n} \simeq \bar{n}_c$. In contrast to the system discussed in Section 1.4.3, the current has a sharp dependence on the dot's energy levels ε_0. I give an example assuming the case $\Gamma_S \ll |\varepsilon_0|, \omega_0$ and $|\varepsilon_0| \approx \omega_0/2$. In the cooling regime,

with $\varepsilon_0 < 0$, we have $\bar{n}_c \ll 1$ and $\gamma_- \ll \gamma_+$, and we can approximate $I_{in} \simeq 2\,e\,\gamma_-$. For $\varepsilon_0 \approx -\omega_0/2$, the inelastic current shows a peak

$$I_{in}\left(\varepsilon_0 \approx -\omega_0/2\right) = I_{in}^{-} \simeq 2e\frac{8\lambda^2\Gamma_S^2\Gamma_N^3}{\omega_0^4\left[\left(\varepsilon_0+\omega_0/2\right)^2+\Gamma_N^2\right]}\,. \tag{1.65}$$

In the regime $\varepsilon_0 > 0$ with $\gamma_+ \gtrsim \gamma_-$ we have $\bar{n}_c > 1$, such that we can approximate $I_{in} \simeq 2e\gamma\bar{n}_c$. Close to $\varepsilon_0 \approx \omega_0/2$ (but far away from the instability region), we can approximate the peak of the inelastic current as

$$I_{in}\left(\varepsilon_0 \approx \omega_0/2\right) = I_{in}^{+} \simeq 2e\frac{8\lambda^2\Gamma_S^2\Gamma_N^3}{\omega_0^4\left[\left(\varepsilon_0-\omega_0/2\right)^2+\Gamma_N^2\right]}\left(\frac{\bar{n}_c(\omega_0/2)}{n_{min}}\right)\,. \tag{1.66}$$

In a such nonequilibrium regime of the oscillator, the peak around $\varepsilon_0 \approx \omega_0/2$ is higher than the peak at $\varepsilon_0 \approx -\omega_0/2$ since the first peak is enhanced by the phonon occupation $\bar{n}_c(\omega_0/2) > 1$ and by the factor $(1/n_{min}) \gg 1$. s

To summarize, in the case of a quantum dot with charge-vibration interaction inducing inelastic Andreev reflections, the effect of the coupling with the resonator appears in the sub-gap transport as sharp, vibrational side-band peaks that are not broadened by the temperature of the normal leads. Then, the strong asymmetry of these two peaks clearly indicates the nonequilibrium state of the oscillator.

1.5 Quantum nanomechanical interferometer

In articles 6 and 7 on the publications list, I studied a nanoresonator with a magnetic electron-vibration coupling operating as a quantum nanomechanical interferometer, in which interference emerges in the electron transport due to the quantum nature of the resonator.

As mentioned above, NEMS are interesting for fundamental research because they can approach the quantum regime at low temperature. A central question is how we can detect quantum states of these mechanical nanoresonators. To address this issue, I studied a model of a nanoelectromechanical system that allows the determination of the quantum nature of the resonator's state by transport measurements. Specifically, I studied the magneto-conductance of the suspended CNT-QD oscillating in the presence of a magnetic field perpendicular to the axis of the nanotube. In the following section, I will explain how this system can readily be used to probe the quantum fluctuations of a suspended vibrating nanotube.

1.5.1 Aharonov-Bohm effect and qualitative description

In this section, I provide a qualitative picture of the quantum nano-mechanical interferometer based on the Aharonov-Bohm effect.

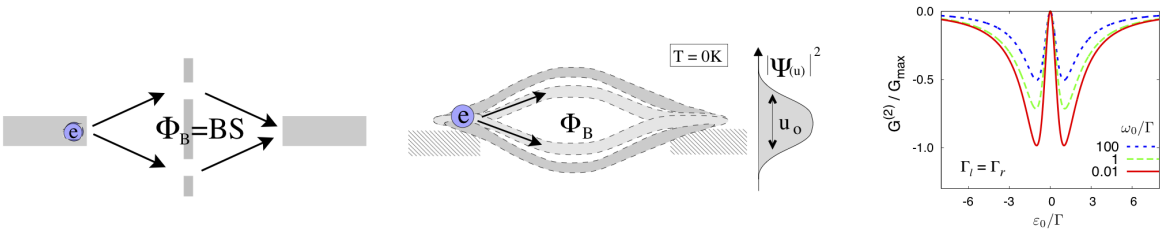

Figure 1.7: Schematic figures to illustrate the quantum nanomechanical interferometer. **Left:** For an electron passing through the two-slit barrier, interference occurs as varying an externally (perpendicular) applied magnetic field B. Interference arises from the fact that the two possible paths have a phase difference proportional to the magnetic flux enclosed by the two paths $\Phi_B = BS$ with S the surface. This is known as the Aharonov-Bohm effect, and the phase difference is given by $\delta\varphi = \Phi_B/\Phi_0$, with $\Phi_0 = h/e$ denoting the flux quantum. **Center:** Vibrating nanotube in the quantum (delocalized) ground state. Starting from the left contact, an electron can arrive at the opposite side by traveling through different paths that eventually interfere as a result of an applied magnetic field. These paths are associated with the probability of finding the fundamental mode of the nanotube at some amplitude, namely the square modulus of the wavefunction $|\Psi(u)|^2$. The latter extends over a length scale of $u_0 \sim (1/m\omega_0)^{1/2}$ (zero-point fluctuations). The net effect is a magneto-conductance $G^{(2)}$ (see text). **Right:** Example of the magneto-conductance $G^{(2)}$ scaled with $G_{max} = 4e^2/h$ at zero temperature and for different values of ω_0/Γ (here, $\Gamma = \Gamma_l = \Gamma_r$) as varying the dot's level ε_0 (viz. the gate voltage). Note that the total conductance is given by $G = G_0 + \phi^2 G^{(2)}$, with $\phi < 1$ (see text).

This effect is a variant of the double slit experiment that is used to illustrate the particle-wave duality in quantum mechanics. For an electron moving in free space through the two-slit barrier, interference appears on the detecting screen at different positions. Alternatively, at a fixed position, one again observes interference fringes as varying an externally applied magnetic field B, perpendicular to the plane of the motion. One can control the interference of two electron paths only via the applied magnetic field, when an electron propagates in a multiply connected region.

In nanoscale devices, the electron trajectories can be efficiently confined in space. In mesoscopic nanoconductors, such as nanorings, the Aharonov-Bohm effect can manifest as a periodic magnetic flux dependence of the conductance of an electron moving from one lead to the opposite lead attached to the ring. In this case, the electron, with the same start and end points, travels along two different routes. Then, the transmission amplitude is given by the sum of $t_{up} + t_{lw}$, with t_{up} representing the transmission via the upper path/branch of the ring and t_{lw} for the lower path. The overall transmission probability is obtained as the square of the sum $|t_{up} + t_{lw}|^2 = |t_{up}|^2 + |t_{lw}|^2 + 2|t_{up}||t_{lw}|\cos\phi$, with ϕ denoting the phase difference between the upper and lower branches. Applying a magnetic flux leads to an additional phase accumulated when the electron propagates through the two arms. One can write the overall transmission probability as $\left|t_{up}e^{i\frac{\delta\varphi}{2}} + t_{lw}e^{-i\frac{\delta\varphi}{2}}\right|^2$ with

$\delta\varphi = \Phi_B/\Phi_0$, denoting Φ_B the magnetic flux threading the loop and $\Phi_0 = h/e$ the flux quantum. If the ring thickness is assumed to be very thin compared to the diameter, the areas enclosed by the outer and inner circumferences are approximatively the same. We then have a well-defined single flux. The linear conductance of the system is related to the transmission probability from left to right and, in the ideal symmetric case, one expects - for weak transmission - $G(B) = G(0)\left|e^{i\frac{\delta\varphi}{2}} + e^{-i\frac{\delta\varphi}{2}}\right|^2$; that is the conductance oscillates with the magnetic field (or the flux) with a single period given by Φ_0.

We now consider the propagation of the electron through a conducting, free-oscillating carbon nanotube suspended between two electrical contacts and hosting a quantum dot. If we view the conducting nanotube as a classical object (almost at rest in the limit of vanishing temperature), then no AB effect can occur in the system, since we have a single trajectory. Remarkably, an AB effect arises if the suspended nanowire behaves properly as a quantum object. In this case, the mechanical ground state is a quantum superposition of displaced oscillator states. When an electron crosses the device, its wavefunction acquires an Aharonov-Bohm phase that depends on the position of the displaced oscillator. The total transmission results from the interference of all electronic trajectories associated with the quantum delocalization of the suspended wire. Assuming that the linear conductance is related to a single event of transmission from left to right, in analogy to the formula of the magneto-conductance of the AB-ring, one would expect

$$G_{AB} = G_t^{(0)}\left|\sum_{u(path)} P_u e^{i\frac{gBLu}{\Phi_0}}\right|^2 \longrightarrow G_t^{(0)}\left|\int du|\Psi(u)|^2 e^{i\frac{gBLu}{\Phi_0}}\right|^2 = G_t^{(0)} e^{-\phi^2} \simeq G_t^{(0)}\left(1-\phi^2\right), \tag{1.67}$$

with u the amplitude (displacement) of the antinode of the fundamental mode, $\Psi(u)$ the quantum ground state wavefunction (Gaussian), the constant $\phi = gBLu_0/\Phi_0$ with g a geometrical factor related to the waveform of the fundamental mode, and u_0 the average quantum fluctuations of the quantum ground state. The factor ϕ is the effective magnetic flux (in units of the flux quantum) through the area swept out by the nanotube of length L and the ground-state quantum fluctuations u_0. For realistic parameters one estimates that $\phi \ll 1$.

1.5.2 Resonant transport

The prediction of the magneto-conductance Eq. (1.67) emerging from the quantum mechanical motion was first obtaind in the tunnel regime (namely, a single-shot electron passage) for a suspended CNT-QD by Shekhter et al. [68]. A similar proposal - employing an Aharonov-Bohm-type setup - was analyzed in [69] to measure the spectrum of the momentum.

Though simple and transparent from a technical point of view, the tunnel regime for the Aharonov-Bohm effect induced by the quantum fluctuations is not optimal for the experimental observation for two reasons: (i) the current is very low, and (ii) electrons

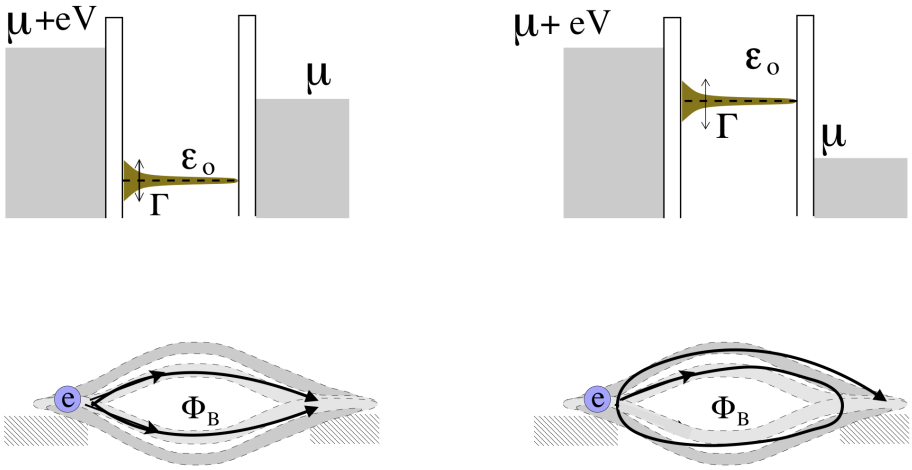

Figure 1.8: A single-level dot between two leads. **Left**: In the out-of-resonance regime (the dot's level is far away from the energy range set by the two chemical potentials), the electron has a small probability of tunneling from left to right (via cotunnelling, a virtual empty state). In a scattering picture, this corresponds to a single passage from left to right. **Right**: In the resonant transport regime, the dot's level is well within the two chemical potentials, and the dot is fully open. In a scattering picture, the electron has a substantial probability of being reflected. As a net effect, there is an enhancement of the overall probability of transmission, even if the individual amplitude of tunneling is small (in analogy to the Fabry-Perot interferometer in optics).

can interfere only once, since a single crossing occurs through the device; as a consequence, the net effect is weak ($\phi \ll 1$). Furthermore, the experimental conditions are stringent: for a nanotube of length $L = 1\mu$m, one finds a zero-point motion of tens of pm, which implies the use of a magnetic field on order of tens of Tesla to achieve variation in the magneto-conductance of a few percent.

Hence, in article 7, I considered the resonant transport through a single electron state of the nanotube. At resonance, the electron channel is fully open. One might expect that the magnetoconductance signal for the suspended nanotube would be greatly enhanced: the electron bounces many times inside the structure before leaving it, thus allowing multiple interference, see Fig. 1.8. Therefore, even if the phase acquired at each passage is small, the accumulated phase can be large.

The quantum nanomechanical interferometer system can be properly described by the following model Hamiltonian

$$\hat{H}_M = \sum_{\nu=l,r} \sum_k (\varepsilon_{\nu k} - \mu_\nu)\, \hat{c}^\dagger_{\nu k} \hat{c}_{\nu k} + \sum_{\nu=l,r} \sum_k \left(t_\nu e^{i\phi_\nu (\hat{b} + \hat{b}^\dagger)}\ \hat{d}\ \hat{c}^\dagger_{\nu k} + \text{h.c.} \right) + \varepsilon_0 \hat{d}^\dagger \hat{d} + \omega_0 \hat{b}^\dagger \hat{b}\ , \tag{1.68}$$

with $\phi_\nu = \phi$ for the left lead and $\phi_\nu = -\phi$. We single out the fundamental bending

mode with eigenfrequency ω_0. The parameter ϕ is therefore the electro-vibration coupling constant of the problem. The magnetic field enters the Hamiltonian through the Aharonov-Bohm phase $\phi\hat{u}$, with $\hat{u} = \hat{b} + \hat{b}^\dagger$, which depends on the quantum displacement operator of the nanotubes' flexural mode. By performing a calculation using the Keldysh nonequilibrium Green's function technique at lowest order in the electron-phonon coupling ϕ, I found that the shape of the resonance as a function of the gate voltage is modified by the magnetic field. As an example of the results, the linear conductance of the system reads as

$$G = \left.\frac{dI}{dV}\right|_{V=0} = G^{(0)}(\varepsilon_0) + \phi^2 G^{(2)}(\varepsilon_0)\,, \tag{1.69}$$

where the unperturbed conductance $G^{(0)}(\varepsilon_0) = 4e^2\Gamma_l\Gamma_r/[(\mu-\varepsilon_0)^2+\Gamma^2]$ for one resonant level and the function $G^{(2)}(\varepsilon_0) < 0$. Compared to the previous result Eq. (1.67), there is a parametric enhancement of the effect at the resonant transport regime. The exact (long) expression for the function $G^{(2)}(\varepsilon_0)$ is reported in my article 7. In the limit of zero temperature $T = 0K$ and far from the resonance $|\varepsilon_0 - \mu| \gg \Gamma$, one finds that $G^{(0)}(\varepsilon_0) \to G_t^{(0)}$ and the formula $G^{(2)}(\varepsilon_0)$ recovers the previous result with $G^{(2)}(\varepsilon_0) \to G_t^{(0)}$, see Eq. (1.67). An example of the behavior of the function $G^2(\varepsilon_0)$ is shown in Fig. 1.7(right). One can observe that, beyond the reduction of the conductance, at resonance and for vanishing temperature, the shape of the conductance resonant peak is also modified, since $G^2(\varepsilon_0)$ has non-monotonic dependence on ε_0. This prominent feature constitutes a measurable signature of the quantum delocalization of the vibrating nanotube.

In any realistic device, both the electrostatic and magnetic effects are present. In a second study, I therefore investigated the interplay and the differences between these two interactions, the magneto-elastic and the (polaron) electrostatic interaction (my article 6). They both affect the charge transport, but in different ways. These effects may be relevant for determining the current-voltage characteristics through suspended nanotubes. Thus, charge transport could be efficiently used to demonstrate the quantum nature of the mechanical vibrations of these tiny objects.

1.6 Effects of the charge-vibration interaction in the current noise

At finite temperature, in a nanoscale conductor as a quantum dot, the thermal noise of the current arises from the fluctuations of the occupation number of energy levels forming the spectrum of the femionic leads.

Electron transport through a nanosystem also displays a current with a different kind of noise when a bias voltage is applied. Indeed, the charge current is in principle time-dependent due to the discreteness of the charge unavoidably appearing in nanoscale conductors, such as in quantum dots. Such current fluctuations associated with the discreteness of the electrical charge are known as "shot noise" [70, 71]. For example, in a tunnel

junction (a thin insulating layer or electric potential between two electrical contacts) electrons are *emitted* from the source lead and have some probability of being transmitted to the drain lead via quantum tunnelling through the barrier.

Generally, the time-fluctuations of the charge current manifest in a finite-frequency current noise $S(\omega)$. This finite frequency noise must be naturally related to the photons emission, as suggested by classical electromagnetism (according to which electromagnetic radiation can indeed be produced by charge fluctuations). More precisely, as a quantum object, the current is associated with a time-dependent operator in the Heisenberg representation $\hat{I}(t)$. Hence, the noise spectral density, defined as

$$S(\omega) = \int dt e^{i\omega t} \langle \hat{I}(t)\hat{I}(0)\rangle \,, \tag{1.70}$$

acquires a frequency-antisymmetric component because of the noncommuting current operators at different times. As a quantum property, the nonsymmetrized finite frequency noise $S(\omega)$ is related to the rate of emission and absorption of photons at the frequency ω [1]. The part of the noise at negative frequencies corresponds to the absorption rate of photons, whereas at positive frequency, the noise is linked to the rate of emitted photons. Therefore, this quantity plays a crucial role in molecular nanojunctions exploited as a source of photons.

In article 1 on my publications list, I investigated the effects of local charge-vibration interaction in the nonsymmetrized current noise $S(\omega)$ of the Holstein model, a single electronic level that is coupled to two metallic leads and to a single vibrational mode - see Eq. (1.5) and Eq. (1.22). Using the Keldysh Green's functions technique, we calculated the nonsymmetrized current noise to the leading order in the charge-vibration interaction λ, including vertex corrections. In this way, the noise is naturally divided into an unperturbed term ($\lambda = 0$) and a correction (of order λ^2), the latter related to interaction with the vibration

$$S(\omega) = S^{(0)}(\omega) + \lambda^2 S^{(1)}(\omega) \,, \tag{1.71}$$

with $S^{(1)}(\omega)$ related to energy exchange (virtual or real emission/absorption) of a single quantum energy of the vibration. $S^{(1)}(\omega)$ encodes the information about the possibility of absorbing or emitting a photon by the whole system formed by the mesoscopic conductor (the quantum dot) and the local vibration. The noise associated with the vibrational-charge interaction shows a complex pattern as a function of the frequency and of the parameters controlling the transmission through the dot, namely $\Gamma_l, \Gamma_r, \varepsilon_0$. Several features, ranging from enhancement to suppression of the noise, occur in different regions of parameters and different frequency scales. A detailed discussion of the general behavior of $S^{(1)}(\omega)$ is provvided in article 1 on the publication list. Here, I note that, depending on the different types of diagrams whose examples are shown in Fig. (1.9), the correction to the noise spectrum $S^{(1)}(\omega)$ can be decomposed as

$$S^{(1)}(\omega) = S_{mf}(\omega) + S_{vc}(\omega) \,, \tag{1.72}$$

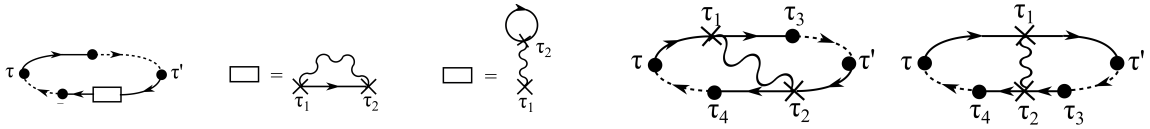

Figure 1.9: Examples of diagrams of the current-current correlator, for the times τ and τ' on the Keldysh close time contour. **Left:** An example of the mean-field diagrams. The solid black line denotes the dot's Green function. The dotted black line is the lead self energy. The wavy line represents the phonon propagator. The empty rectangular box can be one of two diagrams including the phonon propagator: the rainbow diagram or the tadpole diagram. The times τ_1 and τ_2 are internal times to be integrated. **Right:** Examples of the vertex diagrams. The times τ_1, τ_2, τ_3 and τ_4 are internal times to be integrated.

with $S_{mf}(\omega)$ containing the mean field diagram and $S_{vc}(\omega)$ given by the vertex diagrams, see Fig. (1.9). In turn, it is also possible to divide the mean field term into an elastic correction and an inelastic term:

$$S_{mf}(\omega) = S_{ec}(\omega) + S_{in}(\omega)\,. \tag{1.73}$$

In this section, I report an example of the results: the weak tunneling coupling regime between the open dot and the leads such that the transport occurs through a sharp resonant level with the dot's energy level $\varepsilon_0 > 0$, in the limit of vanishing temperature $T = 0K$. For the sake of brevity, I focus the analysis of $S^{(1)}(\omega)$ only on the positive frequency (= the probability of photon emission by the system) as a function of ε_0 for the vibrational frequency $\omega_0 < eV$, with eV as the bias voltage.

I recall first the behavior of the noise $S^{(0)}(\omega)$ in the absence of charge-vibration interaction in the dot. Setting the average chemical potential $\mu = 0$, we assume that the voltage is applied on the left lead $\mu_l = eV$, whereas $\mu_r = \mu = 0$. In this case, electrons emitting photons can tunnel only from left to right. A priori, one would expect that an electron moving from the lead left would have as an upper energy $\omega = eV$. This is indeed the case for the tunnelling junction. By contrast, in the sharp resonant transport regime realized in quantum dots, the electron can mainly tunnel from the left lead to the quantum dot at ε_0, such that the (approximated) maximum energy for emitting a photon is $\omega_{max} \approx eV - \varepsilon_0$, see Fig. 1.10(left). Far away from the chemical potentials of the leads $|eV - \varepsilon_0|, |\varepsilon_0| \gg \Gamma_{l,r}$, the current is almost constant; similarly, $S^{(0)}(\omega)$ is almost a plateau for energy far away from the boundaries $(0, eV)$: as expected for Poissonian processes, the noise is related to the average current. Note that the noise $S^{(0)}(\omega)$ is strongly reduced but not vanishing in the range $eV - \varepsilon_0 < \omega < eV$ for finite tunneling rates. The asymptotic step behavior is only approached in the limit $\Gamma_{l,r} \to 0$.

I discuss briefly the behavior of $S^{(1)}(\omega)$ which is reported in Fig. 1.10(right) as a function of the gate voltage ε_0 and the frequency ω. The mean field terms $S_{ec}(\omega)$ and $S_{in}(\omega)$ have a finite contribution in an extended range of the frequency, whereas the vertex

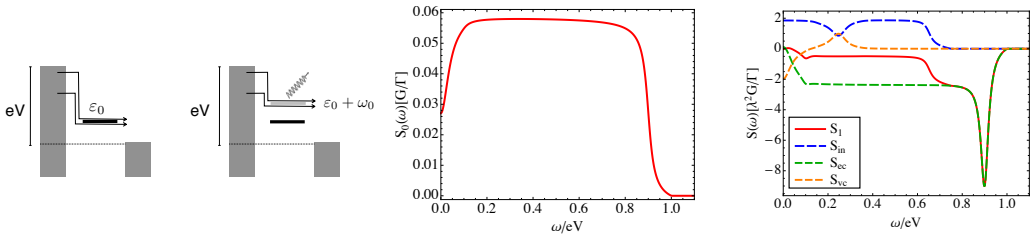

Figure 1.10: **Left:** Schematic picture of an electron tunneling from left to right emitting a photon of frequency ω. In quantum dots with discrete levels, resonant transport occurs and the maximum energy that electrons can emit is, roughly speaking, $\omega_{max} \approx eV - \varepsilon_0$ when only one level is within the bias voltage window. When a tunnelling electron emits a photon of frequency ω *and* a phonon of energy ω_0 into the localized vibration, then the maximum energy of the photon emitted is $\omega_{max} \approx eV - \varepsilon_0 - \omega_0$. **Center:** Behavior of the current noise $S_0(\omega)$ without charge-vibration interaction. Parameters: $\varepsilon_0 = 0.1eV$, $\Gamma_l = \Gamma_r = 0.01eV$ and $T = 0\,K$. **Right:** The leading order correction $S_1(\omega)$ of the finite frequency noise of the current (red line) for $\omega_0 = 0.25eV$. This is composed of three terms. The first two terms are obtained by the mean-field diagrams $S_{mf}(\omega)$ which can be divided into an inelastic term $S_{in}(\omega)$ (dashed blue line) and an elastic correction $S_{ec}(\omega)$ (dashed green line). The dashed orange line is the contribution from the vertex diagrams $S_{vc}(\omega)$.

correction $S_{vc}(\omega)$ is strongly localized in correspondence to characteristic lines that are associated with the resonant transport regime.

The inelastic correction $S_{in}(\omega)$ shows a clear cut-off (smeared on range Γ) at the energy $\omega_{cut} \approx eV - \varepsilon_0 - \omega_0$, see Fig. 1.10(center). The latter quantity corresponds to the maximum energy that an electron can emit as a photon if a phonon of energy ω_0 has also been emitted into the vibration. The three terms sum up in the total function $S^{(1)}(\omega)$ (red line) in Fig. 1.10(right). Roughly speaking, the three contributions compensate for one another: the interesting frequency range, where $S^{(1)}(\omega)$ has a relevant correction, appears after the threshold $\omega = eV - \varepsilon_0$. In this frequency range, we have $S^{(1)}(\omega) \approx S_{ec}(\omega)$, which turns out to be a negative correction in the range $eV - \omega_0 - \varepsilon_0 < \omega < eV - \varepsilon_0$.

In general, we found that the features of the current noise associated with the charge-vibration interaction are strongly governed by all system parameters. A thorough understanding of the lowest-order feature is in any case worthwhile, given the complexity of the physical processes involved in nanocontacts containing a single molecule. The analytic results in the different regimes can serve as a reference for comparison with numerical calculations of realistic molecular nanojunction devices. In particular, these devices are considered to be promising candidates for single-photon sources at the nanoscale [72]. In this context, the current noise is then the central quantity, since it is directly related to the emitted photon spectrum.

Chapter 2

Quantum dissipation in Josephson junction systems

2.1 Context and scientific background

The Josephson junction is one of the most widely used superconducting devices in low-temperature condensed-matter experiments. A single Josephson junction serves as a building block for various sensors and electronic components [73, 74].

On a more fundamental level, the electromagnetic macroscopic degrees of freedom (charge, current, flux) exhibit quantum behavior at very low temperatures (50 mK $\sim$ GHz) in superconducting circuits based on Josephson junctions [75, 76]. Hence, they play an important role in quantum computation and information, as they are the fundamental component of the superconducting quantum bits (qubits) [77]. The reason is that superconductivity provides a typical example of how a complex physical system can behave in an extremely simple collective manner that conceals the microscopic complexity. In a superconductor, the conducting electrons are coupled together in Cooper pairs, and this allows them to form a large-scale condensate, which is a single macroscopic quantum state [78]. Because of this collective behavior, it turns out that it is possible to build superconducting circuits that behave very simply, even at a quantum-mechanical level, despite the fact that they are made up of billions of atoms. A first and striking example is the LC oscillator, which is formed by an inductance L and capacitance C in parallel. In such systems, cooled down to very low temperatures, the collective degree of freedom (viz. the charge fluctuations) does not interact with any other degrees of freedom in the circuit (such as atomic vibrations, etc) - or, at least, it is practically uncoupled - and the circuit can behave as a quantum mechanical oscillator.

However this degree of freedom can often interact strongly with the environment and, as a consequence, its dynamics is affected by dissipation, noise and decoherence. Without any designed adjustment, these systems can operate in a regime in which the quantum effects are fragile. This is not generally a disadvantage. Indeed, Josephson junctions -

with small capacitance - have become paradigmatic systems for studying the decoherence and dissipation of a quantum system coupled to the external world and for analyzing the transition from quantum to classical states [79–83]. Specifically, the quantum dynamics of a single Josephson junction can be described by an effective quantum particle coupled to a bath (i.e. quantum Brownian motion with the Caldeira-Leggett model) [84–88].

2.2 Josephson junction circuits: an experimental overview

Josephson junctions are a versatile circuit element with widespread use in quantum mesoscopic systems, thanks to their intrinsic low dissipation and amenable nonlinearity. This nonlinearity makes it an optimal element in the design of coherent quantum structures. These junctions are the building blocks of superconducting qubits [77,89], hybrid systems (opto- and mechanical- nanodevices) [90] and Josephson photonic circuits, namely Josephson junctions coupled to superconducting microwave cavities [91–99].

The standard example is the circuit QED, which has opened up many new possibilities for the study of the strong interaction between light and matter [100–102]. In these systems, on-chip microwaves cavities consisting of superconducting transmission line resonators are coupled to superconducting Josephson qubits, the latter playing the role of artificial atoms. Owing to the significant tunability of the parameters and accurate control techniques, such devices have paved the way towards lasing [103], the synthesis of arbitrary quantum states of the cavity [104] and the generation of single-photon sources in the microwave domain [105].

Another important aspect is the possibility to wire up different junctions to form more complex quantum circuits, such as 1D chains formed by many junctions. One-dimensional Josephson junction chains are a paradigmatic model for studying the quantum correlations and quantum phase transitions in open, dissipative many-body systems [106]. Josephson junction chains are formed by linear arrays of N superconducting islands, separated by weak Josephson tunnel junctions.
In general, Josephson junction chains exhibit rich and interesting many-body physical properties, that can be influenced relatively accurately by circuit design and fabrication parameters. They have been proposed for the realization of a qubit topologically protected against decoherence [107,108], for the realization of a tunable parametric amplifier in narrow frequency ranges [109] and for the realization of a fundamental current standard in quantum metrology [110]. Significant successes have also been achieved in the fabrication of low-loss high-impedance environments in the form of superinductors [111–113].
Josephson junction chains have constituted the platform of choice for the investigation of quantum fluctuations of the phase induced by charge interactions, i.e. quantum phase slips [114–119], as well as quantum fluctuations of the charge induced by Josephson tun-

neling [120–123]. In the phase regime, where the Josephson energy $E_J = \hbar I_c/(2e)$, with I_c denoting the junction critical current, dominates over the charging energy of the junction $E_C = e^2/(2C_J)$, with C_J as the junction capacitance, Josephson junction chains have been investigated as custom-designed electromagnetic environments, metamaterials implementations [124–127], resonators with tunable non-linearity [128] and in the design of resonant modes in an electromagnetic environment [129].

2.3 Overview of the theoretical technique

The study of quantum dissipation and decoherence dynamics in atomic and mesoscopic systems is driven by the perspective of engineering the reservoirs in order to preserve quantum coherence [130]. This is a crucial point towards the exploitable manipulation and control of individual quantum systems [131–133] and for the realization of future quantum applications. Understanding the influence of the environment on the dynamics of physical systems is hence of paramount importance in the development of quantum-based technologies. However, this issue is also interesting for fundamental research oriented towards fundamental tests of quantum theory [83].

A variety of approaches aiming at a quantum mechanical description of dissipation have been developed. One of the most common approaches is based on the quantum mechanical Langevin equations and the master equations for the density matrix [130, 134, 135]. However, the simplicity of the abovementioned method is balanced out by the fact that concrete results can only be obtained, in general, in a perturbative treatment of the coupling of the system to the environmental bath; the methods are easily implemented in the Markovian limit when the relaxation time of the system is large compared to the (short) time scale of the decay of the correlations in the bath. Alternatively, the functional integral approach (or path integral) of dissipative quantum systems allows for the study of the dynamics at arbitrary damping and arbitrary time scales of the dynamics of the bath. This method was pioneered by Feynman and Vernon [136].

2.3.1 The Caldeira-Leggett model

In this section, I outline the Caldeira-Leggett model [84]. To facilitate concrete results and to simplify the notation, I discuss the case of a quantum particle with two conjugates operators, position and momentum $[\hat{q}, \hat{p}] = i\hbar$. The environment consists of a set of independent harmonic oscillators. The Caldeira-Leggett model for the quantum Brownian motion has the form

$$\hat{H} = \frac{\hat{p}^2}{2m} + V(\hat{q}) + \sum_n \left[\frac{\hat{P}_n^2}{2m_n} + \frac{1}{2} m_n \omega_n^2 \left(\hat{Q}_n - \frac{\lambda_n \hat{q}}{m_n \omega_n^2} \right)^2 \right] \tag{2.1}$$

with the interaction with the environment described by the ensemble of independent harmonic oscillators with the conjugate operators $[\hat{Q}_n, \hat{P}_{n'}] = i\hbar\delta_{n,n'}$. Using the equations

of motion in the Heisenberg picture $\hat{O}(t) = e^{iHt/\hbar}\hat{O}e^{-iHt/\hbar}$, one obtains a generalized quantum Langevin equation:

$$\frac{d\hat{p}(t)}{dt} = -\frac{\partial V(\hat{q})}{\partial \hat{q}} + \hat{F}(t) - \int_{t_0}^{+\infty} dt' \, \eta(t-t') \, m \frac{d\hat{q}(t')}{dt'} \,, \tag{2.2}$$

in which we have introduced t_0 as the initial time for the interaction and the response function as

$$\eta(t) = \frac{\theta(t)}{m} \sum_n \frac{\lambda_n^2}{m_n \omega_n^2} \cos(\omega_n t) \,. \tag{2.3}$$

For times $t > t_0$, the force operator $\hat{F}(t)$ describes the quantum noise. Assuming the continuum limit of the harmonic oscillators, one recovers dissipation in the system. To give an example, the response function describing the ohmic dissipation (with a Drude large frequency cutoff ω_c) is given by

$$\eta(t) = \theta(t) \; \gamma \; \omega_c e^{-\omega_c t} \,, \quad \eta(\omega) = \gamma/(1 + i\omega/\omega_c) \,, \tag{2.4}$$

in which γ is the damping coefficient (with dimensions of a frequency). The response function $\eta(t)$ satisfies causality and the Kramers-Kronig relations. Note that the function $\eta(t) \to 0$ for large times $\omega_c t \gg 1$. Assuming as initial state the total density matrix factorized as $\rho_{t_0} = \rho_0 \rho_{bath}$ with ρ_0 the initial state of the particle and ρ_{bath} the thermal density matrices for the bath, $\rho_{bath} \propto \exp(-\beta \sum_n \omega_n \hat{a}_n^\dagger \hat{a}_n)$, $[\beta = \hbar/(k_B T)]$ then the correlation functions of the noise operators read in the Fourier space ($\hat{F}(\omega) = \int dt \exp(-i\omega t)\hat{F}(t)$) as

$$\langle \hat{F}(\omega)\hat{F}(\omega') \rangle = (2\pi)^2 \delta(\omega + \omega') S(\omega) \,, \tag{2.5}$$

where we have introduced the noise spectral function

$$S(\omega) = \sum_n \hbar\omega_n \left(\frac{\lambda_n^2}{2 m_n \omega_n^2} \right) \left[(n_B(\omega_n) + 1)\delta(\omega + \omega_n) + n_B(\omega_n)\delta(\omega - \omega_n) \right] . \tag{2.6}$$

The noise spectral function can be related to the response function of the bath:

$$\mathrm{Re}[\eta(\omega)] = \frac{\pi}{2m} \sum_n \frac{\lambda_n^2}{m_n \omega_n^2} \left[\delta(\omega - \omega_n) + \delta(\omega + \omega_n) \right] . \tag{2.7}$$

In summary, the quantum Langevin equation describing the dissipative dynamics of the single particle can be obtained by simply closing the equations of motion for the case of linear coupling to the bath. The same approach can be extended in the case of quantum circuits by replacing the position operators with the phases, the momentum with the charge, and so on. An example of this approach in complex quantum circuits is described in my work 9 on the publication list, which sought to implement a tunable ohmic environment at finite frequency.

2.3.2 Path integral in quantum statistical mechanics

In this section, I illustrate the basis of the path integral method in the imaginary time in a heuristic, non-rigorous way. I refer to the books of Feynman [136] and Kleinert [137] for a complete introduction.

As we have seen in the previous section, the standard formulation of quantum dissipation theory is based on the use of a Hamiltonian composed of *system+reservoir*, namely a total Hamiltonian of the form $\hat{H} = \hat{H}_s + \hat{H}_{bath} + \hat{H}_{int}$ with $\hat{H}_s$ for the system of interest (viz. the quantum particle), $\hat{H}_{bath}$ for the bath and $\hat{H}_{int}$ for the interaction. If one combines this starting point with the Caldeira-Leggett model, in which we have a linear interaction with the bosonic operators of the bath (an ensemble of harmonic oscillators), then the path integral turns out to be particularly convenient, since one can integrate out the irrelevant degrees of freedom and construct an object (i.e. the partition function) of the system of interest.

We again start by considering a particle with position $\hat{q}$ and momentum $\hat{p}$ moving in potential $V(\hat{q})$ at thermal equilibrium. The density matrix is given by the Gibbs-Boltzman distribution $\hat{\rho} \propto \exp(-\beta\hat{H})$ with the Hamiltonian $\hat{H} = \hat{K} + \hat{V}$, with $\hat{K} = \hat{p}^2/(2m)$, $\hat{V} = V(\hat{q})$. The latter quantity has a form similar to that of the time evolution operator replaced with an *imaginary time* $-i\beta$. One can factorize the exponential operator in N time slices as $\exp(-\beta\hat{H}) = \prod_{n=0}^{N-1} \exp(-\Delta\tau\hat{H})$ with $\Delta\tau = \beta/N$. Inserting the identity representation $\mathbb{1} = \int dq\, |q\rangle \langle q|$ between the product of the exponential operators, one can write the thermodynamical partition function as

$$\begin{aligned} \mathcal{Z} &= \int dq_0 \, \langle q_0 | \, e^{-\frac{1}{\hbar}\beta\hat{H}} \, |q_0\rangle = \prod_{n=0}^{N-1} \int dq_n \, \langle q_{n+1} | \, e^{-\frac{1}{\hbar}\Delta\tau\hat{H}} \, |q_n\rangle \\ &= \prod_{n=0}^{N-1} \iint \frac{dq_n dp_n}{2\pi\hbar} \, \langle q_{n+1}|p_n\rangle \, \langle p_n | \, e^{-\frac{1}{\hbar}\Delta\tau\left[\hat{K}+\hat{V}\right]} \, |q_n\rangle \ , \end{aligned} \tag{2.8}$$

with the periodic boundary condition $q_0 = q_N$ and using the form for the the identity representation $\mathbb{1} = \int dp\, |p\rangle \langle p| \, /(2\pi\hbar)$. The equation 2.8 s exact, but there is still the problem of calculating the quantity inside the integral $\langle p_n | \, e^{-\Delta\tau\hat{H}/\hbar} \, |x_n\rangle$, as in the starting equation. One cannot generally calculate this matrix element exactly. The problem here is that the Hamiltonian is formed by the kinetic energy operator and the potential operator which do not commute. The important difference is that the *evolution time* $\Delta\tau$ (or the effective temperature) is a much smaller quantity than the time β. Using the Baker-Campbell-Hausdorff formula for two operators, one can show that (Zassenhaus formula)

$$e^{-\frac{1}{\hbar}\Delta\tau\left[\hat{K}+\hat{V}\right]} \approx e^{-\frac{1}{\hbar}\Delta\tau\hat{K}} e^{-\frac{1}{\hbar}\Delta\tau\hat{V}} \cdot e^{-\frac{1}{\hbar^2}\frac{(\Delta\tau)^2}{2}\left[\hat{K},\hat{V}\right]} \cdot e^{-\frac{1}{\hbar^3}\frac{(\Delta\tau)^3}{6}\left\{2\left[\hat{V},\left[\hat{K},\hat{V}\right]\right]+\left[\hat{K},\left[\hat{K},\hat{V}\right]\right]\right\}} \cdot \ldots \tag{2.9}$$

with $[\ldots,\ldots]$ for the commutator between two operators. The equation 2.9 suggests that, in the lowest order of $\Delta\tau$, one can neglect high-order terms and simply treat the

two operators as commuting. Strincly speaking, $\Delta\tau$ is not a dimensionless constant, and one should better estimate the expansion. Furthermore, keeping only the first two terms that are linear in the exponent $\Delta\tau$ is not strictly speaking correct, since they also contain higher-order terms. As observed by Feynman, the crucial point here is in the limit $N \to \infty$, which implies that the time slice becomes infinitesimal $\Delta\tau \to 0$, and this expansion has to meaningful in some sense [136, 138]. A rigorous demonstration was later provided by Trotter, who showed that for two (bounded) operators, the following identity holds [139]

$$e^{-\frac{\beta}{\hbar}\left[\hat{K}+\hat{V}\right]} = \lim_{N\to\infty}\left(e^{-\frac{\Delta\tau}{\hbar}\hat{K}}e^{-\frac{\Delta\tau}{\hbar}\hat{V}}\right)^N . \tag{2.10}$$

It is sufficient to know that, in quantum physics, the Trotter formula holds for the most physically interesting problems of quantum dissipative systems [137]. Formally using the Trotter formula, one can write

$$\begin{aligned}
\mathcal{Z} &= \lim_{N\to\infty}\prod_{n=0}^{N-1}\iint\frac{dq_n dp_n}{2\pi\hbar}\left\langle q_{n+1}|p_n\right\rangle\left\langle p_n\right| e^{-\frac{\Delta\tau}{\hbar}\hat{K}}e^{-\frac{\Delta\tau}{\hbar}\hat{V}}\left|q_n\right\rangle \\
&= \lim_{N\to\infty}\prod_{n=0}^{N-1}\iint\frac{dq_n dp_n}{2\pi\hbar}e^{\frac{i}{\hbar}p_n(q_{n+1}-q_n)-\frac{\Delta\tau}{\hbar}\left[\frac{p_n^2}{2m}+V(q_n)\right]} \\
&= \lim_{N\to\infty}\prod_{n=0}^{N-1}\int dq_n\sqrt{\frac{m}{2\pi\hbar\Delta\tau}}e^{-\frac{\Delta\tau}{\hbar}\left[\frac{1}{2}m\left(\frac{q_{n+1}-q_n}{\Delta\tau}\right)^2+V(q_n)\right]} \equiv \oint\mathcal{D}[q(\tau)]e^{-\frac{1}{\hbar}\mathcal{S}} .
\end{aligned} \tag{2.11}$$

We have used the fact that the states $|p_n\rangle$ and $|q_n\rangle$ are eigenstates of $\hat{K}$ and $\hat{V}$, respectively. In the last equation, we have integrated out the momentum, and one can recognize that the function in the exponent is the time-discretized version of the action S with the associated Lagrangian. This defines the last expression in Eq. (2.11).

Eq. (2.11) can be generalized to the case of many particles - for instance, one particle interacting with a set of harmonic oscillators, namely the Caldeira-Leggett model - see Eq. (2.1). Concretely, the operational task in the path integral formulation is to solve a multidimensional integral and afterwards to calculate the product in the limit $N \to \infty$.

Beyond the direct calculation of the time-discretization formula, another common approach involves transformation in the frequency space. This requires an unitary transformation (unitary Jacobian) on the discrete variables forming the vector $\vec{q} = (q_0, q_1, \ldots, q_{N-1})$. Setting $\bar{N} = N/2-1$ when N is even and $\bar{N} = (N-1)/2$ when N is odd, a possible unitary transformation reads as

$$q_n = \frac{x_0}{\sqrt{N}} + \underbrace{\frac{(-1)^{\frac{N}{2}}x_{\frac{N}{2}}}{\sqrt{N}}}_{\text{if } N \text{ even}} + \sum_{\substack{\ell=1 \\ (\ell\neq\frac{N}{2})}}^{\bar{N}}\sqrt{\frac{2}{N}}\left[\cos\left(\frac{2\pi\ell}{N}n\right)x_\ell^{Re} + \sin\left(\frac{2\pi\ell}{N}n\right)x_\ell^{Im}\right] = \sum_{\ell=0}^{N-1}\frac{e^{-i\frac{2\pi\ell}{N}n}}{\sqrt{N}}\,x_\ell \tag{2.12}$$

with the complex variable $x_\ell = (x_\ell^{Re} + i x_\ell^{Im})/\sqrt{2}$, by setting $x_\ell^{Re} = x_{N-\ell}^{Re}$ and $x_\ell^{Im} = -x_{N-\ell}^{Im}$. Note that the dimension of the vector (independent variables) does not change, $N \to N$.

Using this transformation for the case of the partition function of a free particle in a box of size L, one obtains:

$$\mathcal{Z}_0 = \lim_{N\to\infty}\left(\sqrt{\frac{m}{2\pi\hbar\Delta\tau}}\right)^N \prod_{n=0}^{N-1}\int_{-\sqrt{N}\frac{L}{2}}^{\sqrt{N}\frac{L}{2}} dx_0 \int \prod_{\substack{\ell=1\\(\ell\neq\frac{N}{2})}}^{\bar{N}} dx_\ell^{Re} dx_\ell^{Im}\, \underbrace{dx_{\frac{N}{2}}}\, e^{-\frac{1}{\hbar}S_0}\,, \tag{2.13}$$

with

$$S_0 = \frac{m}{2\Delta\tau}\left[\underbrace{4\,x_{\frac{N}{2}}^2} + \sum_{\substack{\ell=1\\(\ell\neq\frac{N}{2})}}^{\bar{N}} 2\left(1-\cos\left(\frac{2\pi\ell}{N}\right)\right)\left[\left(x_\ell^{Re}\right)^2+\left(x_\ell^{Im}\right)^2\right]\right]. \tag{2.14}$$

Performing the Gaussian integral, one achieves

$$\mathcal{Z}_0 = \left(\sqrt{\frac{m}{2\pi\hbar\Delta\tau}}\right)^N \left(\sqrt{N}L\right)\left(\frac{2\pi\hbar\Delta\tau}{m}\right)^{\bar{N}} \underbrace{\frac{1}{2}\sqrt{\frac{2\pi\hbar\Delta\tau}{m}}} \prod_{\substack{\ell=1\\(\ell\neq\frac{N}{2})}}^{\bar{N}} \frac{1}{2\left[1-\cos\left(\frac{2\pi\ell}{N}\right)\right]} = \frac{L}{\lambda_T} \tag{2.15}$$

with $\lambda_T = \sqrt{m/(2\pi\hbar\beta)}$ denoting the thermal De Broglie wavelength and using the result

$$\underbrace{2}\times\prod_{\ell=1}^{\bar{N}}\left\{2\left[1-\cos\left(\frac{2\pi\ell}{N}\right)\right]\right\} = \underbrace{2}\times\prod_{\ell=1}^{\frac{N}{2}-1}\left\{2\left[1-\cos\left(\frac{2\pi\ell}{N}\right)\right]\right\} = N \quad \text{for} \quad N \text{ even} \tag{2.16}$$

$$\prod_{\ell=1}^{\bar{N}}\left\{2\left[1-\cos\left(\frac{2\pi\ell}{N}\right)\right]\right\} = \prod_{\ell=1}^{\frac{N-1}{2}}\left\{2\left[1-\cos\left(\frac{2\pi\ell}{N}\right)\right]\right\} = N \quad \text{for} \quad N \text{ odd}\,. \tag{2.17}$$

Combining the time slice $\Delta\tau$ with the trigonometric term, one can define the Matsubara frequency as

$$\omega_\ell^2 = \frac{2\left[1-\cos\left(\frac{2\pi\ell}{N}\right)\right]}{\Delta\tau^2} \approx \left(\frac{2\pi\ell}{\beta}\right)^2, \quad \text{for } N \gg 1\,. \tag{2.18}$$

Remarkably, in the limit $N\to\infty$, the two products of the two sequences with the term $\sim[1-\cos(2\pi\ell/N)]$ and with the term $\sim(2\pi\ell/N)^2$ converge to the same result.

Moving from the free particle case, one can repeat similar calculations with a given potential. In this case, it is convenient to scale the partition function of the system with $\mathcal{Z}_0$ and to express the latter quantity in terms of a product of the terms with the Matsubara frequencies. By means of rescaling the variables in the frequency domain, one can show that the following formula holds:

$$\mathcal{Z} = \mathcal{Z}_0 \int\frac{d\tilde{x}_0}{\sqrt{\frac{2\pi\hbar\beta}{m}}}\int\prod_{\ell=1}^{\infty}\frac{d\tilde{x}_\ell^{Re}d\tilde{x}_\ell^{Im}}{\frac{\pi\hbar\beta}{m\beta\omega_\ell^2}}\, e^{-\frac{1}{\hbar}\mathcal{S}[\{\tilde{x}_\ell\}]}\,, \tag{2.19}$$

where the action is expressed in terms of the complex variables $\tilde{x}_\ell = \tilde{x}_\ell^{Re} + i\tilde{x}_\ell^{Im}$ representing the Fourier transform $\tilde{x}_\ell = \int_0^\beta \frac{d\tau}{\beta} x(\tau) e^{i\omega_\ell \tau}$.

Eq. (2.19) is the starting point of the calculations in the Caldeira-Leggett model to integrate out the bath of harmonic oscillators linearly coupled to the particle. The representation of the path integral in terms of the frequency domain is useful in the perturbative method to construct various diagrams. It is also useful for the variational (harmonic) approximations, in which one replaces the nonlinear potential with a simple quadratic potential whose elastic constant is treated as a variational parameter.

2.4 Josephson effect: a simple picture

In this section, I briefly review the basics of the superconductivity theory, a simple description of the Josephson effect and, finally, the Josephson junctions.

Superconductivity allows a macroscopic quantum coherent flow of electrons at sufficiently low temperature. The key property of a superconductor is the existence of the Cooper pair condensate. These pairs are correlated, bound states of two conduction electrons with opposite spins and opposite momenta, that form due to the weak attraction between electrons resulting from the interaction with lattice oscillations (phonons).

In a superconductor, the so-called anomalous average is not zero $\langle \psi_\downarrow(\vec{r})\psi_\uparrow(\vec{r})\rangle \neq 0$ reflecting the fact that the Cooper pairs form a bosonic condensate with a macroscopic population (number of Cooper pairs) in a given state. The ground state of a superconductor is the BCS state (Bardeen-Cooper-Schrieffer), given by

$$|\varphi_{BCS}\rangle = \prod_{\mathbf{k}} \left(u_k + v_k e^{i\varphi} \hat{c}^\dagger_{\mathbf{k}\uparrow} \hat{c}^\dagger_{-\mathbf{k}\downarrow} \right) |0\rangle \tag{2.20}$$

with u_k, v_k real positive number satisfying the relation $u_k^2 + v_k^2 = 1$. The BCS state is a coherent superposition of states with even numbers of electronss. The quantity v_k describes the *wavefunction* of the single Cooper pair, whereas the occupation of the singlet state of opposite momenta is taken into account on average (mean-field approximation) in the BCS state. The key important quantity is the overall phase φ, which plays the role of the phase of the macroscopic wavefunction of the Cooper pairs forming the condensate. More specifically, the (complex) order parameter in a superconductor plays the role of a macroscopic wavefunction of a Cooper pair $\langle \psi_\downarrow(\vec{r})\psi_\uparrow(\vec{r})\rangle \propto \Psi(\vec{r}) = \sqrt{n_s/2}\exp(i\varphi)$ with n_s the electron density of the condensate and φ the phase of the BCS wavefunction.

Remarkably, many of the superconducting properties can be simply derived only by using the wavefunction $\Psi(\vec{r})$, as in basic quantum mechanics. For instance, assuming uniform density n_s, by applying the formula for the current probability associated to $\Psi(\vec{r})$ one can determine that the superfluid velocity is related to the phase gradient $v_s \propto \nabla\varphi$ (with n_s = constant). At a more fundamental level, one can intuitively see why phase fluctuations $\delta\varphi(\vec{r})$ play an important role, in contrast to the density modulation $\delta n_s(\vec{r})$

in the low-temperature system ($T \ll T_c$). The density fluctuations are associated with a variation in the number of Cooper pairs forming the condensate and a finite, large energy (the gap) is required to break them. By contrast, the phase fluctuations are associated to the small change of velocity (kinetic energy) of the Cooper pairs.

The phase difference is also the crucial quantity ruling the Josephson effect: the flow of a superconducting current between two superconducting leads interrupted by, for example, an insulating thin tunneling barrier. Due to quantum tunnelling, a Cooper pair can penetrate through the barrier, and as a result, the wavefunctions of the two condensates - at the left and the right of the barrier ? hybridize, leading to the Josephson effect. Following the approach introduced by Feynman, one can describe the system formed by two leads as a two-component wavefunction of different phases φ_L and φ_R that is governed by an effective tunneling Hamiltonian. Such a phenomenological model leads directly to the Josephson current (dc Josephson effect),

$$I_J = I_C \sin\left(\varphi_L - \varphi_R\right) , \tag{2.21}$$

with I_J the non-dissipative current flowing across the barrier. Here, I_C here is the maximal current sustained by the junction which depends on the microscopic model and details. The result Eq. (2.21) is valid in the lower order in the tunneling, i.e. low transparency. By maintaining a difference between the two chemical potentials of the two superconducting leads $\mu_L - \mu_R = 2eV$, one also obtains the ac-Josephson effect that rules the dynamics of the phase difference:

$$V = \frac{\hbar}{2e} \frac{d\left(\varphi_L - \varphi_R\right)}{dt} . \tag{2.22}$$

The underlying physics of the Josephson effect is based on the general behavior of a macroscopic quantum condensate whose mass flow is hindered by a constriction (the junction). Such physics is universal: it does not occur only in superconducting circuits with weak links but can also manifest in other systems, such as helium superfluids flowing through nanoscale apertures [140, 141] and Bose-Einstein condensates in optical traps [142].

I conclude this section by outlining the standard quantum model to describe Josephson junctions. One can start from the Anderson relation regarding the phase of the BCS wavefunction and the number of particles. From Eq. (2.20), the state with a fixed number of N Cooper pairs can be extracted

$$|N\rangle = \frac{1}{2\pi} \int_0^{2\pi} d\varphi \; e^{-iN\varphi} \;\; |\varphi\rangle \; , \tag{2.23}$$

in which I have simplified the notation $\varphi_{BCS} = \varphi$ in comparison to Eq. (2.20). In other words, the state with fixed number of Cooper pairs has completely indefinite phase. The two different superconducting quantum states in Eq. (2.20) and Eq. (2.23) are similar to what we find in a quantum rotor, where the phase of the particle position is described by the angle operator φ and, in the case of a free rotor, the eigenstates of the Hamiltonian

are the state of given angular momentum N (integer number), since the variable phase is compact ($\varphi + 2\pi$ describes the same state as φ). Then, according to quantum mechanics, one can define the phase and number operator that satisfies the relation

$$\left[e^{-i\hat{\varphi}}, \hat{N}\right] = e^{-i\hat{\varphi}} \quad \text{with} \quad e^{i\hat{\varphi}}\hat{N}e^{-i\hat{\varphi}} = \hat{N} - 1\,, \tag{2.24}$$

with the operator $e^{-i\hat{\varphi}}$ acting as $\sum_N |N-1\rangle\langle N|$. This quantum phase-number uncertainty relation is at the basis of the quantum behavior of the Josephson junction of small capacitance. In an isolated (ideal) Josephson junction, one sets the phase-difference operator $\Delta\hat{\varphi} = \hat{\varphi}_L - \hat{\varphi}_R$ as well as the number difference operator $\Delta\hat{N} = \hat{N}_L - \hat{N}_R$. In this way, one can heuristically obtain the standard model Hamiltonian that describes the Josephson tunnelling junction

$$\hat{H}_{JJ} = \frac{(2e)^2\left(\Delta\hat{N}\right)^2}{2C} - E_J\left[\sum_N |\Delta N - 1\rangle\langle\Delta N| + \text{c.c.}\right] \equiv \frac{\hat{Q}^2}{2C} - E_J\cos\left(\Delta\hat{\varphi}\right)\,, \tag{2.25}$$

where C is the junction capacitance (playing the role of the mass of the rotor) and E_J the Josephson energy (playing the role of the potential energy of the pendulum). The model Eq. (2.25) is justified rigorously by a theoretical calculation based on a microscopic tunnelling Hamiltonian between two BCS superconductors including the charge interaction at the junction [82]. The important degree of freedom in a Josephson junction is thus the difference between the phases of the two superconducting electrodes.

If the junction has a sufficiently large (mass) capacitance, the dynamics is determined by a classical equation of motion that describes the balance of currents. However, in a small-capacitance junction, a quantum mechanical description is needed [82]. The quantum regime requires low temperature (viz. small capacitance), such that the charging energy $\sim e^2/C \gg k_B T$ [78, 82]. Simply put, one recovers a classical description of the pendulum - affected by dissipation and noise - if the temperature is larger than the typical variation in the kinetic energy [88].

The Hamiltonian Eq. (2.25) serves as the starting point to address the problem of quantum Brownian motion when one takes into account that the Josephson junction is affected by dissipative interaction with an external electromagnetic environment. In many theoretical approaches, on the basis that the temperature is much smaller than the superconducting energy gap and the system is at thermal equilibrium, the population of quasi-particles is assumed to be exponentially small, and one focuses on the dissipation related to the external resistors wired to the junction in the circuit. Although it is now known that a nonequilibirum residual quasi-particle distribution can be present in real devices, with drastic effects on the performance of the superconducting qubits [143–146], it turns out that the model of *large gap* (or no quasi-particle dissipation) as given by Eq. (2.25) is expected to be appropriate for studying the quantum dissipative dynamics (quantum Brownian motion) as long as the external dissipation dominates over the effects of the quasi-particles - for instance, if an external resistance shunted in parallel to the Josephson junction is smaller than the resistance associated with the quasi-particles.

2.5 Quantum phase slips

One-dimensional Josephson junction chains are an experimental realization of the 1D quantum phase model that represents a paradigmatic statistical model for illustrating quantum phase transitions [147] and the mapping from a 1D quantum system to a 1D+1 classical one [148]. The theory (for a chain of infinite length, viz. the thermodynamic limit) predicts a quantum phase transition [149]. This corresponds to a superconductor-insulator transition and occurs due to the competition of the Josephson coupling, which enhances global phase coherence, and the electrostatic interaction, which inhibits Cooper pair tunnelling and promotes the charge localization.

In article 13 on the publication list, I studied the effects of nonlinear quantum phase fluctuations, also known as quantum phase slips, in a closed Josephson junction chain (ring) of finite length (N junctions) and threaded by a magnetic flux Φ_B, see Fig. 2.1(a). Using the path integral technique, in the superconducting phase in which the Josephson energy is larger than the charging energy, I calculated the quantum phase slip amplitude. As discussed in detail below, the presence of quantum phase slips changes the ground state energy of the ring, which is directly related to the flux-dependent supercurrent circulating through it $I(\Phi_B)$, see Fig. 2.1(c,d). The main result is that these quantum phase fluctuations in finite systems lead to a remarkable reduction in the maximal supercurrent, see Fig. 2.1(d). I found a non-monotonic behavior of I_{max} increasing the length N. These theoretical results have foreseeable and realistic applications in experimental devices studied in the laboratory that are formed by a finite number N of junctions.
The physics of quantum phase slips is also important in bosonic cold atoms trapped in ring-shaped optical lattice potentials [150–155].

A fundamental contribution on this topic was the work by Matveev et al. [115], who studied quantum phase-slip (QPS) processes in a superconducting nanoring containing a large but finite number of Josephson junctions $N \gg 1$. In my work 13, I went beyond this study to take into account the collective nature of a quantum phase slip, as explained in detail in the next section. In particular, I show relevant finite size effects in a chain of intermediate size, and I also consider the decisive role of the ground capacitance C_0 that was neglected in [115].

Quite simply, a quantum phase slip can be described as a winding by almost 2π (tunnelling) of the phase difference of a single junction, accompanied by a small harmonic displacement of the phase difference in the other $N-1$ junctions, see Fig. 2.1(b). This is a quantum tunnelling between two distinct classical states of the ring with different supercurrents, at given magnetic flux, with which a quantum amplitude is associated. Tunnelling here is possible due to the finite junction mutual capacitance C, which plays the role of inertia. The dynamics $N-1$ junctions are described by a set of harmonic modes (forming the continuum spectrum of the gapless Mooij-Schön modes at finite C_0

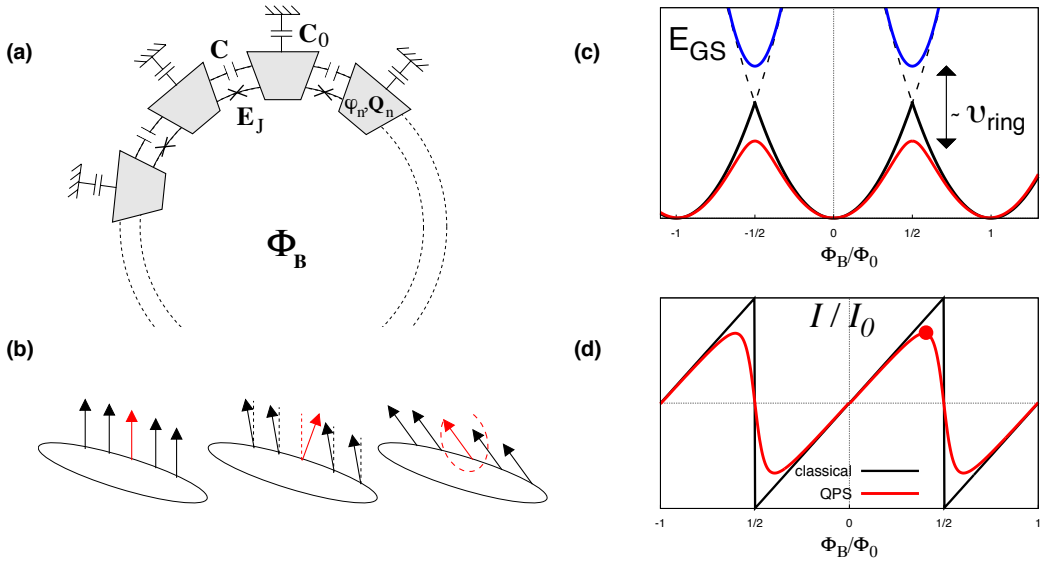

Figure 2.1: **(a)** Ring formed by N superconducting islands separated by N Josephson junctions and threaded by a magnetic flux Φ_B. E_J is the Josephson energy, C the junction capacitance and C_0 the ground capacitance. φ_n and Q_n are, respectively, the superconducting phase and the charge of the $n-$ island. **(b)** The arrows show the phase differences $\Delta\varphi_n = \varphi_{n+1} - \varphi_n$. In the absence of quantum phase fluctuations, the ground state has a uniform distribution of $\Delta\varphi_n^{(m)} = \bar{\theta}_m$ that characterizes the classical state m of the ring. After a quantum phase slips occurs, with the center in one (red) junction, the distribution changes and the ring is in a different classical state (for instance, $m+1$). **(c)** Qualitative behavior of the ground state energy as a function of the magnetic flux Φ_B without quantum phase slips (black line) and including quantum phase slips (red line). The parameter $\nu_{ring} = N\nu$ is the total phase slip amplitude (see text). **(d)** Qualitative behavior of the supercurrent of the ground state as a function of Φ_B scaled with I_0 the maximum classical supercurrent in a ring of size N without quantum phase slips. In the presence of quantum phase slips, the maximum supercurrent is reduced (red dot).

for $N \to \infty$). At finite C_0, this environment contribution leads to a logarithmic divergence in the formula of the phase slip amplitude increasing the chain length. In my article 13, I showed that this logarithmic divergence appears in the semiclassical action of the path integral that controls the quantum phase slip amplitude. Non-logarithmic contributions to the semiclassical action have also been calculated recently [156].

The theoretical model is a homogeneous ring formed by N superconducting islands, separated by N Josephson tunnel junctions, see Fig. 2.1(a). The electrostatic interaction between the metallic islands is modeled by a neighboring capacitance C and by a local ground capacitance C_0, with $E_C = e^2/2C$ and $E_0 = e^2/2C_0$ the corresponding charging

energies. The quantum phase model is [106]

$$H = \frac{1}{2}\sum_{n,m=0}^{N-1} \hat{Q}_n \bar{\bar{C}}^{-1}_{nm} \hat{Q}_m - E_J \sum_{n=0}^{N-1} \cos\left(\Delta\hat{\varphi}_n + \frac{2\pi\Phi_B}{N\Phi_0}\right). \tag{2.26}$$

For each island, the BCS condensate phase $\hat{\varphi}_n$ and the excess charge $\hat{Q}_n$ on the nth island represent the two conjugate variables of the system $[\hat{\varphi}_n, \hat{Q}_n] = 2ei$. $\bar{\bar{C}}$ is the capacitance matrix with matrix elements $\bar{\bar{C}}_{n,m} = (C_0 + 2C)\delta_{n,m} - C(\delta_{n+1,m} + \delta_{n-1,m})$, with the index $n = -1$ corresponding to $N-1$ and $n = 0$ corresponding to N. The relative phase-difference across the nth junction is $\Delta\hat{\varphi}_n = \hat{\varphi}_{n+1} - \hat{\varphi}_n$ for which we have the constraint $\sum_{n=0}^{N-1} \Delta\hat{\varphi}_n = 2\pi m$, where m is an integer [78]. The ground state energy of the ring is directly related to the supercurrent circulating within it

$$I_{GS}(\Phi_B) = \frac{\partial E_{GS}(\Phi_B)}{\partial \Phi_B}. \tag{2.27}$$

E_{GS} and I_{GS} depend periodically on the external magnetic flux Φ_B.

In the classical limit, achieved by neglecting the electrostatic interaction in Eq. (2.26), a given configuration of the phases corresponds to a real physical state *only if* the constraint is satisfied. The minima of the Josephson potential energy in Eq. (2.26), satisfying the constraint, are the classical states of the ring and correspond to uniform distributions of the phase difference $\Delta\varphi_n^{(m)} = \theta_m = 2\pi m/N$ with integer m. They have energy E_m and supercurrent I_m. For fixed flux, the classical ground state has the lowest classical energy $E_{GS}^{(cl)} = \min_m E_m$ with supercurrent $I_{GS}^{(cl)} = \partial E_{GS}^{(cl)}/\partial\Phi_B$. Qualitative behaviors are shown as solid black lines in Fig. 2.1(c,d).

For finite C, C_0, the electrostatic interaction acts as an inertial term on the phases such that quantum fluctuations occur. A priori, a quantum phase slip is a collective process corresponding to the *quantum tunneling in a multidimensional space* of dimension N between two distinct minima of the Josephson potential energy, for instance, between the classical states m and $m+1$. However, due to the constraint relating the phases and the fact that such quantum fluctuations are *rare* (as I explain below), the multidimensional tunneling is reduced to one-dimensional tunneling in which we have only a few relevant trajectories connecting the two states. A possible trajectory is, for instance, when the local phase difference $\Delta\varphi_{n_0}$ at the junction n_0 (the center of the phase slip) winds by an amount of $2\pi(1+1/N)$ and the whole set of phase differences $\{\Delta\varphi_n\}$ $(n \neq n_0)$ shifts in order to preserve the constraint, see Fig. 2.1(b). Such a trajectory is characterized by a quantum amplitude ν.

In the limit $E_J \gg E_C, E_0$, a simple analysis is possible, since the quantum amplitude for this tunnelling event is exponentially small in the ratio E_J/E_C (or E_J/E_0 for not overly long chains, see below), and ν can be computed using the path integral method. However, the total amplitude connecting the classical states is related to the sum of the amplitudes associated with the different trajectories. This total amplitude is simply $\nu_{ring} = N\nu$, since

the system is homogenous and the single trajectory (phase slip event) can occur in any of the junctions, viz. the amplitudes of the single trajectory add up coherently.

The ground state can be obtained by solving the low-energy tight-binding Hamiltonian [115]

$$E_m c_m - N\nu\,(c_{m+1} + c_{m-1}) = E_{GS}\, c_m\,. \tag{2.28}$$

As a consequence, the quantum ground state corresponds to a superposition of different classical states, and this leads to a reduction in the supercurrent. This effect is always dominant close to half flux quantum, where degeneracy of the classical ground states occurs. In summary, by knowledge of ν, we can compute the magnetic flux dependence of the supercurrent of the ground state of the ring in the presence of quantum phase slips.

2.5.1 Single phase slip amplitude

The single quantum phase slip amplitude ν can be computed using the path integral method (more technically, the semiclassical instanton method) in the limit where the Josephson coupling energy E_J dominates over the charging energies, such that the amplitude for QPS to occur is exponentially small. In the phase slip trajectory, the phase differences of the other junctions will vary only slightly $\sim 1/N$. Hence, we can apply the harmonic approximation to describe the dynamics in the junctions $n \neq n_0$. In this way, the Euclidean action used in the path integral is formed by three terms: the first one is related to the junction n_0 (the center of the phase slip) with a nonlinear potential, the second one describes the harmonic modes in the rest of the ring $n \neq n_0$, and the third one is the linear coupling between n_0 and $n \neq n_0$. This is similar to the action of the Caldeira-Leggett model, in which the electromagnetic environment is formed by a set of independent harmonic oscillators acting as an external bath on the winding junction. Then, in the path integral formalism, the harmonic variables can be integrated out and the partition function reads as

$$\mathcal{Z} \sim \mathcal{Z}_{har}^{(N-2)} \oint \mathcal{D}[\theta(\tau)]\, e^{-S_{eff}[\theta(\tau)]}\,, \tag{2.29}$$

where $\mathcal{Z}_{har}^{(N-2)}$ is a partition function of $N-2$ harmonic oscillators, and the effective action for the winding phase difference θ is given by

$$S_{eff} = \int_0^\beta d\tau \left[\frac{\hbar^2}{8e^2}\left(\frac{NC}{N-1} + \frac{C_0}{2}\right)\dot{\theta}^2 - E_J\cos(\theta) + \frac{E_J(\delta_m - \theta)^2}{2(N-1)}\right] + \frac{1}{2}\int_0^\beta d\tau \int_0^\beta d\tau'\, G(\tau-\tau')\theta(\tau)\theta(\tau')\,, \tag{2.30}$$

with $\delta_m = 2\pi\Phi_B/\Phi_0 + m$ and the non-local in time kernel $G(\tau)$, which can be expressed in terms of the Fourier series $G(\tau) = \sum_\ell (1/\beta) G_\ell \exp(i\omega_\ell \tau)$ with $\omega_\ell = 2\pi\ell/\beta$ the Matsubara

frequencies and G_ℓ given by

$$G_\ell = \frac{\hbar^2}{4e^2}\, C_0 \left[\frac{\omega_\ell^2}{2(N-1)}\right] \sum_{k=1}^{k_{max}} \frac{1+\cos\left(\frac{2\pi k}{N-1}\right)}{1-\cos\left(\frac{2\pi k}{N-1}\right)+\frac{\pi^2}{2\lambda^2}\left(\frac{\omega_\ell^2}{\omega_\ell^2+\omega_p^2}\right)}\,, \tag{2.31}$$

with $\lambda = \pi\sqrt{C/C_0}$ and $k_{max} = (N-3)/2$ for odd N or $k_{max} = (N-2)/2$ for even N. Using a transformation, one can show that $G(\omega) = \omega^2 G'(\omega)$, whichs means that the non-local term can be written as $\sim G'(\tau-\tau')\dot{\theta}(\tau)\dot{\theta}(\tau')$. In other words, this term is invariant under a shift of the winding phase $\theta \to \theta + \text{const.}$.

2.5.2 Scaling of the supercurrent

For vanishing ground capacitance C_0, the kernel vanishes ($G_\ell = 0$) in Eq. (2.30), and the effective Lagrangian Eq. (2.30) reduces to the first term: a phase tunnelling in a potential with a renormalized capacitance (mass). In the limit $N \to \infty$ finite size corrections vanish, and we recover the simple action for the single Josephson junction of capacitance C.

From Eq. (2.30), we see that a finite value for N increases the inertial mass C^*/C of the winding phase, leading to a reduction in the charging energy

$$\frac{E_C^*}{E_C} = 1 - \frac{1}{N}\,. \tag{2.32}$$

For the potential in the first term of Eq. (2.30) $V(\theta) = -E_J\cos\theta + E_J(\delta_m-\theta)^2/[2(N-1)]$, one can show that it is a symmetric double well at half flux quantum (close to the degeneracy point of two classical states). Even if $V(\theta)$ is not purely sinusoidal, it is very well approximated by a renormalized cosine potential with a renormalized Josephson energy (energy barrier separating the two wells):

$$\frac{E_J^*}{E_J} = \frac{1}{2}\left[1+\cos\left(\frac{\pi}{N}\right) - \frac{\pi^2}{2N^2}\,(N-1)\right] \simeq 1 - \frac{\pi^2}{4N}\,. \tag{2.33}$$

Another effect that enhances the tunnelling amplitude is the reduction in the distance between the two minima of the effective potential $V(\theta)$, s

$$\frac{\Delta\theta^*}{2\pi} = 1 - \frac{1}{N}\,. \tag{2.34}$$

The three different effects given by Eqs. (2.32), (2.33) and (2.34) combine in the final expression for the renormalized effective amplitude of the quantum tunnelling between the two degenerate minima:

$$\nu_N = \sqrt{\frac{2\pi}{\Delta\theta^*}}\frac{4}{\sqrt{\pi}}\left(8E_J^{*3}E_C^*\right)^{\frac{1}{4}} e^{-\left(\frac{\Delta\theta^*}{2\pi}\right)\sqrt{8\frac{E_J^*}{E_C^*}}} \qquad \left(\overset{N\to\infty}{\longrightarrow} \nu_0 = \frac{4}{\sqrt{\pi}}\left(8E_J^3E_C\right)^{\frac{1}{4}} e^{-\sqrt{8\frac{E_J}{E_C}}}\right). \tag{2.35}$$

The amplitude Eq. (2.35) decreases with the length N, indicating that the latter effects (reduced barrier height and distance between minima) dominate the capacitance renormalization. Because the ground state energy is ruled by the product $\nu_N N$, the maximum supercurrent has a non-monotonic dependence on the total length N.

Increasing the length (more precisely for $N^2\nu \sim 2\pi^2 E_J$), the maximum supercurrent shifts from the half flux quantum (the point of classical degeneracy). The current-phase relation is strongly modified passing from a sawtooth to a sinusoidal function [115], see Fig. 2.1(d). The potential $V(\theta)$ is asymmetric, and one must calculate the renormalized amplitude ν_{as}.
However, by increasing the length N of the system, the finite size effects discussed above at half quantum flux vanish as $1/N$. In my work I showed that the finite-size corrections due to the asymmetry of the barrier vanish more rapidly, specifically as $1/N^2$. Consequently, one can neglect the difference between ν_{as} and ν_N. To demonstrate the latter result, I used the fact that, for an asymmetric potential, the tunnelling energy splitting between the two levels can be expressed as a geometrical average

$$\nu_{as} \simeq \sqrt{\nu_L \nu_R}\,, \tag{2.36}$$

where ν_L and ν_R represent the tunnelling energy splitting for two symmetric double-well potentials s obtained by mirroring the asymmetric double-well potential of interest. Despite the fact that quantum tunnelling has been studied since the advent of quantum mechanics, I could not find in the literature (or textbooks) a simple formula for tunneling in generic asymmetric double-well potentials (without dissipation). I therefore derived the analytical formula Eq. (2.36) based on the Wentzel-Kramers-Brillouin semiclassical approach for this kind of problem. This is reported in my article 14 on the publications list. In this work I also examined two different examples of asymmetric potentials: the cases in which the two localized levels are degenerate, and that in which they are not degenerate.

Restoring the ground capacitance C_0 in the problem, we focus on the analysis of the case at half flux quantum $\delta = \pi$. Using the semiclassical instanton approach [157, 158], the QPS amplitude reads as

$$\nu = A \exp\left[-S_{eff}^{(cl)}/\hbar\right], \tag{2.37}$$

where $S_{eff}^{(cl)}$ is the effective action evaluated at the *classical* path $\theta_{cl}(\tau)$, the asymptotic path that minimizes the action and connects the two relevant minima in the limit $\beta \to \infty$, *i.e.*, the instanton solution. The prefactor A is related to the quantum fluctuations around this minimum path [137]. The *classical* path in a cosine potential in the presence of a non-local in time kernel in the action is generally not solvable. To analyze the scaling behavior of the phase slip amplitude, I used a parabolic approximation by using an effective double well described by two parabolas that mimic the potential $V(\theta)$. In this case, the *classical* path can be calculated exactly even with the kernel non-local in time [159]. For further technical details, I refer to my paper 13.

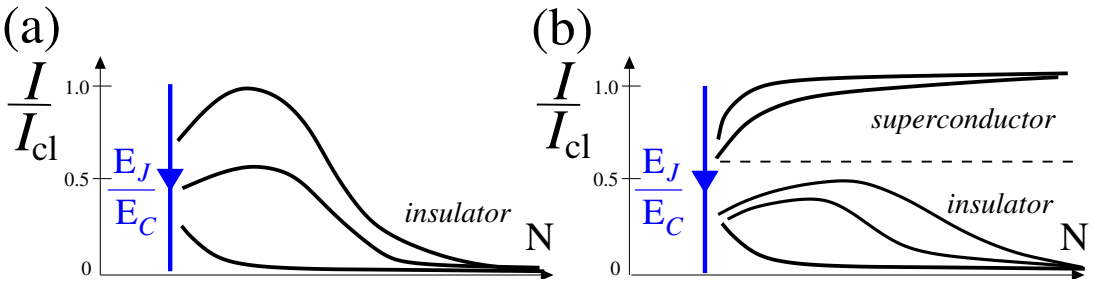

Figure 2.2: Schematic picture of the maximum supercurrent in Josephson junction rings (scaled with the maximum classical value $I_{cl} = \pi I_J/N$ without quantum phase slips) as a function of the size N. E_J is the Josephson energy and E_C is the charging energy associated with the junction capacitance. **(a)** Vanishing ground capacitance $C_0 = 0$. Finite size effects give rise to a nonmonotonic dependence at large ratio E_J/E_C. **(b)** Finite ground capacitance $C_0 = C/2$ ($E_0 = 2E_C$). Depending on the ratio $E_J/E_C = 2E_J/E_0$ the scaling of the supercurrent has a different asymptotic behavior as increasing N.

In Fig. 2.2, I report a summary that outlines the main results. In Fig. 2.2(a) the case $C_0 = 0$ is shown. In this limit, when $N \gg 1$, finite size effects vanish ,and ν_N converges to the constant ν_0, such that $N\nu_N$ increases with the length and the maximum supercurrent $I_{\max}$ vanishes exponentially, see Fig. 2.2(a), at large $N \gg 1$. However, as we have discussed above, in finite systems we find a *reduction* of the effective QPS amplitude ν_N by *increasing* the size N, and the final outcome is that the maximum supercurrent $I_{\max}$ shows a non-monotonic behavior as a function of N for sufficiently large values of the ratio E_J/E_C.

An example of the behavior at $C_0 \neq 0$ is given in Fig. 2.2(b). When the capacitance to ground C_0 is restored, the winding junction and the $N-1$ harmonic junctions interact directly. This leads to the appearance of an ensemble of dispersive electrodynamics modes, similar to the case of a Josephson junction coupled to a (finite length) LC-transmission line.

The tunneling phase couples to these modes in much the same way as a quantum particle to a harmonic bath in the Caldeira-Leggett model. In particular, one can show that the low-frequency modes with linear dispersion give rise to a finite friction for the tunnelling phase dynamics in the limit $N \to \infty$.

At finite N, the coupling with the low-frequency modes strongly affects the quantum phase slip amplitude. Indeed, one obtains the following scaling for the phase slip amplitude: $\nu \sim \nu_0/N^\alpha$ for $N \gg 1$ where $\alpha \propto (E_J/E_0)^{1/2}$. Depending on the value of α, the total phase slip amplitude $N\nu(N) \sim N^{1-\alpha}$ that determines the low-energy properties of the system (ground state and its supercurrent) either tends to zero, when $\alpha \gg 1$, or grows linearly, when $\alpha \ll 1$, indicating that the system either displays superconducting or insulating behavior, as can be seen in Fig. 2.2(b). This behavior is reminiscent of the dissipative phase transition [85] occurring in a single junction in an electromagnetic environment

[157, 158]. For intermediate sizes of the ring, finite size effects occur, yielding a non-monotonic behavior of the maximum supercurrent in the insulating regime, similar to what happens in the case $C_0 = 0$.

2.6 Dissipative frustration in quantum systems

2.6.1 Noncommuting dissipative interactions

Remarkably, an open quantum system coupled to two independent environments by canonically conjugate operators shows an enhancement of the quantum fluctuations. This result can be understood by considering the two baths as two detectors continuously coupled to the system and measuring two noncommutating observables simultaneously. This frustration of decoherence and dissipation can be attributed to the noncommuting nature of the conjugate coupling operators that prevents the selection of an appropriate pointer basis to which the quantum system could relax.

For the quantum damped harmonic oscillator, it is known that the quantum fluctuations of the operator to which the bath is coupled are squeezed and those of its conjugate variable are enhanced in such a way that the Heisenberg uncertainty principle holds [88]. In my work 10 on the publications list, I considered a symmetric environmental coupling for the position $\hat{q}$ and for the momentum $\hat{p}$ of a quantum harmonic oscillator in the case of ohmic dissipation with a Drude large frequency cut-off. I obtained analytical formulas that allow detailed analysis of the enhancement of the quantum fluctuations and the role of the temperature as well as that of the high-frequency cut-off of the bath's spectrum. The analytic results show that such quantum fluctuations (squeezed or enhanced) are observable at low temperatures $T < T^*$, where T^* is the typical temperature below which finite temperature corrections are negligible and the fluctuations of the particle are controlled by the quantum contribution.

I generalized the Caldeira-Leggett model considering two baths forming two separate sets of harmonic oscillators. The starting model Hamiltonian is

$$\begin{aligned}\hat{H}_g = \frac{\hat{p}^2}{2m} + \frac{m\omega_0^2}{2}\hat{q}^2 + \sum_n \left[\frac{\hat{P}_{q,n}^2}{2m_{q,n}} + \frac{1}{2} m_{q,n}\omega_{q,n}^2 \left(\hat{Q}_{q,n} - \frac{\lambda_{q,n}\hat{q}}{m_{q,n}\omega_{q,n}^2} \right)^2 \right] \\ + \sum_n \left[\frac{1}{2m_{p,n}} \left(\hat{P}_{p,n} - \frac{\lambda_{p,n}\hat{p}}{m\omega_{p,n}\omega_0} \right)^2 + \frac{1}{2} m_{p,n}\omega_{p,n}^2 \hat{Q}_{p,n}^2 \right]\end{aligned} \tag{2.38}$$

with the two conjugate operators $[\hat{q}, \hat{p}] = i\hbar$ and the interaction with the environment described by two ensembles of independent harmonic oscillators with the conjugate operators $[\hat{Q}_{\nu,n}, \hat{P}_{\nu,n'}] = i\hbar\delta_{\nu,\nu'}\delta_{n,n'}$ where $\nu = q, p$ are the two bath indices. Using the equations of motion in the Heisenberg picture $\hat{O}(t) = e^{iHt/\hbar}\hat{O}e^{-iHt/\hbar}$, one obtains a generalized

quantum Langevin equation:

$$\frac{d\hat{p}(t)}{dt} = -m\omega_0^2\hat{q}(t) + \hat{F}_q(t) - \int_{t_0}^{+\infty} dt'\,\eta_q(t-t')\,m\frac{d\hat{q}(t')}{dt'}\,, \tag{2.39}$$

$$m\frac{d^2\hat{q}(t)}{dt^2} = \frac{d\hat{p}(t)}{dt} + \hat{F}_p(t) + \int_{t_0}^{+\infty} dt'\,\eta_p(t-t')\,\frac{1}{\omega_0^2}\frac{d^2\hat{p}(t')}{dt'^2}\,, \tag{2.40}$$

in which we have introduced t_0 as the initial time for the interaction and the two response functions of the two baths with a form similar to Eqs. (2.3) and (2.4) and characterized by the two damping parameters γ_q and γ_p. To simplify, I assumed the same high frequency cut-off ω_c.
Assuming as initial state the total density matrix factorized as $\rho_{t_0} = \rho_0\rho_q\rho_p$ with ρ_0 the initial state of the oscillator and $\rho_{q,p}$ the thermal density matrices for the two baths $\rho_\nu \propto \exp(-\beta\sum_n \omega_{\nu,n}\hat{a}^\dagger_{\nu,n}\hat{a}_{\nu,n})$, the correlation functions of the noise operators read as

$$\langle\hat{F}_\nu(\omega_1)\hat{F}_\nu(\omega_2)\rangle = (2\pi)^2\delta(\omega_1+\omega_2)\left[\delta_{\nu q} + \left(\frac{\omega}{\omega_0}\right)^2\delta_{\nu p}\right]S_\nu(\omega_1)\,, \tag{2.41}$$

with the noise spectral function $S_\nu(\omega_1)$ similar to Eq. (2.6) for $\nu = q, p$.

Assuming $t_0 \to -\infty$, the generalized quantum Langevin equations (2.39) and (2.40) can be solved using the Fourier transform, and it is possible to compute the correlation functions of the oscillators for arbitrary products of the position and momentum. In particular, the two fluctuations of the position and momentum, after some algebra, are

$$\begin{bmatrix} \langle\hat{Q}^2\rangle \\ \langle\hat{P}^2\rangle \end{bmatrix} = \begin{bmatrix} \langle\hat{q}^2\rangle/q_0^2 \\ \langle\hat{p}^2\rangle/p_0^2 \end{bmatrix} = -\frac{1}{\pi\omega_0}\int_{-\infty}^{+\infty} d\omega\,\coth(\beta\omega/2)\,\mathrm{Im}\left(\frac{1}{D(\omega)}\begin{bmatrix} \omega_0^2 + i\omega\eta_p(\omega) \\ \omega_0^2 + i\omega\eta_q(\omega) \end{bmatrix}\right) \tag{2.42}$$

with the normalization $q_0^2 = \hbar/(2m\omega_0)$ and $p_0^2 = m\hbar\omega_0/2$ and the Heisenberg's uncertainty relation in the form $\langle\hat{Q}^2\rangle\langle\hat{P}^2\rangle \geq 1$. The denominator is given by

$$D(\omega) = \omega_0^2 - \omega^2 + i\omega[\eta_q(\omega) + \eta_p(\omega)] - \frac{\omega^2}{\omega_0^2}\eta_q(\omega)\eta_p(\omega)\,. \tag{2.43}$$

Provided that the poles of the functions $D(z)$ - with z complex - always have the same sign for the imaginary part, then we can calculate the integral using the residues theorem for a closed curve lying only in one half of the complex plane that contains only the poles of function $\coth(\beta\omega/2)$. The latter correspond to the Matsubara frequencies $z_k = i\omega_k = i2\pi k/\beta$ with integer k

$$\begin{bmatrix} \langle\hat{Q}^2\rangle \\ \langle\hat{P}^2\rangle \end{bmatrix} = \frac{2}{\beta\omega_0} + \frac{4}{\beta\omega_0}\sum_{k=1}^{+\infty}\frac{1}{D(-i\omega_k)}\begin{bmatrix} \omega_0^2 + \omega_k\eta_p(-i\omega_k) \\ \omega_0^2 + \omega_k\eta_q(-i\omega_k) \end{bmatrix}\,. \tag{2.44}$$

The formulas for the two quadratures are symmetric under interchange of the two response functions $\eta_q \leftrightarrow \eta_p$, i.e.

$$\langle\hat{Q}^2\rangle = \sigma(\eta_q,\eta_p) \equiv \sigma_q\,, \quad \langle\hat{P}^2\rangle = \sigma(\eta_p,\eta_q) \equiv \sigma_p\,. \tag{2.45}$$

Due to this symmetry, hereafter we discuss the function σ_q. It should be noted that the result (2.44) can be also obtained using the path integral. This confirms the initial assumption that the poles of the functions $D(z)$ always have the same sign for the imaginary part (as it is also possible to show explicitly in the ohmic case).

Formula 2.44 is valid for an arbitrary spectral environmental function. For the ohmic case, the Eq. (2.44) reads explicitly as

$$\sigma_q = \frac{2}{\beta\omega_0} + \frac{4}{\beta\omega_0}\sum_{k=1}^{+\infty} \frac{\omega_0^2(\omega_c+\omega_k)^2 + \gamma_p\omega_k\omega_c(\omega_c+\omega_k)}{(\omega_k^2+\omega_0^2)(\omega_c+\omega_k)^2 + (\gamma_q+\gamma_p)\omega_k\omega_c(\omega_c+\omega_k) + \omega_k^2(\frac{\gamma_q\gamma_p}{\omega_0^2})\omega_c^2}\,. \quad (2.46)$$

The sum over the Matsubara frequencies Eq. (2.46) can be carried out analytically if one introduces the frequencies Ω_i as the negative roots of the quartic polynomial in ω_n of the denominator appearing in Eq. (2.46).

For sufficiently high temperature, such that $\beta\Omega_i/(2\pi) \ll 1$ for $i = 1, \ldots, 4$, the theoretical formula recovers the result of the equipartition theorem (the classical limit). Going further in the high-temperature expansion, one can obtain quantum corrections to the classical result that are proportional to the thermal de Broglie wavelength

$$\langle q^2\rangle_{high-T} = \frac{k_BT}{m\omega_0^2} + \frac{1}{6}\left(\frac{\hbar^2}{2mk_BT}\right)\left(1+\frac{\gamma_p\omega_c}{\omega_0^2}\right) \quad (2.47)$$

Even if the temperature is relatively high $k_BT \gg \hbar\omega_0$, quantum corrections due to the dissipative interaction can become parametrically relevant in the presence of the interaction with a second bath via the momentum operator for $\gamma_p\omega_c/\omega_0^2 \sim 1$. The result (2.47) represents the dual expression of the standard, damped harmonic oscillator with ohmic-Drude dissipation, for which we have $\langle p^2\rangle_{high-T} \simeq \langle p^2\rangle_{(cl)} + m\gamma_q\omega_c\hbar^2/(12k_BT)$ [88] in the limit $\omega_c \gg (\omega_0, \gamma_q)$.

In the opposite low-temperature regime, defined by $\beta\Omega_i/(2\pi) \gg 1$ for $i = 1, \ldots, 4$, one obtains quadratic corrections in T:

$$\sigma_q^{(low-T)} = \sigma_q^0 \; + \frac{2\pi}{3}\left(\frac{\gamma_q}{\omega_0}\right)\left(\frac{k_BT}{\hbar\omega_0}\right)^2. \quad (2.48)$$

Thus, for sufficiently low temperature $T \ll T_q^*$, defined by

$$T_q^* = \min\left[\{\hbar|\Omega_i|\}, \sqrt{\frac{3\omega_0}{2\pi\gamma_q}}\hbar\omega_0\right] \quad (i = 1, \ldots, 4)\,, \quad (2.49)$$

we can neglect the finite temperature effects for the fluctuations of the position operator $\hat{q}$. By interchanging the damping coefficients $\gamma_q \leftrightarrow \gamma_p$, a similar expression holds for the temperature threshold T_p^* for the quantum regime and for the quantum fluctuations σ_p^0 of the momentum operator $\hat{p}$.

In the limit of low temperature, we can focus on the ground state fluctuations in the different regimes. When one dissipative coupling overhelms the second dissipative interaction, one recover the results of a harmonic oscillator coupled to a single bath. This limit is defined by $\gamma_p \ll (\omega_0/\omega_c)^2\gamma_q/4$ (viz. the bath coupled to the oscillator via the position $\hat{q}$ dominates) or equivalently by $\gamma_q \ll (\omega_0/\omega_c)^2\gamma_p/4$ (viz. the bath coupled to the oscillator via the momentum $\hat{p}$ dominates). In these regimes, one of the two fluctuations of the oscillator is quenched $\langle\hat{Q}^2\rangle < 1$ *or* $\langle\hat{P}^2\rangle < 1$: the quantum fluctuations of the quadrature coupled to the bath are squeezed and those of the conjugate variable are enhanced. The more interesting regime is when dissipation leads to the enhancement of both quantum fluctuations, $\langle\hat{Q}^2\rangle \gg 1$ *and* $\langle\hat{P}^2\rangle \gg 1$. This occurs in the cross-over regime when both dissipative interactions are relevant.

Far away from the single bath regime, $|\gamma_q - \gamma_q| < 2\omega_0$, all frequencies are complex, and it is possible to show that the relaxation dynamics of the harmonic oscillator is always underdamped, i.e. the dynamical correlation functions always exhibit an oscillatory decay even for large damping. In the limit $\omega_0, \gamma_q, \gamma_p \ll \omega_c$, I obtained the following analytic expression for the zero-temperature fluctuations

$$\sigma_q^0 \approx \frac{2}{\pi(1+\rho^2)}\left[\frac{\gamma_p}{\omega_0}\left(\ln\left(\frac{\omega_c}{\omega_0}\right) + \rho\arctan(\rho) + \ln(1+\rho^2)\right) + \frac{\left(1+\frac{\gamma_p}{\omega_0}\Delta\Gamma_{q,p}\right)}{\sqrt{\left|1-\Delta\Gamma_{q,p}^2\right|}}\mathrm{F}_{q,p}\right] \tag{2.50}$$

with $\rho = \sqrt{\gamma_q\gamma_p}/\omega_0$, $\Gamma = (\gamma_q+\gamma_p)/(2\omega_0)$ and $\Delta\Gamma_{q,p} = (\gamma_q-\gamma_p)/(2\omega_0)$ and

$$\mathrm{F}_{q,p} = \begin{cases} \arctan\left(\sqrt{1-\Delta\Gamma_{q,p}^2}\,/\,\Gamma\right) & \text{for} \quad |\Delta\Gamma_{q,p}| < 1 \\ \operatorname{arctanh}\left(\sqrt{\Delta\Gamma_{q,p}^2-1}\,/\,\Gamma\right) & \text{for} \quad |\Delta\Gamma_{q,p}| > 1 \end{cases} . \tag{2.51}$$

In the regime in which the two dissipative interaction compete, Eq. (2.50) shows that the fluctuations have a *nonmonotic* behavior as increasing the dissipation, keeping constant the ratio γ_p/γ_q, This result was obtained numerically in [160], whereas I provided an analytic formula. The regime of *enhancement* of quantum fluctuations corresponds to the case in which *both* fluctuations of $\hat{q}$ and $\hat{p}$ grow with increasing dissipative coupling constant γ_q and γ_p. An example is shown in Fig. 2.3. We note that the curve $\gamma_q = \gamma_p$ is identical for the position and momentum fluctuations; the other curves appear different, as we plot the fluctuations as a function of the parameter γ_q only.

In summary, I show that in the intermediate range of damping defined by $(\gamma_q, \gamma_p) \sim \omega_0$, it is possible to achieve a strong enhancement of the quantum fluctuations due to the competition between two dissipative interactions through two noncommuting operators. Such dissipative frustration can result in a remarkable effect in the phase diagram of a many-body system, as explained in the next section.

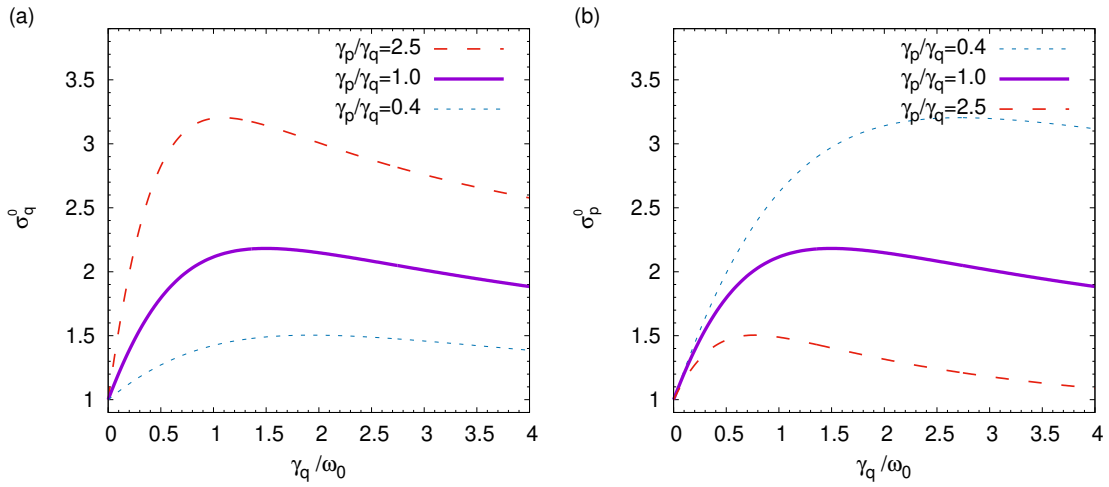

Figure 2.3: Results for the harmonic oscillator of frequency ω_0 with two noncommuting dissipative interactions characterized by the two damping parameters: γ_q (damping related to dissipative coupling through the position) and γ_p (damping related to dissipative coupling through the momentum). The scaled zero-temperature quantum fluctuations of **(a)** $\hat{q}$ and **(b)** $\hat{p}$ in the large cutoff expansion, as a function of the (position) damping γ_q. The different curves are for three different ratios of the two damping parameters $\gamma_p/\gamma_q = 2.5, 1, 0.4$. The cutoff frequency is $\omega_c/\omega_0 = 80$.

2.6.2 Phase diagram of Josephson junction chains

In my work 8 on the publications list, I studied the phase diagram of the dissipative quantum phase transition in a 1D phase model in the presence of dissipative frustration. This system can be simply realized with Josephson junction chains. The main result is that the critical line separating the two phases of the phase diagram is nonmonotonic. Moreover, interesting features occur in two thermodynamics quantities: the purity, which quantifies the degree of correlation between the system and the environment, and the logarithmic negativity, an entanglement measure that encodes the internal quantum correlations.

We consider a Josephson junction chain in the self-charging limit where we disregard capacitances between the islands. This is not relevant for the discussion of the effects of the dissipative frustration on the quantum phase transition in the chain. In this case, the Hamiltonian simplifies to

$$\hat{H}_{JJ0} = \sum_{n=0}^{N-1} \left[\frac{\hat{Q}_n^2}{2C_0} - E_J \cos\left(\Delta\hat{\varphi}_n\right) \right], \tag{2.52}$$

and periodic boundary conditions $\varphi_N = \varphi_0$. In the harmonic regime $E_J \gg E_0$, the intrinsic zero-temperature (quantum) fluctuations of the system are governed by the ratio

$g = \sqrt{E_J/(8E_0)}$ (increasing g, the phase fluctuations decrease). As explained above, the one-dimensional Josephson junction chains show a quantum phase transition, which can be mapped to a classical two-dimensional Berlinski-Kosterlitz-Thouless (BKT) transition, at a critical point g_c. For $g < g_c$, the phases are uncorrelated and the Josephson junction chain is an insulator. For $g > g_c$, the chain is superconducting with a (quasi-long) range ordering.

To discuss the effect of the dissipative frustration, we use the Caldeira-Leggett model and consider local ohmic baths coupled to each phase difference $\Delta\hat{\varphi}_n$ and local ohmic baths coupled to each charge $\hat{Q}_n$ of the superconducting islands. Fig. 2.4(a) shows a possible realization of such a system. The shunt resistance between the superconducting islands R_s leads to a (conventional) dissipation affecting the phase difference, and the resistance to the ground R_g leads to the (unconventional) charge dissipation.

Using the imaginary time path integral formalism, one can represent the partition function as $\mathcal{Z}_{\text{eff}} = \prod_{n=0}^{N-1} \oint_c \mathcal{D}[\varphi_n(\tau)]\ e^{-\mathcal{S}[\{\varphi_n(\tau)\}]/\hbar}$, with the Euclidean action

$$\mathcal{S} = \mathcal{S}_d + \sum_{n=0}^{N-1} \int_0^\beta d\tau \left[\frac{\hbar C_0}{8e^2} \dot{\varphi}_n^2(\tau) - E_J \cos\left(\Delta\varphi_n(\tau)\right) \right], \tag{2.53}$$

where the dissipative part, with the function $F(\tau)$ affecting the phase difference, and the function $\widetilde{F}(\tau)$ affecting the total charge, reads as

$$\mathcal{S}_d = \sum_{n=0}^{N-1} \left[-\frac{1}{2} \int_0^\beta\!\!\int_0^\beta d\tau d\tau'\, F(\tau-\tau') \left|\Delta\varphi_n(\tau) - \Delta\varphi_n(\tau')\right|^2 + \frac{1}{2} \int_0^\beta\!\!\int_0^\beta d\tau d\tau'\, \widetilde{F}(\tau-\tau')\, \dot{\varphi}_n(\tau)\, \dot{\varphi}_n(\tau') \right]. \tag{2.54}$$

Using the Matsubara frequencies $\omega_l = 2\pi l/\beta$ in the frequency space, the function $F(\tau)$ consists of $F_l \propto (R_q/R_s)|\omega_l|$, whereas the function associated with the charge dissipation corresponds to $\widetilde{F}_l \propto -R_g C_0 |\omega_l|/(1 + R_g C_0 |\omega_l|)$. It is natural to define a dissipative parameter for conventional dissipation as $\alpha = R_q/R_s$, and for unconventional dissipation as $\widetilde{\alpha} = R_g/R_q$, with $R_q = h/2e^2$ being the quantum of resistance.

As the partition function of the whole action is not exactly solvable due to the cosine interaction, we use a self-consistent harmonic approximation (SCHA [161]. In this approach, the cosine is approximated by an effective parabolic interaction with variational interaction strength. The SCHA allows determination of a qualitative phase diagram of the Josephson chain. By varying the parameters $\alpha, \widetilde{\alpha}$ and g we can determine a critical value for a phase transition.

The quantum fluctuations of a system affected by dissipative couplings to noncommuting observables can exhibit a non-monotonic behavior as a function of the damping, as explained in the previous section.

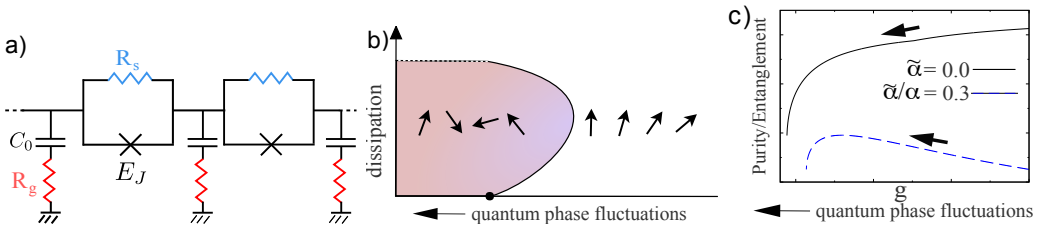

Figure 2.4: **(a)** 1D chain of superconducting islands with Josephson coupling of energy E_J and a capacity to the ground C_0. The shunt resistance R_s corresponds to a dissipative coupling for the difference between the superconducting phases $\Delta\varphi_n = \varphi_{n+1} - \varphi_n$, whereas the resistance to the ground R_g yields a dissipative coupling in the charge Q_n. The dimensionless parameters for the coupling strengths of the two dissipative interactions are, respectively, $\alpha = R_q/R_s$ and $\tilde{\alpha} = R_g/R_q$, with R_q the quantum of resistance. **(b)** Qualitative quantum phase diagram with dissipative frustration, $\alpha \sim \tilde{\alpha}$. **(c)** Qualitative results for the purity and the logarithmic negativity (as an entanglement measure) as functions of $g = \sqrt{E_J/(8E_0)}$ for $\tilde{\alpha} = 0$ and $\tilde{\alpha}/\alpha = 0.3$.

We analyze this dissipative frustration by fixing the ratio $\widetilde{\alpha}/\alpha$. If the quantum fluctuations are too large the phase transition to an insulator occurs. Consequently, this nonmonotonic behavior of the phase fluctuations in the presence of dissipative frustration can lead to a situation in which the system is superconducting for small and large damping but in the intermediate regime is an insulator. Hence, a non-monotonic phase transition line emerges in the phase diagram, see Fig. 2.4(b).

In addition to affecting the phase diagram, dissipation also influences quantum correlations. To study these effects, we calculated the purity as a measure of correlations between the system and the environment and the logarithmic negativity as a measure of entanglement in the Josephson junction chain. As the qualitative behavior of the two quantities is the same, we summarize the results in a single schematic plot in Fig. 2.4(c).

The purity is defined as $\mathcal{P} = \mathrm{Tr}\left(\rho_{sc}^2\right)$, where ρ_{sc} is the reduced density matrix describing the one-dimensional chain within the SCHA. In the non-dissipative case, the chain remains in a pure state and $\mathcal{P} = 1$, whereas for a statistical mixture $\mathcal{P} < 1$. Fig. 2.4(c) shows $\mathcal{P}$ as a function of the parameter g. For conventional dissipation ($\widetilde{\alpha} = 0$), the purity decreases for lower values of g (i.e. enhancing phase fluctuations). Here, conventional dissipation counteracts the increase in the phase fluctuations and leads to an incoherent mixing of the states. In the presence of both dissipative couplings ($\widetilde{\alpha} \neq 0$), the purity increases with decreasing g. The unconventional part of the dissipation acts in favor of an enhancement of phase fluctuations and leads to a more pure state.

We also computed the bipartite entanglement for two subsystems A and B of the ring, namely we have calculated the logarithmic negativity via a partial transposition of the density matrix $\rho_{sc} \to \rho_{sc}^{T_A}$. We cut the ring in two parts, with $N_A + N_B = N$. The

superscript T_A denotes the transposition of the part of ρ_{sc} corresponding to subsystem A. We calculate the covariance matrix $\sigma[\rho_{sc}^{T_A}]$ and with this the logarithmic negativity for Gaussian states $E_{\mathcal{N}}[\hat{\rho}_{sc}] = -\sum_k \log_2(\min[1,(2c_k)])$, where c_k represent the symplectic eigenvalues of the covariance matrix [162].

The amount of entanglement generally depends on the partition of the Josephson junction ring. However, in all the cases, we found a common feature, namely that the purity has the same qualitative behavior as reported in Fig. 2.4(c).
We can explain this result according to the following argument. The Josephson coupling naturally determines correlations in the system. In the same way, the conventional (phase) dissipation enforces correlations, since it favors the phase coherence in the chain. Hence, an increase of the quantum phase fluctuations (a decrease of g) results in a reduction in the correlations. However, quantum correlations cannot be present at all in the pure classical limit, namely when all the phases are aligned. This fact indicates that the quantum correlations are determined by a subtle interplay between the Josephson coupling and the electrostatic interaction. Indeed, the unconventional (charge) dissipation operates in a way very similar to the electrostatic interaction enhancing the quantum phase fluctuations in the system. This explains the different, qualitative scaling of the amount of entanglement in the presence of unconventional (charge) dissipation.

In summary, dissipative frustration on the superconductor-insulator phase transition in a chain of Josephson junctions is achieved via the coupling to the environment through two noncommuting observables. The critical line is nonmonotonic when the ratio of the two dissipative coupling strengths is fixed. This peculiar behavior can be traced back to the nonmonotonic zero-temperature fluctuations yielded by dissipative frustration. Because dissipative frustration is a purely quantum effect, it is interesting to analyze the influence of dissipation on system-environment correlations and on the internal quantum correlations. Indeed, the purity and the logarithmic negativity as functions of the parameter g show different scaling behavior. These results demonstrate that dissipative frustration can lead to interesting effects and novel features in the physics of open quantum many-body systems.

Chapter 3

Future research projects: a few examples

My theoretical questions are inspired by the physics of engineered quantum systems, such as nanoelectromechanical systems, superconducting quantum circuits and qubits, and hybrid photonic systems.

Such systems are fascinating because of their complexity: they typically operate far from equilibrium and can be very strongly nonlinear, allowing us to explore a wide range of quantum dynamical properties.

Another important aspect is that such systems realize artificial many-body systems in which the interacting units must be considered as open/dissipative quantum systems, since their interaction with the environment cannot be neglected.

I am currently interested in: (i) exploring strategies for creating, detecting and eventually controlling quantum states in engineered coherent systems, and (ii) the theoretical understanding of the interplay between quantum coherence, interactions and nonlinearity.

3.1 Electron-vibration interaction: mesoscopic QED

The subject of quantum transport in systems characterized by electron-phonon or electron-photon coupling is a topic in which I have acquired relevant experience in recent years and upon which I plan to base my future research activity.

Cavity QED allowed the study of the light-matter interaction at the most fundamental level. Other systems are based on this architecture, such as superconducting qubits coupled to microwave cavities (circuit QED), in which an artificial atom is integrated into nanocircuits on a chip.

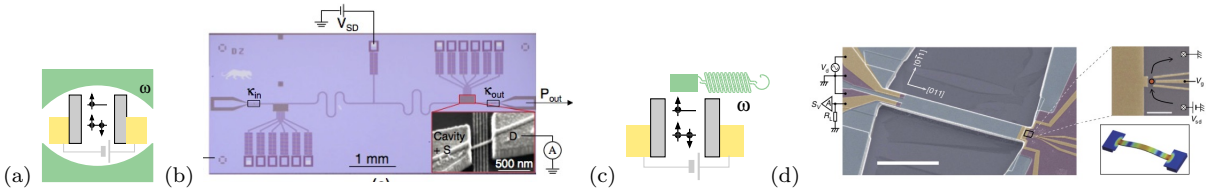

Figure 3.1: Examples of nanoscale hybrid systems formed by quantum dots coupled to localized resonators. **(a)** Cartoon of a photon microwave cavity coupled to a dot. **(b)** Optical micrograph of a semiconductor double quantum dot embedded in a high-quality-factor microwave cavity (from [163]). **(c)** Cartoon of a mechanical nanoresonator coupled to a dot. **(d)** Scanning electron microscope image of a device formed by a gate-defined quantum dot integrated into a piezoelectricity-based mechanical resonator (from [27]).

More recently, a new architecture has been realized with experimental mesoscopic devices in which the superconducting qubit is replaced by a quantum conductor (mesoscopic QED). These hybrid circuits with quantum conductors coupled to localized harmonic oscillators - such as microwave photon cavities [34–36] or mechanical resonators [14, 20, 27] - have become commonly studied systems across a number of experiments. A schematic picture of the prototypal system/model is given in Fig. 3.1. A new aspect here is the single-electron quantum transport that occurs in the mesoscopic conductor, with various phenomena (Coulomb blockade, interference effects, etc.). Quantum dots are natural candidates for exploring the rich physics of electron-vibration interaction given their tunability. Their versatility is also a key issue, as it is possible to connect quantum dots at different types of electrodes (normal metal, superconductor or ferromagnet) [35,51]. These systems - which are well controlled and characterized - can be used as ideal platforms to study fundamental questions in condensed matter at the interface between nonlinear quantum dynamics and nonequilibrium regime.

More specifically, these hybrid nanoscale systems combine different types of quantum degrees of freedom and serve as ideal platforms to explore correlations between charge transport and the emitted radiation or the induced mechanical vibrations. I aim to explore several theoretical issues, for example: (i) the nonequilibrium (potentially quantum) states of the oscillator; (ii) the effect of back-action of the oscillator on the transport properties; (iii) the generation of quantum (entangled) states in many oscillator systems; and (iv) nonlinear (anharmonic) effects in quantum oscillators. In this context, a starting model Hamiltonian that captures the essential aspects of the problem is given by

$$H = H_{leads} + H_{tun} + H_{dot} + H_{res} + H_{int}\,, \tag{3.1}$$

with H_{leads} denoting the Hamiltonian of the leads/contacts, H_{tun} the tunnelling part and H_{dot} the dot's Hamiltonian interacting with the resonator H_{res} via H_{int}.

3.1.1 Example of recent results

Hybrid systems combine elemental components with distinct tunable properties, offering a way to explore novel mechanisms of coherent energy exchange. Ultimately, these systems can encode a single-atom laser that exhibits unique features compared to conventional lasers such as the absence of threshold, self-quenching and sub-Poissonian statistics. Single-atom lasers have been realized in cavity QED [164], in circuit QED [103] and recently in double quantum dots coupled to microwave cavities [34, 163].

Recently, together with my PhD student (Mantovani), I studied a spin-valve quantum dot system that can encode an efficient single-atom laser characterized by a dynamical multistability [40], see Fig. 3.2. This represents a significant theoretical advance , since multistability is a peculiar phenomenon that arises in nonlinear driven systems out of equilbrium. Just for comparison, for example, multistability was achieved in cavity QED only by using a controlled steady stream of excited two level atoms interacting sequentially with the field and in a fixed amount of time [165]. Because the electron passage through the dot is a random process, a priori multistability is not evident in quantum dots. We have also demonstrated that multistability is theoretically associated with the breaking down of one of the standard approximations, the so-called Rotating Wave Approximation (RWA), opening new theoretical perspectives for a large class of quantum nanoscale systems (I note that in cavity QED, for instance, multistability occurs but within the RWA).

Research into the behavior of systems beyond the RWA has attracted immense interest recently, though usually this requires the difficult-to-access regime of extremely strong coupling strengths.

In this work [40], I showed that the laser-like dynamics facilitates the breakdown of the RWA at much weaker couplings, thereby opening up a promising route for the study

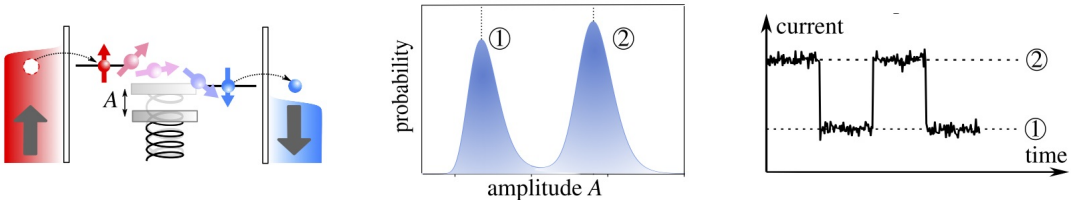

Figure 3.2: **Left:** spin-polarized electrons are injected from a ferromagnetic contact into a quantum dot. The resonator (photon cavity or nanomechanical resonator) interacts with the dot's spin. The system realizes a highly efficient single-atom laser with dynamical multistability. **Center:** In a bistable regime, for instance, the resonator can oscillate in two possible ways, characterized by different amplitudes in the semiclassical picture. These correspond to the two maxima in the distribution of the Fock states. **Right:** Because the charge current is determined by the resonator's state, the current behaves like a *telegraph* when monitored over time, as a manifestation of the lasing bistability regime occurring in the resonator (see [40] for more details).

of unconventional coherent interactions.

3.1.2 Future projects

(A) Switching dynamics in a bistable quantum dot laser

In the abovementioned theoretical works on dynamical multistability in a quantum dot (spin-valve) laser, we solved a density matrix equation for the system of interest (formed by the dot and the oscillator), having traced out the leads. The steady-state solution of such an equation (with the rich phase diagram including different types of multistabilities) was found either numerically or analytically in some limit cases, with an excellent agreement between the two methods. When a (classical or quantum) system becomes, for example, dynamically bistable, a natural theoretical issue is the description of the switching dynamics between the two possible steady states of vibration. These switching dynamics were not investigated in the previous work, which was limited to the analysis of the average steady-state distribution of the resonator?s energy (Fock number distribution).

In an upcoming project, I plan to analyze the switching dynamics in a bistable quantum dot (spin-valve) laser, Fig. 3.3(left). This requires going beyond the computation of the steady-state density matrix to properly take into account the role of the shot-noise associated with the single tunnelling event beyond the average charge current. This objective can be accomplished by deriving a quantum Fokker-Planck equation in the phase space representation (for instance, the Glauber-Sudarshan $P(\alpha)$ representation). By opportunely extending this method in order to include the degrees of freedom of the dot, from preliminary calculations, one can show that such a distribution becomes a tensor $P_{ss'}(\alpha)$. The label s and s' refer to the three possible state of the dot (spin up, spin down and empty, since double occupancy is forbidden by the strong local Coulomb repulsion). The next step is to find a strategy to solve the set of coupled nonlinear equations for the functions $P_{ss'}(\alpha)$ under the assumption of some adiabatic regime (for instance, slow relaxation time of the resonator).

I have worked on a similar problem - the switching dynamics of a classical nanomechanical Duffing resonator - in collaborations with Prof. Mark Dykman (Michigan State University) and I thereby acquired a certain experience that I now aim to exploit for the quantum case. For instance, I studied the switching dynamics of a driven Duffing nonlinear resonator in the presence of nonlinear dissipation (friction and noise) [166] , which was not previously investigated in the literature. In particular, we found that the nonlinear friction leads to a strong variation of the critical switching point between the two stable states of the Duffing resonator in the bistability regime.

(B) Lasing in multiple-dot systems and time-dependent transport

The previous results concern the spin-valve system in which I proposed to encode a spin-vibration interaction (for instance, through the presence of a strong magnetic field in the

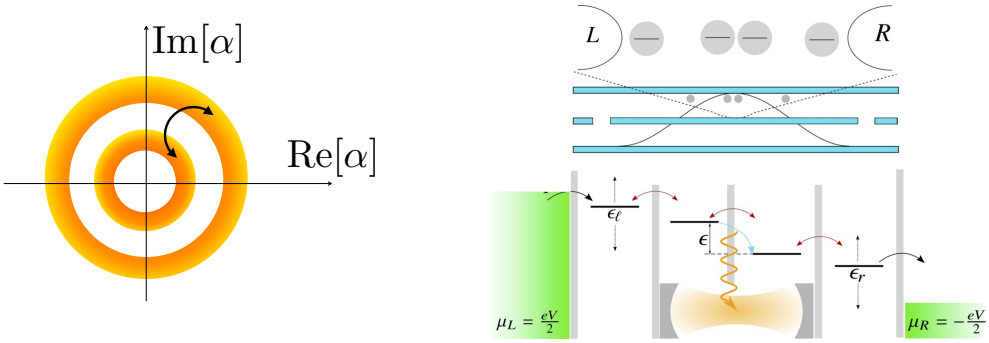

Figure 3.3: **Left:** Cartoon of a distribution function in the phase space representation of a quantum harmonic oscillator, with the two quadratures x_1 and x_2, in a bistability regime. The objective of one project is to address the switching dynamics between two stable states. **Right:** Schematic picture of a multiple quantum dot system interacting with a microwave photon cavity. The central double quantum dot is coupled to the resonator and tunnelling-coupled to lateral (injecting) quantum dots. The latter dots are connected to source (L) and drain (R) electrodes. The energy levels of the dots are tuned via the gate electrodes.

space occupied by the nanomechanical resonator, see Chapter 1). Although it is within the reach of the state of the art of these devices, thus far single-atom lasing has only been achieved in double dots characterized by a dipole interaction (via a double gate capacitance) with the microwave photon cavity. However, the efficiency realized is low and, indeed, lasing has been accomplished in a cavity coupled at least to two double dots [34] or by applying a time-dependent signal in addition to the dc bias voltage [163]. This can be explained by many reasons, such as the unavoidable interaction with the surrounding phonons of the nanocontacts embedding the quantum dots.

Beyond specific issues of technological origin, lasing in the double dots is also intrinsically limited by the unavoidable elastic tunneling associated with the partial delocalization of the electron orbitals. This implies a balance between the pumping efficiency and the coherent coupling to the resonator. Simply put, the elastic (non-emitting) tunnelling events through the higher-energy dot level are perfectly blocked when the two levels of the two separated dots are not hybridized. However, in this case, lasing is also absent, since no tunnelling can occur at all between the two dots in series.

My next project seeks to overcome this effect by proposing a multiple-dot system. Exploiting the fact that resonant transport can occur in quantum dots, the energy levels of, for instance, four dots in series can be arranged in an optimal configuration in order to suppress the elastic tunnelling transmission and enhance the coherent interaction of the charge with the cavity. In a simple scenario, the system is formed by a central double dot, which is coupled to the cavity via the gates, and by other two lateral dots that stay between the central double dot and the left and right lead, respectively, see Fig. 3.3(right). These additional dots act as energy filters for a tunnelling electron, such that this electron

has a greater probability of leaving the central double dot - by tunnelling out to the right lead - only after having emitted a photon.
On the basis of my previous studies, I am convinced that such a system is a promising way to achieve an efficient single-atom laser. One possible theoretical goal is to demonstrate that lasing in a multiple-dot system occurs in a range of interaction coupling strength (λ) in which there is no lasing for the case of a simple double dot with the same coupling strength.
Another interesting perspective is to introduce an additional ingredient in the study of the four-dot system: the use of a time-dependent gate for the lateral dots, see Fig. 3.3(right). This idea is inspired by the results of lasing in cavity QED. Here, high-efficiency lasing (up to multistability of the resonator) is achieved by pumping a steady stream of excited two-level atoms interacting sequentially with the field of the cavity at a fixed, tailored amount of time [165]. The underlying microscopic mechanism is based on a kind of matching of the interacting time of the atom with the period of the coherent cycles involving, for instance, the excited state of the atom and n photons in the cavity and the ground state and $n+1$ photons. In the same spirit, an engineered time-dependent protocol was used to generate an arbitrary single Fock state [104]. I have the perspective of realizing a similar mechanism in the multiple quantum dot system with the suitable use of a time-dependent control of the energy levels in order to adjust the injection (and extraction) of the electron in the central double dot interacting with the cavity. I have already planned a work-package for this project that I have proposed to my PhD student working on this topic (M. Mantovani).

(C) Entanglement between two resonators using a Cooper beam splitter

In mesoscopic QED, one of the theoretical challenges is the identification of fundamental mechanisms leading to the formation of quantum states or nonclassical correlations by electron transport. Within this perspective, my future plans have the objective of studying proposals for producing quantum entangled states between two remote resonators via electron transport.
The interaction between the vibration and the electron spin - which I explored in my previous work - is unique and can lead to peculiar effects that do not arise, for instance, in the case of charge-vibration interaction. Indeed, coupling the vibration with the spin represents a natural proposal for generating quantum entangled states between two mechanical oscillators. The latter goal can be achieved by exploiting the spin entanglement in a BCS superconductors Cooper pair, viz. a singlet state. These states represent one of the most simple and accessible entangled quantum systems on demand in quantum nanoelectronic devices.

One of my future projects has the objective of theoretically demonstrating entanglement between the two resonators induced by the spin-vibration. Specifically, I plan to study a three-terminal devices (the so-called Cooper-pair beam splitter), see Fig. 3.4. In this device, pairwise entangled spins can be injected in two separated dot levels. The split-

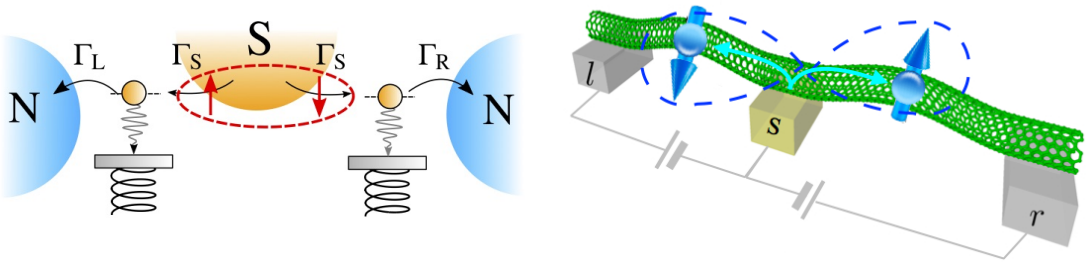

Figure 3.4: **Left:** A schematic picture of the so-called Cooper pair splitter: the pair of electrons forming the spin singlet are transferred from the superconductor to the two quantum dots. **Right:** Possible realization with two suspended carbon nanotube quantum dots.

ting of the singlet can be enforced by local (intra-dot) Coulomb interactions that inhibit the transfer of the Cooper pair in a single dot. Technically speaking, this process is called crossed Andreev reflection: the two electrons forming a singlet state are transferred from the superconductor to the two separated quantum dots. Each individual spin then locally interacts with one resonator. Owing to this direct interaction and to the entangled state of the electrons, one expects the formation of entangled states between the two resonators.

A first simple way to approach this problem is to focus on the large superconducting gap regime (the gap Δ much larger than other energy scales). Then, one can consider the effective pairing Hamiltonian in each dot, as described in the section 1.4.4. Another simplification that facilitates identification of the solution but keeps all the essential aspects is to assume a large bias limit for the normal lateral leads playing the role of simple sinks for the electrons forming the singlet. In this regime, one can tackle the problem by setting up the effective master equation - in the Lindblad form - and solving it numerically or analytically in some opportune limit.

(D) Entanglement between two resonators using quantum transport

I conclude this section by overviewing a second project on the topic of quantum correlations between two resonators generated by quantum (nonlocal) electron transport.

The basic model is outlined in Fig. 3.5. I aim to study a parallel double quantum dot device operating as a single electron splitter interferometer, with each dot linearly coupled to a local photon cavity. I want to explore how quantum correlation between the two oscillators is generated by the coherent transport of a single electron passing simultaneously through the two different dots.

The theoretical target is the computation of the covariance of the correlation functions between the two resonators. Assuming that the interaction strength between the dot's charge and each resonator is weak, I will use the perturbative approach based on the Keldysh nonequilibrium Green's functions to compute the bosonic correlator functions

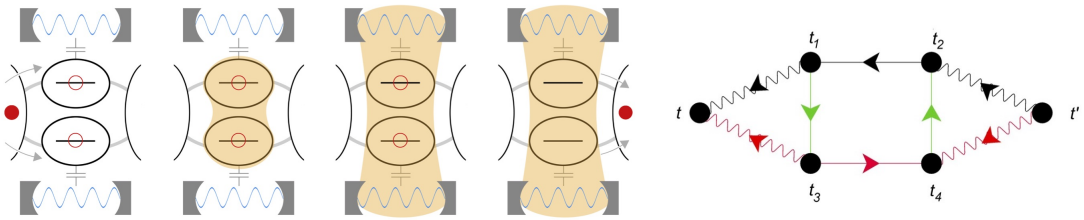

Figure 3.5: **Left:** Schematic picture of two parallel double dots between two leads. In coherent transport regime, a single electron propagates simultaneously through the two dots and interacts with the two remote resonators (microwave photon cavities). In simple terms, after an elemental passage, entanglement is created between the two resonators. **Right:** Examples of the vertex diagrams needed to compute the correlation functions of the two resonators (see text). The wavy lines are the bosonic propagators (red and black for the two different resonators), and the solid lines are the dot Green?s functions according to the color code: black for the diagonal part G_{11} of the dot 1, red for the diagonal part G_{22} on the dot 2, and green for the off-diagonal Green?s function G_{12} between the dot 1 and 2.

involving the two oscillators. This implies that one must carry out a calculation up to the fourth order in the dot-oscillator interaction strength, taking into account vertex diagrams, Fig. 3.5 (right). Diagrams to the second order in the coupling $\sim \lambda^2$ cannot contain any correlations between the two resonators, since the electron sees only one of the two resonators in the virtual (elastic) or real (inelastic) exchange of energy.
Quantum correlations are demonstrated and quantified by analyzing the correlation functions of the two resonators and testing the violation of the Cauchy-Schwarz inequality. This requires calculations of the type called vertex diagrams, whose examples are reported in Fig. 3.5 (right), to the fourth order in the coupling constant $\sim \lambda^4$.

I have already planned a work-package for this project that I have proposed to my PhD student working on this topic (F. Hellbach).

3.2 Decoherence and dissipation in many-body systems

Owing to recent experimental progress, the study of artificial quantum many-body systems, or synthetic quantum matter, has attracted great interest. Mesoscopic systems such as bosons in optical lattices or superconducting circuits made by qubits (spins) are the most remarkable experimental platforms. Other typical examples are optomechanical systems formed by photonic cavities and nanomechanical resonators integrated in hybrid devices.
These systems pave the way for the study of theoretical issues of many-body problems in nonequilibrium states, such as quantum quenching, quantum phase-transitions in the presence of external driving, dissipative phase transitions or, more generally, nonequilibrium quantum phase transitions in driven-dissipative systems and anomalous scaling in

relaxation dynamics.
Moreover, these mesoscopic systems - with intermediate size between the macroscopic and the microscopic - also have another important property that distinguishes them from the strongly correlated bulk systems: their interaction with the environment cannot be neglected. This means that they must be theoretically treated as open, dissipative quantum systems. This is indeed the typical case for the superconducting qubits formed by macroscopic circuits and the optomechanical systems formed by photon cavities and mechanical resonators. Understanding the effects of the environment on the quantumness of such systems is also an important issue for the control and manipulation of the individual coherent systems. Devising methods to control and suppress decoherence is therefore a key issue for various present and future applications in quantum measuring devices and in quantum computation.
In the past, quantum dissipative dynamics and decoherence have been theoretically analyzed primarily in individual open systems (for example, the spin-boson model); only in recent years has there been a novel interest in addressing this problem in many-body systems. A clear understanding of the effects of an environment on correlated quantum many-body systems is presently lacking.

3.2.1 Example of recent results

In a first work [167], together with my two PhD students (H. Weisbrich and C. Saussol), I studied the decoherence dynamics of a quantum Ising lattice of finite size with a transverse dissipative interaction: namely, the coupling with the bath is assumed to be perpendicular to the direction of the spin interaction and parallel to the external transverse magnetic field.
In the limit of a small transverse field, the eigenstates and spectrum are obtained by a strong coupling expansion, from which we derived the Lindblad equation in the Markovian limit. At temperatures lower than the energy gap and for weak dissipation, the decoherence dynamics can be addressed by taking only the two degenerate ground states and the first excited subspace into account. The latter is formed by pairs of domain walls (or kinks), which are quantum delocalized along the chain due to the small magnetic field. We found that some of these excited states form a relaxation-free subspace; that is, they do not decay to the ground states.
In a more recent work [168], together with one of my PhD students (H. Weisbrich), I studied the decoherence and relaxation dynamics of topological states in an extended class of quantum Ising chains that can present a multidimensional ground-state subspace, see Fig. 3.6. The leading interaction between the spins and the environment was assumed to be the local fluctuations of the transverse magnetic field. By deriving the Lindblad equation using the many-body states, we investigated the relation between decoherence, energy relaxation and topology. In particular, in the topological phase and at low temperature, we analyzed the dephasing rates between the different degenerate ground states.

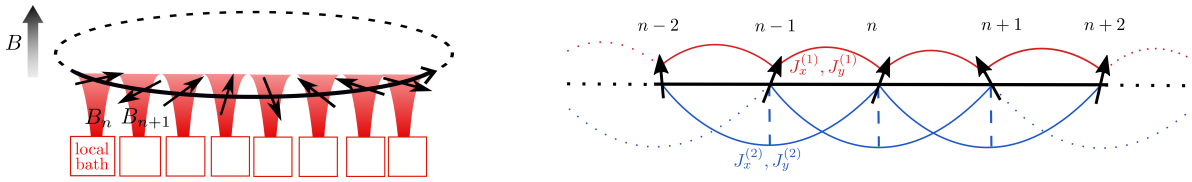

Figure 3.6: **Left:** Model of the interacting spin chain with local coupling to the environment. Each spin is coupled to a local bath via the spin component parallel to the magnetic field of the Ising model. **Right:** Example of extended Ising model: in addition to the usual nearest-neighbor two-body interaction (with coupling constant $J_x^{(1)}$ or $J_y^{(1)}$) the chain has a next nearest neighbor interaction that couples, for example, two spins at position $n-1$ and $n+1$ in the x- (or y-)component and the z-component of the intermediate spin at position n (see [168] for details).

3.2.2 Future projects

The abovementioned works [167] and [168] define one possible scheme of addressing this topic, namely by starting from an integrable spin lattice model and treating the dissipative coupling with the environment in the Markovian regime (Lindblad) using an opportune perturbative expansion.
My research program on this topic will focus on the study of decoherence and nonequilibrium quantum dynamics in (i) spin lattices with engineered interactions and (ii) spin lattices with engineered dissipation
Concerning the first point, my work plan is to consider spin lattices in which each spin is coupled to a dissipative bath, as occurs in experimental systems such as superconducting qubits, and to discuss the effect of the interactions between the spins and those of an external driving on the spin lattice. I aim to investigate tailored quasi-1D lattices with some topological constraints and/or geometrical frustrations. An example of interesting geometry is a chain of triangular plaquettes with antiferromagnetic interaction, see 3.7 (left). The research hypothesis is that the strong quantum correlations among qubits created by interaction and enhanced by topology/geometry can compete with dissipative interaction with the environment such that decoherence dynamics can be drastically slowed down. In other words, the goal is to enhance the internal quantum correlation among the spins in order to compete with the detrimental, dissipative effects of the environment.

To outline the research strategy, the first steps will be: (i) analysis of the model without dissipation (possibly to search for an exact solution) and (ii) derivation of the Lindblad equation, assuming the Markovian limit, on the basis of the many-body states. The dissipative interaction with the environment is assumed according to the natural situation occurring in experimental devices. For example, each spin can can be considered to be coupled to its local thermal bath. This approach is motivated by the perspective of realizing these lattices with real superconducting qubits in which the dissipative interaction with the bath is completely generic and affects all spins of the system, generally in an uncorrelated way.

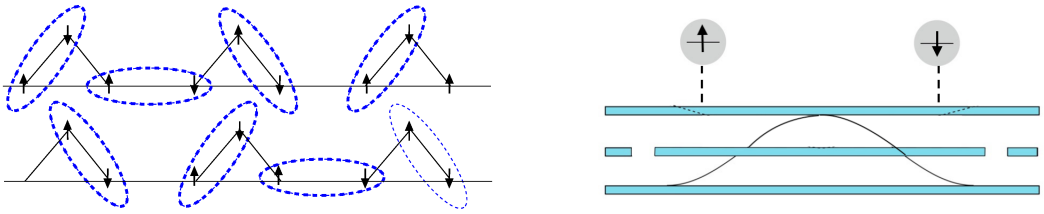

Figure 3.7: **Left:** Example of a chain of spin formed by triangular plaquettes with antiferromagnetic interaction. Due to the geometric frustration, different ways of pairing the nearest-neighbor spins are possible. **Right:** Example of engineered dissipation: two spin (qubits) coupled to a driven microwave cavity of frequency ω_c. The sum of the two energy levels of the spin (qubit frequencies) $\omega_{q,1} + \omega_{q,2}$ match the detuning between the frequency ω_L of the pumping laser of the cavity, viz. $\omega_L - \omega_c = \omega_{q,1} + \omega_{q,2}$. This leads to an enhancement of correlated energy relaxation in which the two qubits can relax simultaneously by emitting a photon into the cavity.

Regarding the second research direction, in general, dissipation - the coupling of a system with its environment - produces decoherence, with the tendency to destroy and erase the interesting quantum effects responsible for the power of quantum computation. However, it can also have exactly the opposite effect: it acts as a resource for quantum computation without the requirement to attain a purely coherent quantum dynamics. This corresponds to the strategy of engineered dissipation. I plan to develop projects on this topic with the objective of controlling the dynamics of superconducting qubits embedded in designed electromagnetic environments. The ultimate goal in this approach is to design in an opportune way the interaction between the lattice of spin and the environment such that the latter can drive the spins towards the desired final (quantum) state.
An example of elemental units producing nontrivial dissipation is a system formed by two spins, both coupled to a driven microwave resonator, see Fig. 3.7(right). In this case, one can envisage the implementation of nonlocal dissipation that translates into nonlocal dissipative Lindblad operators. The latter ingredient is crucial for encoding non-trivial dissipation that can stabilize nonclassical states.
Finally, I again intend to analyze the possibility of experimentally implementing these ideas with superconducting qubits based on Josephson junctions coupled to microwave cavities, with the ultimate perspective of increasing the decoherence time through designed dissipation.
I have already planned a work-package for this project that I have proposed to my PhD student working on this topic (H. Weisbrich).

Bibliography

[1] Y. V. Nazarov and Y. M. Blanter, *Quantum Transport: Introduction to Nanoscience*. New York: Cambridge University Press, 2009.

[2] J. C. Cuevas and E. Scheer, *Molecular Electronics: An introduction to Theory and Experiment*. Singapore: World Scientific, 2010.

[3] M. P. Blencowe, "Nanoelectromechanical systems," *Contemporary Physics*, vol. 46, p. 249, 2005.

[4] Y. S. Greenberg, Y. A. Pashkin, and E. Il'ichev, "Nanomechanical resonators," *Physics-Uspekhi*, vol. 55, p. 382, 2012.

[5] M. Poot and H. van der Zant, "Mechanical systems in the quantum regime," *Physics Reports*, vol. 511, p. 273, 2012.

[6] H. Park, J. Park, A. K. L. Lim, E. H. Andersen, A. P. Alivisatos, and P. L. McEuen, "Nanomechanical oscillations in a single $c-60$ transistor," *Nature*, vol. 407, p. 57, 2000.

[7] S. V. Aradhya and L. Venkataraman, "Single-molecule junctions beyond electronic transport," *Nat. Nanotechnol.*, vol. 8, p. 399, 2013.

[8] K. J. Franke and J. I. Pascual, "Effects of electron-vibration coupling in transport through single molecules," *J. Phys.: Condens. Matter*, vol. 24, p. 394002, 2012.

[9] R. Leturcq, C. Stampfer, K. Inderbitzin, L. Durrer, C. Hierold, E. Mariani, M. G. Schultz, F. von Oppen, and K. Ensslin, "Franck-Condon blockade in suspended carbon nanotube quantum dots," *Nat. Physics*, vol. 5, p. 327, 2009.

[10] A. K. Hüttel, B. Witkamp, M. Leijnse, M. R. Wegewijs, and H. S. J. van der Zant, "Pumping of Vibrational Excitations in the Coulomb-Blockade Regime in a Suspended Carbon Nanotube," *Phys. Rev. Lett.*, vol. 102, p. 225501, 2009.

[11] G. A. Steele, A. K. Hüttel, B. Witkamp, M. Poot, H. B. Meerwaldt, L. P. Kouwenhoven, and H. S. J. van der Zant, "Strong Coupling Between Single-Electron Tunneling and Nanomechanical Motion," *Science*, vol. 325, p. 1103, 2009.

[12] B. Lassagne, Y. Tarakanov, J. Kinaret, D. Garcia-Sanchez, and A. Bachtold, "Coupling Mechanics to Charge Transport in Carbon Nanotube Mechanical Resonators," *Science*, vol. 325, p. 1107, 2009.

[13] M. Ganzhorn and W. Wernsdorfer, "Dynamics and Dissipation Induced by Single-Electron Tunneling in Carbon Nanotube Nanoelectromechanical Systems," *Phys. Rev. Lett.*, vol. 108, p. 175502, 2012.

[14] A. Benyamini, A. Hamo, S. V. Kusminskiy, F. von Oppen, and S. Ilani, "Real-space tailoring of the electron-phonon coupling in ultraclean nanotube mechanical resonators," *Nat. Physics*, vol. 9, p. 1, 2014.

[15] R. G. Knobel and A. N. Cleland, "Nanometre-scale displacement sensing using a single electron transistor," *Nature*, vol. 424, p. 291, 2003.

[16] A. D. Armour, M. P. Blencowe, and Y. Zhang, "Classical dynamics of a nanomechanical resonator coupled to a single-electron transistor," *Phys. Rev. B*, vol. 69, p. 125313, 2004.

[17] Y. M. Blanter, O. Usmani, and Y. V. Nazarov, "Single-electron tunneling with strong mechanical feedback," *Phys. Rev. Lett.*, vol. 93, p. 136802, 2004.

[18] N. M. Chtchelkatchev, W. Belzig, and C. Bruder, "Charge transport through a single-electron transistor with a mechanically oscillating island," *Physical Review B*, vol. 70, p. 193305, 2004.

[19] C. B. Doiron, W. Belzig, and C. Bruder, "Electrical transport through a single-electron transistor strongly coupled to an oscillator," *Physical Review B*, vol. 74, p. 205336, 2006.

[20] A. Naik, O. Buu, M. D. LaHaye, A. D. Armour, A. A. Clerk, M. P. Blencowe, and K. C. Schwab, "Cooling a nanomechanical resonator with quantum back-action," *Nature*, vol. 443, p. 193, 2006.

[21] M. P. Blencowe, J. Imbers, and A. D. Armour, "Dynamics of a nanomechanical resonator coupled to a superconducting single-electron transistor," *New J. Phys.*, vol. 7, p. 236, 2005.

[22] V. Koerting, T. L. Schmidt, C. B. Doiron, B. Trauzettel, and C. Bruder, "Transport properties of a superconducting single-electron transistor coupled to a nanomechanical oscillator," *Physical Review B*, vol. 79, p. 134511, Apr. 2009.

[23] A. Erbe, C. Weiss, W. Zwerger, and R. H. Blick, "Nanomechanical Resonator Shuttling Single Electrons at Radio Frequencies," *Phys. Rev. Lett.*, vol. 87, p. 096106, 2001.

[24] L. Y. Gorelik, A. Isacsson, Y. M. Galperin, R. I. Shekhter, and M. Jonson, "Coherent transfer of Cooper pairs by a movable grain," *Nature*, vol. 411, p. 454, 2001.

[25] F. Pistolesi, "Full counting statistics of a charge shuttle," *Phys. Rev. B*, vol. 69, p. 245409, 2004.

[26] E. M. Weig, R. H. Blick, T. Brandes, J. Kirschbaum, W. Wegscheider, M. Bichler, and J. P. Kotthaus, "Single-Electron-Phonon Interaction in a Suspended Quantum Dot Phonon Cavity," *Phys. Rev. Lett.*, vol. 92, p. 046804, 2004.

[27] Y. Okazaki, I. Mahboob, K. Onomitsu, S. Sasaki, and H. Yamaguchi, "Gate-controlled electromechanical backaction induced by a quantum dot," *Nature Communications*, vol. 7, p. 11132, 2016.

[28] J. Moser, A. Eichler, J. Güttinger, M. I. Dykman, and A. Bachtold, "Nanotube mechanical resonators with quality factors of up to 5 million," *Nature Nanotechnology*, vol. 9, p. 1007, 2014.

[29] M. Dykman, *Fluctuating Nonlinear Oscillators: From Nanomechanics to Quantum Superconducting Circuits*. Oxford University Press, 2012.

[30] M. Galperin, M. A. Ratner, and A. Nitzan, "Hysteresis, Switching, and Negative Differential Resistance in Molecular Junctions: A Polaron Model," *Nano Lett.*, vol. 5, no. 1, p. 125, 2005.

[31] D. Mozyrsky, M. B. Hastings, and I. Martin, "Intermittent polaron dynamics: Born-oppenheimer approximation out of equilibrium," *Phys. Rev. B*, vol. 73, p. 035104, 2006.

[32] G. Micchi, R. Avriller, and F. Pistolesi, "Mechanical Signatures of the Current Blockade Instability in Suspended Carbon Nanotubes," *Phys. Rev. Lett.*, vol. 115, no. 20, p. 206802, 2015.

[33] D. Radić, A. Nordenfelt, A. M. Kadigrobov, R. I. Shekhter, M. Jonson, and L. Y. Gorelik, "Spin-Controlled Nanomechanics Induced by Single-Electron Tunneling," *Phys. Rev. Lett.*, vol. 107, no. 23, p. 236802, 2011.

[34] Y. Y. Liu, J. Stehlik, C. Eichler, M. J. Gullans, J. M. Taylor, and J. R. Petta, "Semiconductor double quantum dot micromaser," *Science*, vol. 347, p. 285, Jan. 2015.

[35] J. J. Viennot, M. C. Dartiailh, A. Cottet, and T. Kontos, "Coherent coupling of a single spin to microwave cavity photons," *Science*, vol. 349, p. 408, July 2015.

[36] A. Stockklauser, P. Scarlino, J. V. Koski, S. Gasparinetti, C. K. Andersen, C. Reichl, W. Wegscheider, T. Ihn, K. Ensslin, and A. Wallraff, "Strong Coupling Cavity QED with Gate-Defined Double Quantum Dots Enabled by a High Impedance Resonator," *Physical Review X*, vol. 7, p. 011030, Mar. 2017.

[37] O. Dmytruk, M. Trif, C. Mora, and P. Simon, "Out-of-equilibrium quantum dot coupled to a microwave cavity," *Phys. Rev. B*, vol. 93, p. 075425, Feb 2016.

[38] N. Lambert, F. Nori, and C. Flindt, "Bistable photon emission from a solid-state single-atom laser," *Phys. Rev. Lett.*, vol. 115, p. 216803, Nov 2015.

[39] O. Dmytruk, M. Trif, and P. Simon, "Cavity quantum electrodynamics with mesoscopic topological superconductors," *Physical Review B*, vol. 92, p. 245432, Dec. 2015.

[40] M. Mantovani, A. D. Armour, W. Belzig, and G. Rastelli, "Dynamical multistability in a quantum-dot laser," *Physical Review B*, vol. 99, p. 045442, 2019.

[41] S. Sapmaz, P. Jarillo-Herrero, Y. M. Blanter, and H. S. J. v. d. Zant, "Coupling between electronic transport and longitudinal phonons in suspended nanotubes," *New J. Phys.*, vol. 7, p. 243, 2005.

[42] B. J. LeRoy, J. Kong, V. K. Pahilwani, C. Dekker, and S. G. Lemay, "Three-terminal scanning tunneling spectroscopy of suspended carbon nanotubes," *Phys. Rev. B*, vol. 72, p. 075413, 2005.

[43] Y. Wang and F. Pistolesi, "Sensitivity of mixing-current technique to detect nanomechanical motion," *Physical Review B*, vol. 95, p. 035410, 2017.

[44] A. D. O'Connell, M. Hofheinz, M. Ansmann, R. C. Bialczak, M. Lenander, E. Lucero, M. Neeley, D. Sank, H. Wang, M. Weides, J. Wenner, J. M. Martinis, and A. N. Cleland, "Quantum ground state and single-phonon control of a mechanical resonator," *Nature*, vol. 464, p. 697, 2010.

[45] A. Eichler, M. del Álamo Ruiz, J. A. Plaza, and A. Bachtold, "Strong Coupling between Mechanical Modes in a Nanotube Resonator," *Phys. Rev. Lett.*, vol. 109, p. 025503, 2012.

[46] S. Sahoo, T. Kontos, J. Furer, C. Hoffmann, M. Gräber, A. Cottet, and C. Schönenberger, "Electric field control of spin transport," *Nat. Phys.*, vol. 1, p. 99, 2005.

[47] F. Kuemmeth, S. Ilani, D. C. Ralph, and P. L. McEuen, "Coupling of spin and orbital motion of electrons in carbon nanotubes," *Nature*, vol. 452, p. 448, 2008.

[48] J. Atalaya and L. Y. Gorelik, "Spintronics-based mesoscopic heat engine," *Phys. Rev. B*, vol. 85, p. 245309, 2012.

[49] A. Pályi, P. R. Struck, M. Rudner, K. Flensberg, and G. Burkard, "Spin-Orbit-Induced Strong Coupling of a Single Spin to a Nanomechanical Resonator," *Phys. Rev. Lett.*, vol. 108, p. 206811, 2012.

[50] J. Schindele, A. Baumgartner, R. Maurand, M. Weiss, and C. Schönenberger, "Nonlocal spectroscopy of Andreev bound states," *Phys. Rev. B*, vol. 89, p. 045422, 2014.

[51] J. Gramich, A. Baumgartner, and C. Schönenberger, "Resonant and Inelastic Andreev Tunneling Observed on a Carbon Nanotube Quantum Dot," *Phys. Rev. Lett.*, vol. 115, p. 216801, 2015.

[52] J. Rammer, *Quantum Field Theory of Nonequilibrium States.* New York: Cambridge University Press, 1 ed., 2007.

[53] Y. Meir and N. S. Wingreen, "Landauer formula for the current through an interacting electron region," *Phys. Rev. Lett.*, vol. 68, p. 2512, 1992.

[54] J. D. Teufel, T. Donner, D. Li, J. W. Harlow, M. S. Allman, K. Cicak, A. J. Sirois, J. D. Whittaker, K. W. Lehnert, and R. W. Simmonds, "Sideband cooling of micromechanical motion to the quantum ground state," *Nature*, vol. 475, p. 359, 2012.

[55] M. Aspelmeyer, T. J. Kippenberg, and F. Marquardt, "Cavity optomechanics," *Rev. Mod. Phys.*, vol. 86, p. 1391, 2014.

[56] I. Martin, A. Shnirman, L. Tian, and P. Zoller, "Ground-state cooling of mechanical resonators," *Phys. Rev. B*, vol. 69, p. 125339, 2004.

[57] F. Pistolesi, "Cooling a vibrational mode coupled to a molecular single-electron transistor," *J. Low Temp. Phys.*, vol. 154, p. 199, 2009.

[58] S. Zippilli, G. Morigi, and A. Bachtold, "Cooling Carbon Nanotubes to the Phononic Ground State with a Constant Electron Current," *Phys. Rev. Lett.*, vol. 102, p. 096804, 2009.

[59] G. Sonne, M. E. Peña-Aza, L. Y. Gorelik, R. I. Shekhter, and M. Jonson, "Cooling of a Suspended Nanowire by an ac Josephson Current Flow," *Phys. Rev. Lett.*, vol. 104, p. 226802, 2010.

[60] F. Santandrea, L. Y. Gorelik, R. I. Shekhter, and M. Jonson, "Cooling of Nanomechanical Resonators by Thermally Activated Single-Electron Transport," *Phys. Rev. Lett.*, vol. 106, p. 186803, 2011.

[61] G. Sonne and L. Y. Gorelik, "Ground-State Cooling of a Suspended Nanowire through Inelastic Macroscopic Quantum Tunneling in a Current-Biased Josephson Junction," *Phys. Rev. Lett.*, vol. 106, p. 167205, 2011.

[62] L. I. Glazman and R. I. Shekhter, "Inelastic resonant tunneling of electrons through a potential barrier," *Sov. Phys. JETP*, vol. 67, p. 163, 1988.

[63] S. Braig and K. Flensberg, "Vibrational sidebands and dissipative tunneling in molecular transistors," *Phys. Rev. B*, vol. 68, p. 205324, 2003.

[64] A. Mitra, I. Aleiner, and A. J. Millis, "Phonon effects in molecular transistors: Quantal and classical treatment," *Phys. Rev. B*, vol. 69, p. 245302, 2004.

[65] J. Koch, F. von Oppen, and A. V. Andreev, "Theory of the Franck-Condon blockade regime," *Physical Review B*, vol. 74, p. 205438, 2006.

[66] R. Egger and A. O. Gogolin, "Vibration-induced correction to the current through a single molecule," *Physical Review B*, vol. 77, p. 113405, 2008.

[67] A. Braggio, M. Governale, M. G. Pala, and J. König, "Superconducting proximity effect in interacting quantum dots revealed by shot noise," *Solid State Communications*, vol. 151, p. 155, 2011.

[68] R. I. Shekhter, L. Y. Gorelik, L. I. Glazman, and M. Jonson, "Electronic Aharonov-Bohm Effect Induced by Quantum Vibrations," *Physical review letters*, vol. 97, p. 156801, 2006.

[69] C. B. Doiron, B. Trauzettel, and C. Bruder, "Measuring the momentum of a nanomechanical oscillator through the use of two tunnel junctions," *Phys. Rev. Lett.*, vol. 100, p. 027202, 2008.

[70] Y. M. Blanter and M. Büttiker, "Shot noise in mesoscopic conductors," *Physics Reports*, vol. 336, p. 1, 2000.

[71] R. Landauer, "Condensed-matter physics: The noise is the signal," *Nature*, vol. 392, pp. 658–, 1998.

[72] L. Zhang, Y.-J. Yu, L.-G. Chen, Y. Luo, B. Yang, F.-F. Kong, G. Chen, Y. Zhang, Q. Zhang, Y. Luo, J.-L. Yang, Z.-C. Dong, and J. G. Hou, "Electrically driven single-photon emission from an isolated single molecule," *Nature Communications*, vol. 8, p. 580, 2017.

[73] A. Barone and G. Paternò, *Physics and Applications of the Josephson Effect*. New York: John Wiley and Sons, 1982.

[74] K. K. Likharev, *Dynamics of the Josephson Junctions and Circuits*. London: Gordon and Breach Science Publishers, 1986.

[75] G.-L. Ingold and Y. V. Nazarov, *Single charge tunneling: Coulomb blockade phenomena in nanostructures*, ch. 2. Springer, 1992.

[76] M. H. Devoret, *Quantum Fluctuations (Les Houches Session LXIII)*. Amsterdam: Elsevier, 2002.

[77] Y. Makhlin, G. Schön, and A. Shnirman, "Quantum-state engineering with Josephson-junction devices," *Rev. Mod. Phys.*, vol. 73, p. 1, 2001.

[78] M. Tinkham, *Introduction to Superconductivity*. New York: Dover Publications, Inc., 2 ed., 1996.

[79] J. M. Martinis, M. H. Devoret, and J. Clarke, "Energy-level quantization in the zero-voltage state of a current-biased josephson junction," *Phys. Rev. Lett.*, vol. 55, p. 1543, 1985.

[80] M. H. Devoret, J. M. Martinis, and J. Clarke, "Measurements of macroscopic quantum tunneling out of the zero-voltage state of a current-biased josephson junction," *Phys. Rev. Lett.*, vol. 55, p. 1908, 1985.

[81] A. J. Leggett and A. Garg, "Quantum mechanics versus macroscopic realism: Is the flux there when nobody looks?," *Phys. Rev. Lett.*, vol. 54, p. 857, 1985.

[82] G. Schön and A. Zaikin, "Quantum coherent effects, phase transitions, and the dissipative dynamics of ultra small tunnel junctions," *Physics Reports*, vol. 198, p. 237, 1990.

[83] A. J. Leggett, "Testing the limits of quantum mechanics: motivation, state of play, prospects," *Journal of Physics: Condensed Matter*, vol. 14, p. R415, 2002.

[84] A. O. Caldeira and A. J. Leggett, "Quantum tunnelling in a dissipative system," *Ann. Phys.*, vol. 149, p. 374, 1983.

[85] A. Schmid, "Diffusion and localization in a dissipative quantum system," *Phys. Rev. Lett.*, vol. 51, p. 1506, 1983.

[86] S. Bulgadaev, "Phase diagram of a dissipative quantum system," *JETP Letters*, vol. 39, p. 314, 1984.

[87] A. J. Leggett, S. Chakravarty, A. Dorsey, M. Fisher, A. Garg, and W. Zwerger, "Dynamics of the dissipative two-state system," *Rev. Mod. Phys.*, vol. 59, p. 1, 1987.

[88] U. Weiss, *Quantum Dissipative Systems*. Singapore: World Scientific Publishing, 2012.

[89] M. Devorert and R. J. Schoelkopf, "Superconducting Circuits for Quantum Information: An Outlook," *Science*, vol. 339, p. 1169, 2013.

[90] Z.-L. Xiang, S. Ashhab, J. You, and F. Nori, "Hybrid quantum circuits: Superconducting circuits interacting with other quantum systems," *Rev. Mod. Phys.*, vol. 85, p. 623, 2013.

[91] M. Hofheinz, F. Portier, Q. Baudouin, P. Joyez, D. Vion, P. Bertet, P. Roche, and D. Esteve, "Bright side of the coulomb blockade," *Phys. Rev. Lett.*, vol. 106, p. 217005, 2011.

[92] Y. A. Pashkin, H. Im, J. Leppäkangas, T. F. Li, O. Astafiev, A. A. Abdumalikov, E. Thuneberg, and J. S. Tsai, "Charge transport through ultrasmall single and double josephson junctions coupled to resonant modes of the electromagnetic environment," *Phys. Rev. B*, vol. 83, p. 020502, 2011.

[93] F. Chen, A. J. Sirois, R. W. Simmonds, and A. J. Rimberg, "Introduction of a dc bias into a high-q superconducting microwave cavity," *Applied Physics Letters*, vol. 98, p. 132509, 2011.

[94] M. C. Cassidy, A. Bruno, S. Rubbert, M. Irfan, J. Kammhuber, R. N. Schouten, A. R. Akhmerov, and L. P. Kouwenhoven, "Demonstration of an ac josephson junction laser," *Science*, vol. 355, p. 939, 2017.

[95] A. D. Armour, M. P. Blencowe, E. Brahimi, and A. J. Rimberg, "Universal quantum fluctuations of a cavity mode driven by a josephson junction," *Phys. Rev. Lett.*, vol. 111, p. 247001, 2013.

[96] V. Gramich, B. Kubala, S. Rohrer, and J. Ankerhold, "From coulomb-blockade to nonlinear quantum dynamics in a superconducting circuit with a resonator," *Phys. Rev. Lett.*, vol. 111, p. 247002, 2013.

[97] M. Trif and P. Simon, "Photon cross-correlations emitted by a josephson junction in two microwave cavities," *Phys. Rev. B*, vol. 92, p. 014503, 2015.

[98] O. Dmytruk, M. Trif, and P. Simon, "Josephson effect in topological superconducting rings coupled to a microwave cavity," *Phys. Rev. B*, vol. 94, p. 115423, 2016.

[99] M. Westig, B. Kubala, O. Parlavecchio, Y. Mukharsky, C. Altimiras, P. Joyez, D. Vion, P. Roche, D. Esteve, M. Hofheinz, M. Trif, P. Simon, J. Ankerhold, and F. Portier, "Emission of nonclassical radiation by inelastic cooper pair tunneling," *Phys. Rev. Lett.*, vol. 119, p. 137001, 2017.

[100] A. Wallraff, D. I. Schuster, A. Blais, L. Frunzio, R. S. Huang, J. Majer, S. Kumar, S. M. Girvin, and R. J. Schoelkopf, "Strong coupling of a single photon to a superconducting qubit using circuit quantum electrodynamics," *Nature*, vol. 431, p. 162, 2004.

[101] A. Blais, R.-S. Huang, A. Wallraff, S. M. Girvin, and R. J. Schoelkopf, "Cavity quantum electrodynamics for superconducting electrical circuits: An architecture for quantum computation," *Physical Review A*, vol. 69, p. 062320, 2004.

[102] S. M. Girvin, M. H. Devoret, and R. J. Schoelkopf, "Circuit qed and engineering charge-based superconducting qubits," *Physica Scripta*, vol. 2009, p. 014012, 2009.

[103] O. Astafiev, K. Inomata, A. O. Niskanen, T. Yamamoto, Yu, Y. Nakamura, and J. S. Tsai, "Single Artificial-Atom Lasing," *Nature*, vol. 449, p. 588, 2007.

[104] M. Hofheinz, E. M. Weig, M. Ansmann, R. C. Bialczak, E. Lucero, M. Neeley, A. D. O'Connell, H. Wang, J. M. Martinis, and A. N. Cleland, "Generation of Fock states in a superconducting quantum circuit," *Nature*, vol. 454, p. 310, 2008.

[105] A. A. Houck, D. I. Schuster, J. M. Gambetta, J. A. Schreier, B. R. Johnson, J. M. Chow, L. Frunzio, J. Majer, M. H. Devoret, S. M. Girvin, and R. J. Schoelkopf, "Generating single microwave photons in a circuit," *Nature*, vol. 449, pp. 328–331, Sept. 2007.

[106] R. Fazio and H. van der Zant, "Quantum phase transitions and vortex dynamics in superconducting networks," *Physics Reports*, vol. 355, p. 235, 2001.

[107] L. B. Ioffe, M. V. Feigel'man, A. Ioselevich, D. Ivanov, and M. Troyer, "Topologically protected quantum bits using Josephson junction arrays.," *Nature*, vol. 415, p. 503, 2002.

[108] S. Gladchenko, D. Olaya, E. Dupont-Ferrier, B. Douçot, L. B. Ioffe, and M. E. Gershenson, "Superconducting nanocircuits for topologically protected qubits," *Nature Physics*, vol. 5, p. 48, 2009.

[109] M. A. Castellanos-Beltran, K. D. Irwin, G. C. Hilton, L. R. Vale, and K. W. Lehnert, "Amplification and squeezing of quantum noise with a tunable Josephson metamaterial," *Nature Physics*, vol. 4, p. 929, 2008.

[110] W. Guichard and F. W. J. Hekking, "Phase-charge duality in Josephson junction circuits: Role of inertia and effect of microwave irradiation," *Physical Review B*, vol. 81, p. 064508, 2010.

[111] V. E. Manucharyan, J. Koch, and L. I. Glazman, "Fluxonium: Single Cooper-Pair Circuit Free of Charge Offsets," *Science*, vol. 326, p. 113, 2009.

[112] N. A. Masluk, I. M. Pop, A. Kamal, Z. K. Minev, and M. H. Devoret, "Microwave Characterization of Josephson Junction Arrays: Implementing a Low Loss Superinductance," *Physical Review Letters*, vol. 109, p. 137002, 2012.

[113] M. T. Bell, I. A. Sadovskyy, L. B. Ioffe, A. Y. Kitaev, and M. E. Gershenson, "Quantum superinductor with tunable nonlinearity," *Physical Review Letters*, vol. 109, p. 137003, 2012.

[114] H. S. J. van der Zant, C. J. Muller, L. J. Geerligs, C. J. P. M. Harmans, and J. E. Mooij, "Coherent phase slip in arrays of underdamped Josephson tunnel junctions," *Physical Review B*, vol. 38, p. 5154, 1988.

[115] K. A. Matveev, A. I. Larkin, and L. I. Glazman, "Persistent Current in Superconducting Nanorings," *Physical Review Letters*, vol. 89, p. 096802, 2002.

[116] I. M. Pop, I. Protopopov, F. Lecocq, Z. Peng, B. Pannetier, O. Buisson, and W. Guichard, "Measurement of the effect of quantum phase slips in a Josephson junction chain," *Nature Physics*, vol. 6, p. 589, 2010.

[117] I. M. Pop, B. Douçot, L. Ioffe, I. Protopopov, F. Lecocq, I. Matei, O. Buisson, and W. Guichard, "Experimental demonstration of Aharonov-Casher interference in a Josephson junction circuit," *Physical Review B*, vol. 85, p. 094503, 2012.

[118] V. E. Manucharyan, N. A. Masluk, A. Kamal, J. Koch, L. I. Glazman, and M. H. Devoret, "Evidence for coherent quantum phase slips across a Josephson junction array," *Physical Review B*, vol. 85, p. 024521, 2012.

[119] A. Ergül, T. Weißl, J. Johansson, J. Lidmar, and D. B. Haviland, "Spatial and temporal distribution of phase slips in Josephson junction chains," *Scientific Reports*, vol. 7, p. 11447, 2017.

[120] Z. Hermon, E. Ben-Jacob, and G. Schön, "Charge solitons in one-dimensional arrays of serially coupled Josephson junctions," *Physical Review B*, vol. 54, p. 1234, 1996.

[121] D. B. Haviland and P. Delsing, "Cooper-pair charge solitons: The electrodynamics of localized charge in a superconductor," *Physical Review B*, vol. 54, p. R6857, 1996.

[122] S. Corlevi, W. Guichard, F. W. J. Hekking, and D. B. Haviland, "Coulomb blockade of Cooper pair tunneling and parity effects in the Cooper pair transistor," *Physical Review B*, vol. 74, p. 224505, 2006.

[123] S. V. Syzranov, K. B. Efetov, and B. L. Altshuler, "dc Conductivity of an Array of Josephson Junctions in the Insulating State," *Physical Review Letters*, vol. 103, p. 127001, 2009.

[124] C. Hutter, E. A. Tholén, K. Stannigel, J. Lidmar, and D. B. Haviland, "Josephson junction transmission lines as tunable artificial crystals," *Physical Review B*, vol. 83, p. 014511, 2011.

[125] D. Zueco, J. J. Mazo, E. Solano, and J. J. García-Ripoll, "Microwave photonics with josephson junction arrays: Negative refraction index and entanglement through disorder," *Physical Review B*, vol. 86, p. 024503, 2012.

[126] M. Taguchi, D. M. Basko, and F. W. J. Hekking, "Mode engineering with a one-dimensional superconducting metamaterial," *Physical Review B*, vol. 92, p. 024507, 2015.

[127] W. Zhang, W. Huang, M. E. Gershenson, and M. T. Bell, "Josephson Metamaterial with a Widely Tunable Positive or Negative Kerr Constant," *Physical Review Applied*, vol. 8, p. 051001, 2017.

[128] T. Weißl, B. Küng, E. Dumur, A. K. Feofanov, I. Matei, C. Naud, O. Buisson, F. W. J. Hekking, and W. Guichard, "Kerr coefficients of plasma resonances in josephson junction chains," *Physical Review B*, vol. 92, p. 104508, 2015.

[129] J.-P. Martinez, S. Leger, N. Gheereart, R. Dassonneville, L. Planat, F. Foroughi, Y. Krupko, O. Buisson, C. Naud, W. Guichard, S. Florens, I. Snyman, and N. Roch, "Probing a transmon qubit via the ultra-strong coupling to a Josephson waveguide," *arXiv:1802.00633*, 2018.

[130] H.-P. Breuer and F. Petruccione, *The Theory of Open Quantum Systems*. Oxford University Press, 2007.

[131] J. M. Raimond, M. Brune, and S. Haroche, "Manipulating quantum entanglement with atoms and photons in a cavity," *Rev. Mod. Phys.*, vol. 73, p. 565, 2001.

[132] S. Haroche, "Nobel Lecture: Controlling photons in a box and exploring the quantum to classical boundary," *Rev. Mod. Phys.*, vol. 85, p. 1083, 2013.

[133] D. J. Wineland, "Nobel Lecture: Superposition, entanglement, and raising Schrödinger's cat," *Rev. Mod. Phys.*, vol. 85, p. 1103, 2013.

[134] H. J. Carmichael, *Statistical Methods in Quantum Optics 1*. Springer-Verlag Berlin Heidelberg, 1999.

[135] C. Gardiner and P. Zoller, *Quantum noise*. Springer-Verlag Berlin Heidelberg, 2000.

[136] R. P. Feynman and A. R. Hibbs, *Quantum mechanics and path integrals*. Dover Publications Inc., 2010.

[137] H. Kleinert, *Path Integrals in Quantum Mechanics, Statistics, Polymer Physics, and Financial Markets*. Singapur: World Scientific, 2009.

[138] R. P. Feynman, "Space-time approach to non-relativistic quantum mechanics," *Rev. Mod. Phys.*, vol. 20, p. 367, 1948.

[139] H. Trotter, "On the product of semigroups of operators," *Proc. Amer. Math. Soc.*, vol. 10, p. 545, 1959.

[140] S. Pereverzev, A. Loshak, S. Backhaus, J. Davis, and R. Packard, "Direct measurement of the current-phase relation of a superfluid 3he-b weak link," *Nature (London)*, vol. 388, p. 449, 1997.

[141] K. Sukhatme, Y. Mukharsky, T. Chui, and D. Pearson, "Observation of the ideal josephson effect in superfluid 4he," *Nature (London)*, vol. 411, p. 280, 2001.

[142] S. Levy, E. Lahoud, I. Shomroni, and J. Steinhauer, "The a.c. and d.c. Josephson effects in a Bose–Einstein condensate," *Nature*, vol. 449, p. 579, 2007.

[143] J. M. Martinis, M. Ansmann, and J. Aumentado, "Energy Decay in Superconducting Josephson-Junction Qubits from Nonequilibrium Quasiparticle Excitations," *Physical review letters*, vol. 103, p. 097002, 2009.

[144] P. J. de Visser, J. J. A. Baselmans, P. Diener, S. J. C. Yates, A. Endo, and T. M. Klapwijk, "Number Fluctuations of Sparse Quasiparticles in a Superconductor," *Physical review letters*, vol. 106, p. 167004, 2011.

[145] G. Catelani, R. J. Schoelkopf, and L. I. Glazman, "Relaxation and frequency shifts induced by quasiparticles in superconducting qubits," *Physical Review B*, vol. 84, p. 064517, 2011.

[146] I. M. Pop, K. Geerlings, G. Catelani, R. J. Schoelkopf, L. I. Glazman, and M. H. Devoret, "Coherent suppression of electromagnetic dissipation due to superconducting quasiparticles," *Nature*, vol. 508, p. 369, 2014.

[147] S. Sachdev, *Quantum phase transitions*. Wiley Online Library, 2007.

[148] S. L. Sondhi, S. M. Girvin, J. P. Carini, and D. Shahar, "Continuous quantum phase transitions," *Review Modern Physics*, vol. 69, p. 315, 1997.

[149] R. M. Bradley and S. Doniach, "Quantum fluctuations in chains of josephson junctions," *Physical Review B*, vol. 30, p. 1138, 1984.

[150] L. Amico, D. Aghamalyan, F. Auksztol, H. Crepaz, R. Dumke, and L. C. Kwek, "Superfluid qubit systems with ring shaped optical lattices," *Scientific Reports*, vol. 4, p. 4298, 2014.

[151] M. Cominotti, M. Rizzi, D. Rossini, D. Aghamalyan, L. Amico, L. C. Kwek, F. Hekking, and A. Minguzzi, "Optimal scaling of persistent currents for interacting bosons on a ring," *The European Physical Journal Special Topics*, vol. 224, p. 519, 2015.

[152] D. Aghamalyan, M. Cominotti, M. Rizzi, D. Rossini, F. Hekking, A. Minguzzi, L. C. Kwek, and L. Amico, "Coherent superposition of current flows in an atomtronic quantum interference device," *New Journal of Physics*, vol. 17, p. 045023, 2015.

[153] D. Aghamalyan, N. T. Nguyen, F. Auksztol, K. S. Gan, M. M. Valado, P. C. Condylis, L. C. Kwek, R. Dumke, and L. Amico, "An atomtronic flux qubit: a ring lattice of Bose–Einstein condensates interrupted by three weak links," *New Journal of Physics*, vol. 18, p. 075013, 2016.

[154] L. Amico, G. Birkl, M. Boshier, and L. C. Kwek, "Focus on atomtronics-enabled quantum technologies," *New Journal of Physics*, vol. 19, p. 020201, 2017.

[155] L. Amico, D. Basko, F. S. Bergeret, O. Buisson, H. Courtois, R. Fazio, W. Guichard, A. Minguzzi, J. Pekola, and G. Schön, "Mesoscopic electron transport and atomic gases, a review of Frank W. J. Hekking's scientific work," *SciPost Physics*, vol. 5, p. 009, 2018.

[156] A. E. Svetogorov, M. Taguchi, Y. Tokura, D. M. Basko, and F. W. J. Hekking, "Theory of coherent quantum phase slips in Josephson junction chains with periodic spatial modulations," *Physical Review B*, vol. 97, p. 104514, 2018.

[157] S. E. Korshunov, "Zero-phonon friction mechanism for linear defects in quantum crystals," *Sov. Phys. JETP*, vol. 63, p. 1242, 1986.

[158] S. E. Korshunov, "Effect of dissipation on the low-temperature properties of a tunnel-junction chain," *Sov. Phys. JETP*, vol. 68, p. 609, 1989.

[159] U. Weiss, H. Grabert, P. Hänggi, and P. Riseborough, "Incoherent tunneling in a double well," *Phys. Rev. B*, vol. 35, p. 9535, 1987.

[160] A. Cuccoli, N. Del Sette, and R. Vaia, "Reentrant enhancement of quantum fluctuations for symmetric environmental coupling," *Physical Review E*, vol. 81, p. 041110, 2010.

[161] G. Rastelli and S. Ciuchi, "Wigner crystallization in a polarizable medium," *Physical Review B*, vol. 71, p. 184303, 2005.

[162] G. Adesso and F. Illuminati, "Entanglement in continuous-variable systems: recent advances and current perspectives," *Journal of Physics A: Mathematical and Theoretical*, vol. 40, p. 7821, 2007.

[163] Y. Y. Liu, J. Stehlik, C. Eichler, X. Mi, T. R. Hartke, M. J. Gullans, J. M. Taylor, and J. R. Petta, "Threshold Dynamics of a Semiconductor Single Atom Maser," *Physical review letters*, vol. 119, p. 097702, Aug. 2017.

[164] J. McKeever, A. Boca, A. D. Boozer, J. R. Buck, and H. J. Kimble, "Experimental realization of a one-atom laser in the regime of strong coupling," *Nature*, vol. 425, p. 268, 2003.

[165] H. Walther, B. T. H. Varcoe, B.-G. Englert, and T. Becker, "Cavity quantum electrodynamics," *Rep. Prog. Phys.*, vol. 69, p. 1325, 2006.

[166] M. I. Dykman, G. Rastelli, M. L. Roukes, and E. M. Weig, "Resonantly induced friction and frequency combs in driven nanomechanical systems," *Phys. Rev. Lett.*, vol. 122, p. 254301, 2019.

[167] H. Weisbrich, C. Saussol, W. Belzig, and G. Rastelli, "Decoherence in the quantum Ising model with transverse dissipative interaction in the strong-coupling regime," *Physical Review A*, vol. 98, p. 052109, 2018.

[168] H. Weisbrich, W. Belzig, and G. Rastelli, "Decoherence and relaxation of topological states in extended quantum Ising models," *SciPost Physics*, vol. 6, p. 037, 2019.